CHARACTERIZING THE INTERACTIONS OF APTAMERS WITH THEIR LIGANDS USING ISOTHERMAL TITRATION CALORIMETRY AND FLUORESCENCE SPECTROMETRY

KABISAN THAVASEELAN

A DISSERTATION SUBMITTED TO THE FACULTY OF GRADUATE STUDIES IN FULFILLMENT OF THE REQUIREMENTS FOR THE DEGREE OF MASTERS OF CHEMISTRY

GRADUATE PROGRAM IN CHEMISTRY
YORK UNIVERSITY
TORONTO, ONTARIO

SEPTEMBER 2024
©KABISAN THAVASEELAN 2024

Abstract

Aptamers are short single-stranded DNA or RNA molecules that are selected to bind a target often with high affinity and specificity. Some of these targets include small molecules, proteins, nucleic acids, cells and tissues. Isothermal Titration Calorimetry (ITC) and Fluorescence Spectrometry were employed to characterize the binding interactions of aptamers with their ligands. This dissertation comprises two separate research projects; in the first project, ITC was used to explore how the binding affinity of structure-switching aptamers toward their ligand varies when altering the NaCl concentration. It was shown that the binding affinity of MN19, a variant of the cocaine-binding aptamer, decreases when the NaCl concentration is increased from 140 mM to 1000 mM. The affinity increases again when the NaCl concentration is increased to 2000 mM.

The next project showcases the use of fluorescence spectrometry to characterize the interactions of methylene blue with different aptamers. Methylene blue is a redox-reporter which is used in Electrochemical aptamer-based biosensing platforms. It was shown that methylene blue binds to the MN19 aptamer, and therefore, it was of interest to see if methylene blue binds to other aptamers and to explore any similarities in their aptamer structures. Fluorescence spectrometry was used to see if methylene blue binds to other aptamers by measuring the change in fluorescence intensity of methylene blue and if binding occurred, the binding affinity was quantified. It was determined that methylene blue may be interacting and binding tightly to DNA aptamer structures which includes bulges and stem-loops but may be binding very weakly to duplex DNA such as the Dickerson Drew Dodecamer and a Hexamer.

Acknowledgements

I would like to thank my family and friends for their continuous love and support during the completion of this program. It would not have been possible for me to complete my research without your endless words of kindness and motivation. A huge thanks to my mother Thushitha Thavaseelan for her consultation which has helped me push through the completion of my Masters. I also would like to thank my father Thavaseelan Suppiah for his dedication in providing for the family allowing me to be able to pursue my Masters.

I also sincerely thank my supervisor Professor Philip E. Johnson for accepting me into his lab and providing me with the necessary facilities and guidance to help me complete my project. Being a part of your lab has helped me build on my critical thinking skills on this journey as a scientist. I am extremely grateful for the opportunities and assistance you have given me to allow me to explore beyond my potential. I want to also thank my committee members Professors Ryan Hili and Logan Donaldson for the advice and feedback you provided me about my work.

A special thanks to Dr. Aron A. Shoara for training me and providing me with the necessary assistance in using the fluorescence spectrometer along with data fitting and analysis. Thank you for the endless amounts of advice, support and knowledge to help me succeed in this project. I also would like to express my gratitude to Yunus Kaiyum for sharing your ideas through discussions and being available for advice and support whenever possible to help me grow as a scientist. The amount of time you spent for training me on using the isothermal titration calorimetry machine is very much appreciated. Thank you to Dr. Zach Churcher for also being a mentor to me and for your tremendous amounts of feedback. I also would like to thank Emily Chao for your kind friendship and assistance which has made me have an enjoyable time during my project. Thank you to all past and present lab members of the Johnson lab for their help.

Table of Contents

List of Abbreviations

DNA- Deoxyribonucleic Acid

ssDNA- single-stranded DNA

RNA- Ribonucleic Acid

SELEX- Systemic Evolution of Ligands by Exponential enrichment

PCR- Polymerase Chain Reaction

PDAC- Pancreatic Ductal Adenocarcinoma

UV-Vis- Ultraviolet-Visible

ITC- Isothermal Titration Calorimetry

NMR- Nuclear Magnetic Resonance

ΔH- Change in enthalpy

ΔS- Change in entropy

K_a- association constant

K_d- dissociation constant

IDT- Integrated DNA Technologies

PBS- Phosphate-Buffered Saline

OD- Optical Density

E-AB- Electrochemical Aptamer-Based

λ_{ex}- excitation wavelength

λ_{em}- emission wavelength

DDD- Dickerson Drew Dodecamer

SJH- Hexamer

List of Tables

List of Figures

Chapter 1. Background and Introduction

Introduction to Aptamers

Deoxyribonucleic acid (DNA) is one of the most significant molecules within cells of living organisms. It contains genetic information that is read in cells to be transcribed into messenger RNA (mRNA), which is then translated into proteins necessary for living things to function and survive.[1] A common structure of DNA, the double helix, helps this information to be replicated and passed onto future generations. Nucleic acids can be arranged in various ways, each with its own unique structure and function. Aptamers are a class of nucleic acids that can fold into unique three-dimensional structures.[2] Aptamers are short single-stranded DNA or RNA molecules that can bind to a target often with high affinities and specificities. Some include small molecules, proteins, nucleic acids, cells and tissues.[3]

Regardless of the similarity between their nucleic acid structures, DNA and RNA aptamers exhibit noticeable differences. DNA nucleotides have a C-H bond in the 2' position of the deoxyribose sugar while RNA nucleotides have a hydroxyl group (-OH) in the 2' position of its ribose sugar.[4] This significant difference makes DNA aptamers possess an advantage over RNA aptamers with regards to stability. This is because the C-H bond at the 2' position of DNA makes the DNA aptamer less reactive while the -OH group at the 2' position of RNA is susceptible to hydrolysis, making the RNA aptamer unstable.[4] To elaborate, the 2'OH group performs a nucleophilic attack on the phosphodiester bond, causing a breakage in RNA strands at the P-O 5' ester bond, which is catalyzed by the nucleases enzyme.[5] Therefore, modifications such as removing the -OH group at this position can prevent the RNA from undergoing cleavage by nucleases which can eventually help the RNA aptamer become more stable as the DNA aptamer. Furthermore, chemical modifications can be made to nucleic acid libraries such as in SELEX which can enhance the ability of aptamers to interact with their target and broaden their target spectrum.[6]

SELEX

The aptamers that we work with in our lab are selected in a process called Systemic Evolution of Ligands by Exponential enrichment (SELEX). This process was developed

independently in 1990 by two research laboratories, the Gold and Szostak groups.[7] Tuerk and Gold were using SELEX to have an RNA sequence bind a T4 DNA Polymerase.[8] On the other hand, Ellington and Szostak used this in vitro selection method to have RNA sequences that can bind to a variety of organic dyes from a population of random sequence RNA molecules.[9] Using this method, they isolated aptamer sequences that can bind their target of interest.

Standard SELEX

The first SELEX method, Standard or Classical SELEX, begins with a selection stage where a large diverse oligonucleotide library is created with predesigned primer-binding domains for Polymerase Chain Reaction (PCR) amplification as shown in Figure 1.[7] Step 1 shows the incubation of this library with a target of interest. Some sequences bind to the target whereas some sequences do not. Step 2 shows that the unbound sequences are removed and separated from the ones that do demonstrate binding for the target, allowing the completion of the partitioning phase. Step 3 shows that the bound sequences are eluted from the target. Step 4 shows the amplification stage where the bound sequences are collected and PCR is performed for several rounds for enrichment of sequences.[7] These stages are repeated until the library that was initially started with, turns into a collection of sequences that demonstrate affinity for the target of interest. This collection is then cloned and sequenced (Figure 1).

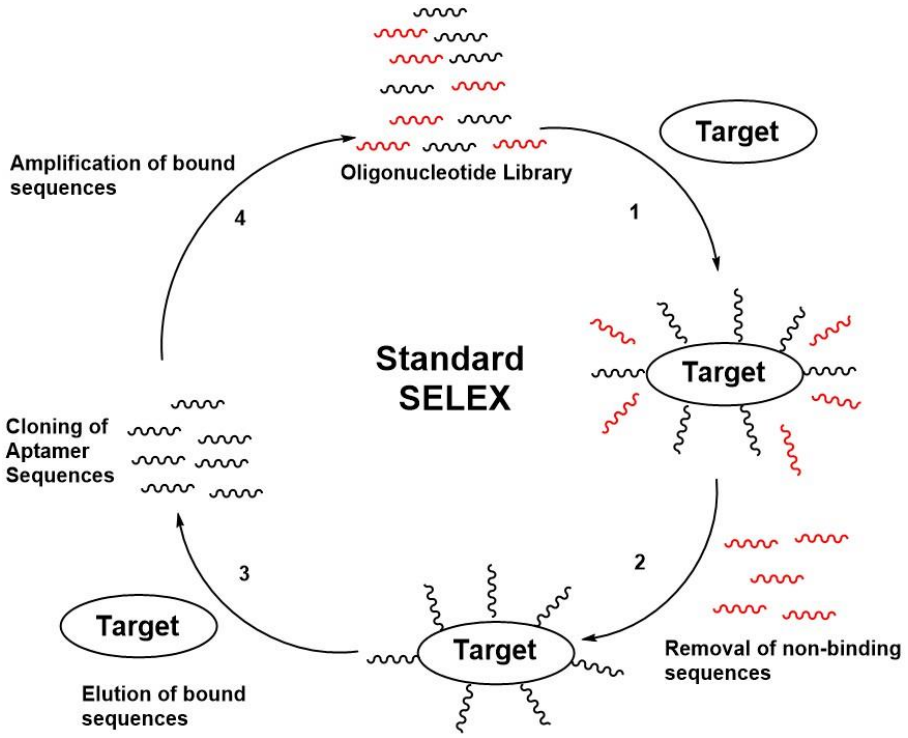

Figure 1. Diagram of the standard SELEX procedure.

Capture-SELEX

A derivative of the original SELEX method can be classified as Capture-SELEX. This process is almost like Standard SELEX with a few exceptions. This process starts with the hybridization of a single-stranded DNA (ssDNA) library with biotinylated capture-oligonucleotides.[10] This is done by having a docking site on the ssDNA that has complementarity to the capture-oligonucleotide which then hybridizes through Watson-Crick base-pairing. Another step involves immobilizing the biotinylated hybridized oligonucleotides onto streptavidin magnetic beads which act as a form of solid support. Using a magnetic rack, these beads are then washed multiple times to remove any residual or non-specific sequences. Counter-selection is performed to identify and remove any non-specific targets that may bind to the library.[10] Positive selection is then conducted to detect any binding interactions of the aptamer with the target molecule. The elution step is then performed to isolate the aptamer-target complexes, ideally possessing higher binding affinities compared to the capture-oligonucleotide aptamer complexes. PCR amplification is then performed on this eluted ssDNA library for enrichment of sequences. The ssDNA library is regenerated to conduct Capture-SELEX for

multiple rounds. Finally, aptamer sequences are identified with sequencing after multiple rounds of Capture-SELEX have been conducted.[10]

Aptamer Structure

DNA is composed of nucleotides, each containing a deoxyribose pentose sugar, nitrogenous base and phosphate group. These nucleotides commonly form a double-stranded helical structure with antiparallel strands.[1] Watson-Crick base-pairing stabilizes this DNA structure through hydrogen bonding between adenine and thymine, and cytosine and guanine nitrogenous bases (Figure 2).[1] The double-helix structure features major and minor grooves due to uneven spacing of opposing nucleotides along the helical axis, with the sugar-phosphate backbone on the outside of the double-helix while the nitrogenous bases are in the middle of the double-helix.[1]

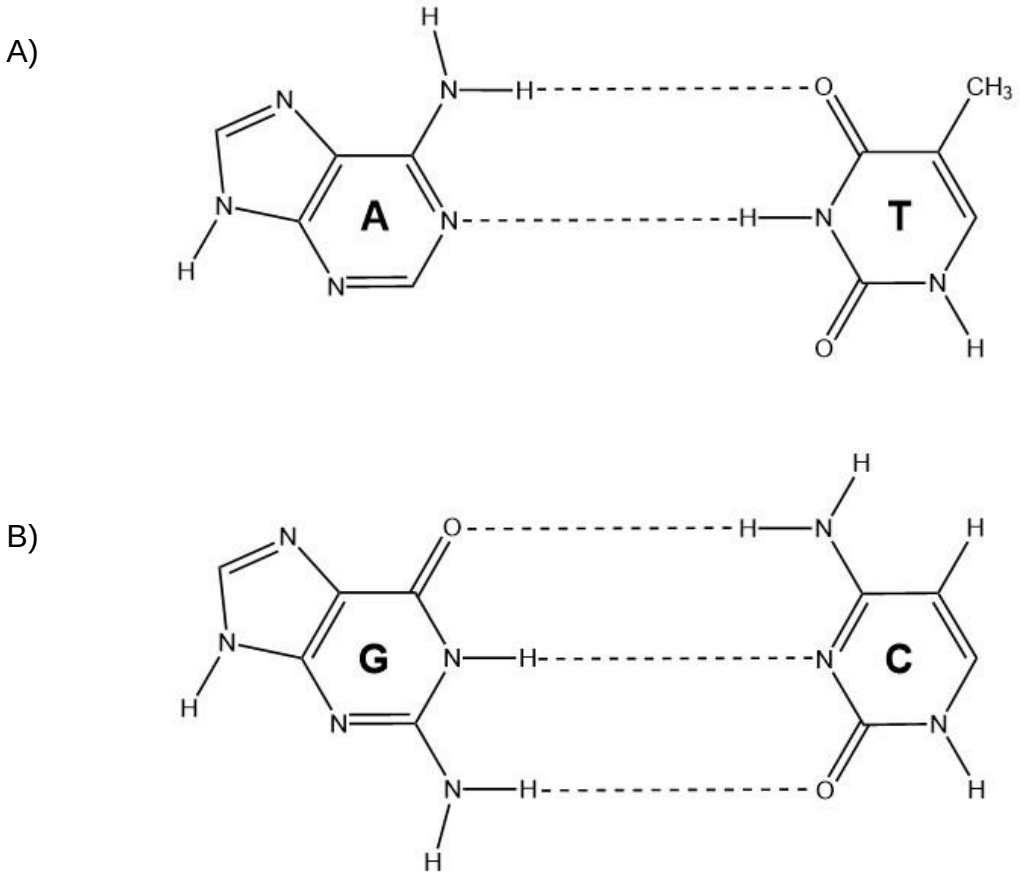

Figure 2. Watson-Crick base-pairs: A) Adenine-Thymine; B) Guanine-Cytosine. The base marked with an A is Adenine; T is Thymine; G is Guanine; C is Cytosine.

Different DNA sequences can be used to design a variety of aptamers. Furthermore, unique secondary structures can be seen because of aptamer folding and some of these structures include but are not limited to a stem, loop or a bulge.[11-12] These structures play a crucial role in target recognition and any interference with these structures can impair binding. A bulge-hairpin secondary structure motif was shown with streptavidin-binding DNA aptamers that were isolated from different libraries from different laboratories. In addition, nucleotides important for binding in the loop and bulge area were identified in high affinity sequences.[11] Therefore, if nucleotides vary from the ones observed in this region, it may or may not affect the binding affinity towards its target. Illustrations of some of the mentioned secondary structures are seen in Figure 3 for a couple of aptamers. Figure 3A shows Caff209, a variant of the caffeine-binding aptamer, containing a stem-loop structure in its predicted secondary structure. Figure 3B shows MTX5, a version of the methotrexate-binding aptamer, containing a bulge structure in its predicted secondary structure. In addition, secondary structures can fold into three-dimensional conformations. With the use of π-π stacking interactions and hydrogen bonding among nucleotides, electrostatic repulsion is mitigated when folding into three-dimensional structures.[12]

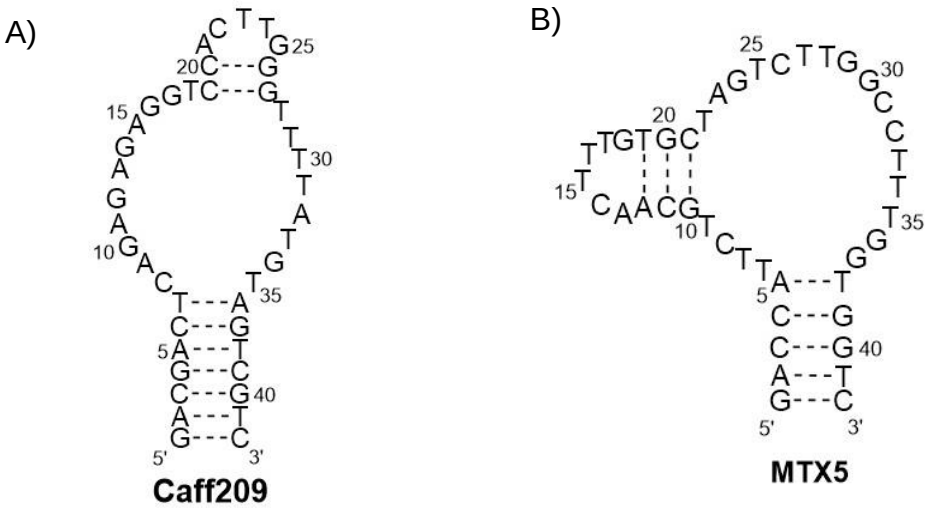

Figure 3. Illustrations of some of the secondary structures seen for aptamers. (A) shows Caff209, a variant of the caffeine-binding aptamer and it contains a stem-loop structure in its predicted secondary structure. (B) shows MTX5, a version of the methotrexate-binding aptamer and it contains a bulge structure in its predicted secondary structure.

The Cocaine-Binding Aptamer

The cocaine-binding aptamer is a well-behaved DNA aptamer where its structure consists of three stems organized around a three-way junction. In 2000, Stojanović *et al.* selected the first cocaine-binding aptamer, MNS4.1, through standard SELEX.[13] The secondary structure of MNS4.1 was determined through mutational analyses that include both random and targeted mutations.[13] The aptamer contains 38 nucleotides which are predominantly connected through Watson-Crick base-pairing. There are 5 non-Watson-Crick base-pairs: 3 GA base-pairs observed in stem 1 and 1 GT and 1 GA base-pair observed in stem 3. The cocaine-binding site on the aptamer is located within the lipophilic cavity, formed at the three-way junction. Figure 4 shows that in the free state of the aptamer where no cocaine is present, stem 3 is not formed. However, upon addition of cocaine, the stem is assembled and aids in the formation of the aptamer's three-way junction structure. It was also found that the aptamer binds to cocaine with a K_d range of 0.4-10 μM.[13]

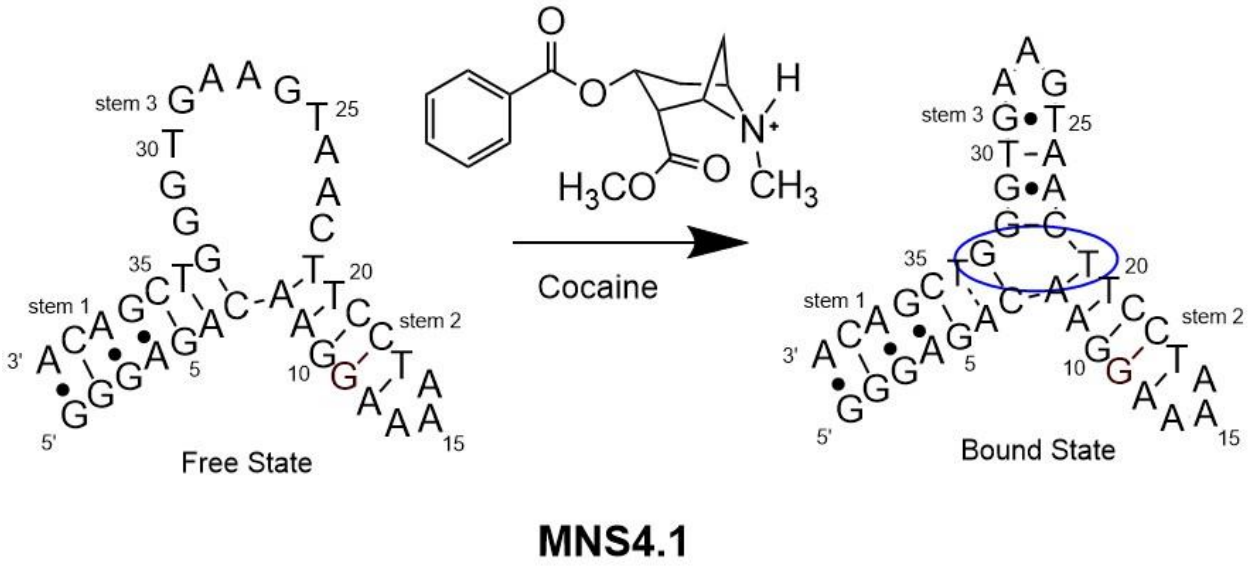

Figure 4. Binding mechanism of the MNS4.1 aptamer. In the free state, stem 3 is not formed. Upon cocaine binding, stem 3 folds to form the three-way junction. The blue oval in the bound state represents cocaine binding at the ligand-binding site located at the three-way junction of the aptamer. Dashed lines represent Watson-Crick base-pairs and black dots represent non-Watson-Crick base-pairs on the secondary structure of the aptamer in the free and bound states.

The cocaine-binding aptamer continues to be extensively studied for the purposes of small-molecule sensing as it was found that the aptamer binds to quinine and quinine analogs tighter than the ligand it was originally selected for.[14] Variants of this aptamer have been

demonstrated to bind quinine approximately 30-fold tighter than cocaine and one of these is identified as MN4, a commonly studied variant of the cocaine-binding aptamer in our lab.[15] When looking at Figure 5, this aptamer consists of 36 nucleotides and the secondary structure is pre-formed in the free-state. With the addition of ligand, there are no observable changes in its secondary structure which shows that this aptamer variant has no structure-switching folding mechanism upon binding.[14] However, another variant of the cocaine-binding aptamer was identified as MN19 and was constructed by shortening the stem 1 of MN4 to three base-pairs. By doing so, it is observed that the aptamer is loosely folded in the free-state and upon binding ligand, a structure-switching folding mechanism is observed (Figure 6).[14] NMR studies confirm that the stem 2 and 3 in the free-state in the aptamer are formed while stem 1 is not.[16] Figure 6 shows that upon ligand addition, the base-pairs in stem 1 start to form and the structure is rigidified. This ligand-induced folding mechanism was seen for both cocaine and quinine binding. Therefore, the key difference seen in this comparison is that MN4 is a non-structure-switching aptamer and MN19 is a structure-switching aptamer.

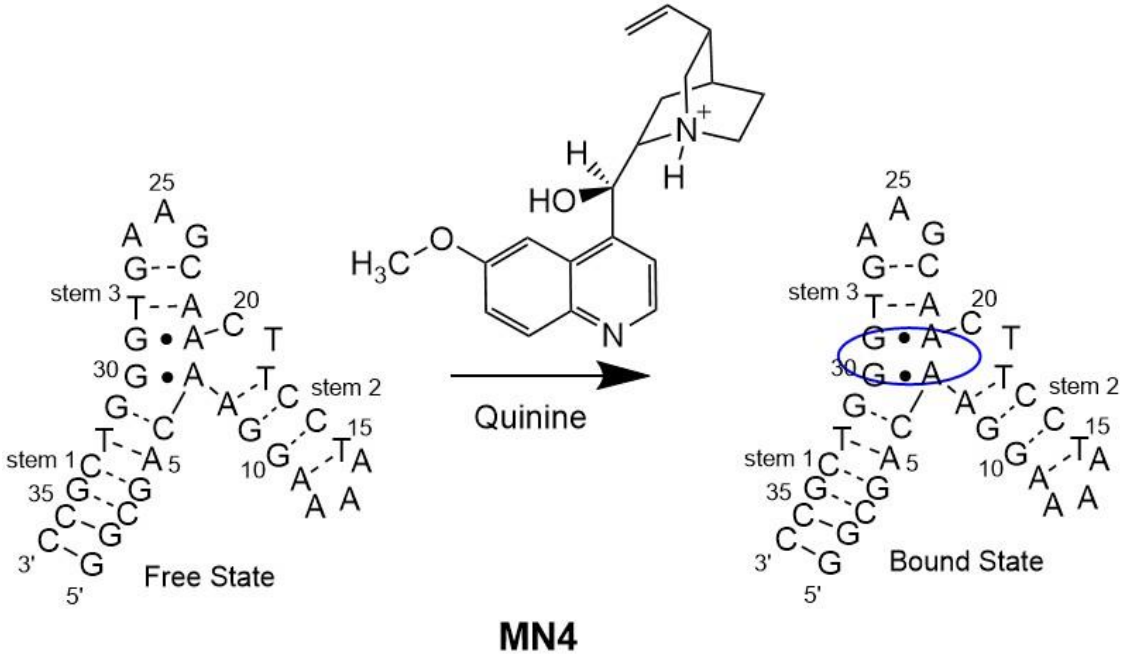

Figure 5. Binding mechanism of the MN4 aptamer. In the free state, the aptamer has a preformed structure. Upon ligand binding, there is no change in its structure. The blue oval represents quinine which binds at the ligand-binding site. Dashed lines represent Watson-Crick base-pairs and black dots represent non-Watson-Crick base-pairs on the secondary structure of the aptamer in the free and bound states.

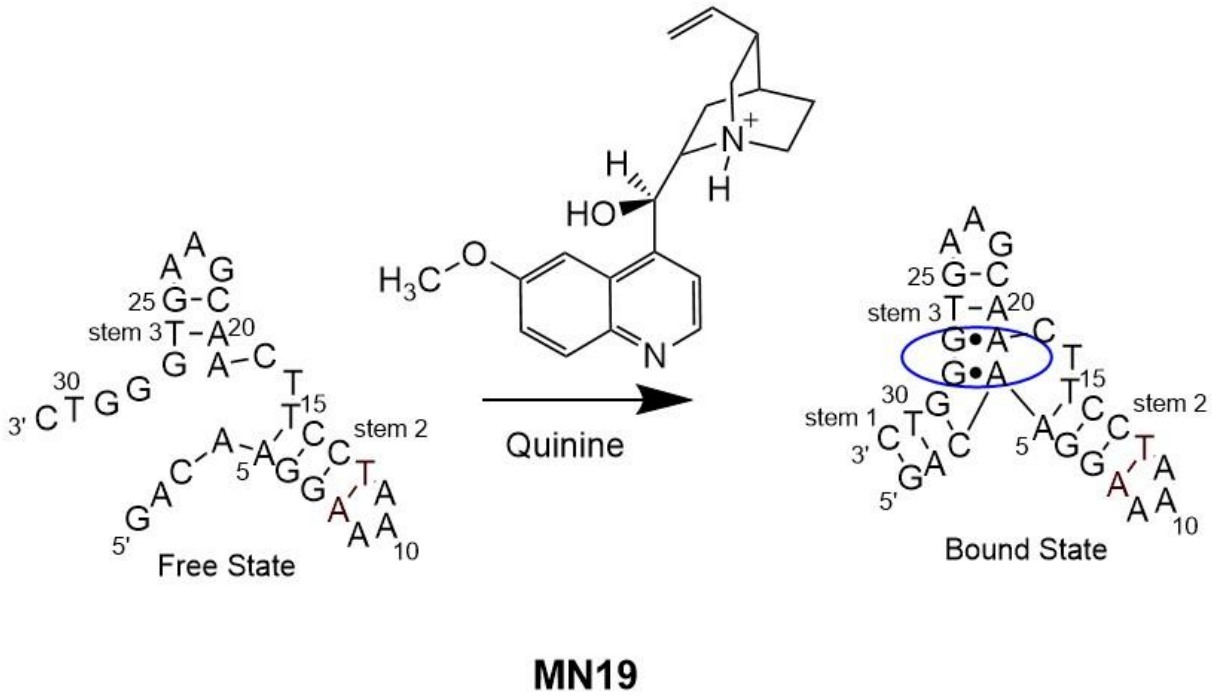

Figure 6. Binding mechanism of the MN19 aptamer. In the free state, the aptamer is loosely folded or unfolded. Upon ligand binding, the stem 1 forms to have a rigidified structure of the aptamer. The blue oval represents quinine which binds at the ligand-binding site. Dashed lines represent Watson-Crick base-pairs and black dots represent non-Watson-Crick base-pairs on the secondary structure of the aptamer in the free and bound states.

Aptamer Applications

The application of aptamers as therapeutic or diagnostic agents in environmental or clinical settings has been discussed by Yang Zhang *et al*. This includes monitoring food safety, environmental contamination, cancer detection and recognition of stem cell markers.[17] Aptamers are capable of monitoring and reducing environmental pollutants and the illnesses associated with them. Some pollutants include antibiotics, heavy metals, toxins, and pathogens which can affect the nervous, endocrine and reproductive systems.[17] Antibiotics that are administered to farm animals can build up in their tissues and can be transmitted to humans during the consumption of said animal. To tackle this problem, aptamers have been created to target antibiotics such as chloramphenicol and tetracycline.[17]

The development of timely and reliable aptamers for cancer diagnosis and treatment is also important. Wu *et al.* have developed a truncated DNA aptamer referred to as XQ-2d which was selected for pancreatic ductal adenocarcinoma (PDAC) with high affinity and specificity.[18] The aptamer specifically binds to PL45 cells with a binding affinity in the nanomolar range. This

was determined by the aptamer's ability to recognize PL45 tumour cells in mice. The aptamer also demonstrates an improved recognition ratio for 40 tissue sections of clinical PDAC samples when compared to the library initially started with in cell-SELEX selection.[18] This shows how this aptamer can be a potential candidate that can aid in the diagnosis and treatment of PDAC.

Aptamers also have been employed for the recognition of stem cell markers. Some comprehensive studies have been done which have identified several cell surface molecules on embryonic stem cells.[19] Some molecules are significant as they help characterize cellular phenotypes and help regulate the differentiation state. Aptamers have been isolated that can differentiate between mouse embryonic cells from differentiated mouse cell lines and monitor the differentiation process of these stem cells.[19] Thus, these aptamers can be promising for the development of molecular probes.

Electrochemical aptamer-based (E-AB) biosensors are another promising application of aptamers. They can be used to monitor molecules directly in undiluted complex matrices, such as plasma, serum and other bodily fluids, and in the body with efforts of overcoming barriers in personalized medicine.[20] The E-AB sensing platform depends on a redox-reporter, methylene blue, which is modified onto an aptamer that is then attached to a gold electrode surface through thiol chemistry. The electrochemical signal produced from this platform occurs from the aptamer undergoing a conformational change when ligand binding occurs, moving methylene blue closer to the electrode surface and therefore, altering its electron transfer rates. However, it was found that with the MN19 aptamer, the signal generated from this platform relies on a redox-reporter-ligand competition mechanism.[20] As seen in Figure 7, methylene blue is covalently attached to MN19 on its 3' end and it binds at or near the ligand binding site on the aptamer. This results in a folded conformation of the aptamer. When cocaine is added, it competes with the bound methylene blue and displaces it from the binding site, changing its distance from the electrode surface and therefore, altering its electron transfer rates (Figure 7).

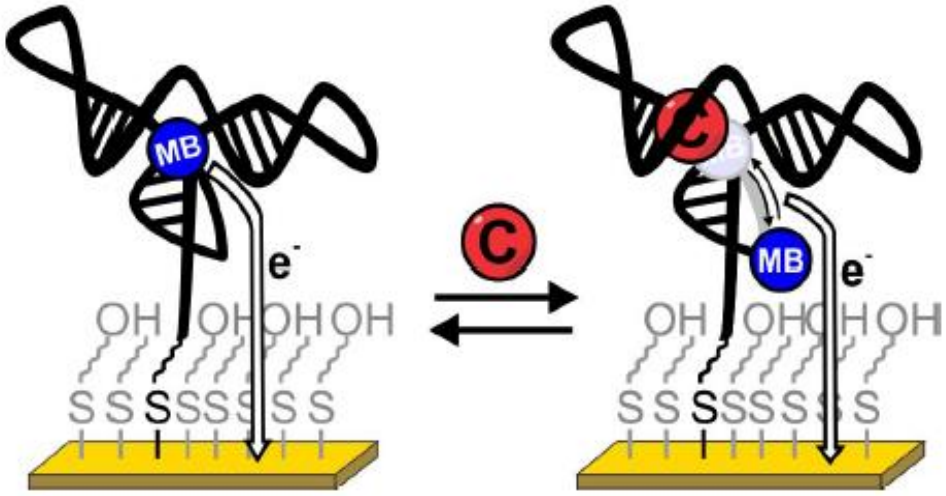

Figure 7. Schematic representation of the E-AB biosensing platform. Reprinted with permission from Dauphin-Ducharme, P.; Churcher, Z.R.; Shoara, A.A.; Rabarimehr, E.; Slavkovic, S.; Fontaine, N.; Boisvert, O.; Johnson, P.E. Redox Reporter - Ligand Competition to Support Signaling in the Cocaine-Binding Electrochemical Aptamer-Based Biosensor. *Chemistry*. **2023**, *29*(35), e202300618. DOI:10.1002/chem.202300618. Copyright 2023 Wiley-VCH.

Given the specific applications, it is important to highlight the properties of aptamers that offer advantages over antibodies and makes them more suitable for the mentioned applications. Aptamers are easily produced in a time and cost-efficient process, and they are generally more stable when compared to antibodies.[21] Aptamers also can be produced without the requirement of an immune response. Since aptamers are chemically synthesized, they are easy to modify at any position of the nucleotide chain. Even though antibodies can also be chemically modified, targeted modifications are difficult to perform.[21] Aptamers can also be selected for targets that antibodies cannot be selected for. For example, aptamers can be selected against toxic compounds that can kill an animal during the antibody production against the compound. Aptamers are also considered more thermally stable, as they can be easily restored back to their original state after unfolding at high temperatures and be repeatedly used. Lastly, aptamers are smaller in size, enhancing their ability for transport and tissue penetration but also makes them easy to filter out the renal system.[21]

Nevertheless, understanding how aptamers function during binding interactions is important. By learning about how they function, it can provide insight if modifications can be made to optimize their binding abilities with their target. There are a wide range of techniques

that have been used to study these aptamer-target binding interactions such as gel and capillary electrophoresis, ultraviolet-visible (UV-Vis) absorption, circular dichroism, surface plasmon resonance, nuclear magnetic resonance (NMR), isothermal titration calorimetry (ITC) and fluorescence spectrometry.[22]

Isothermal Titration Calorimetry

Isothermal Titration Calorimetry (ITC) is a technique used to study the thermodynamic properties of aptamer-ligand interactions. ITC can be performed under different solution conditions, and it also has the benefit of being a non-destructive label-free technique.[23] Some properties that this technique provides us with are the stoichiometry of an interaction (n), equilibrium binding constants (K_a or K_d), enthalpy (ΔH) and entropy (ΔS). Figure 8A shows that in a typical ITC instrument, there are two cells placed in an adiabatic jacket where one cell is a reference cell and the other is a sample cell, where the aptamer is loaded.[23] During an experiment, these two cells are maintained at a constant temperature. Ligand is loaded into a syringe which is then titrated into the sample cell in known aliquots. As ligand is gradually titrated into the aptamer, binding occurs as seen in Figure 8B. As a result of an exothermic binding event, the temperature of the sample cell increases when ligand is added. Because of this, the power being supplied to the heater surrounding the sample cell decreases to decrease the temperature of the sample cell and have it isothermal with the reference cell. This leads to obtaining exothermic peaks in the raw experimental data where each peak corresponds to a ligand injection as seen in Figure 8C.[23] Positive peaks would be observed for an endothermic binding event. Many injections are performed and when the ligand binding sites on the aptamer become saturated, there will be a gradual decrease in the size of the peaks observed in the raw data until only heats of dilution of ligand are observed. Integration is performed on the power supplied per unit time to obtain the heat per mole of injectant in reference to the molar ratio.[23] Data fitting is then done on the integrated thermogram to obtain the thermodynamic parameters of the aptamer-ligand interaction such as binding affinity (K_a), enthalpy (ΔH), and stoichiometry (n). The sigmoidal-shaped curve in Figure 8C indicates that binding occurs between the cocaine-binding aptamer and its target ligand.

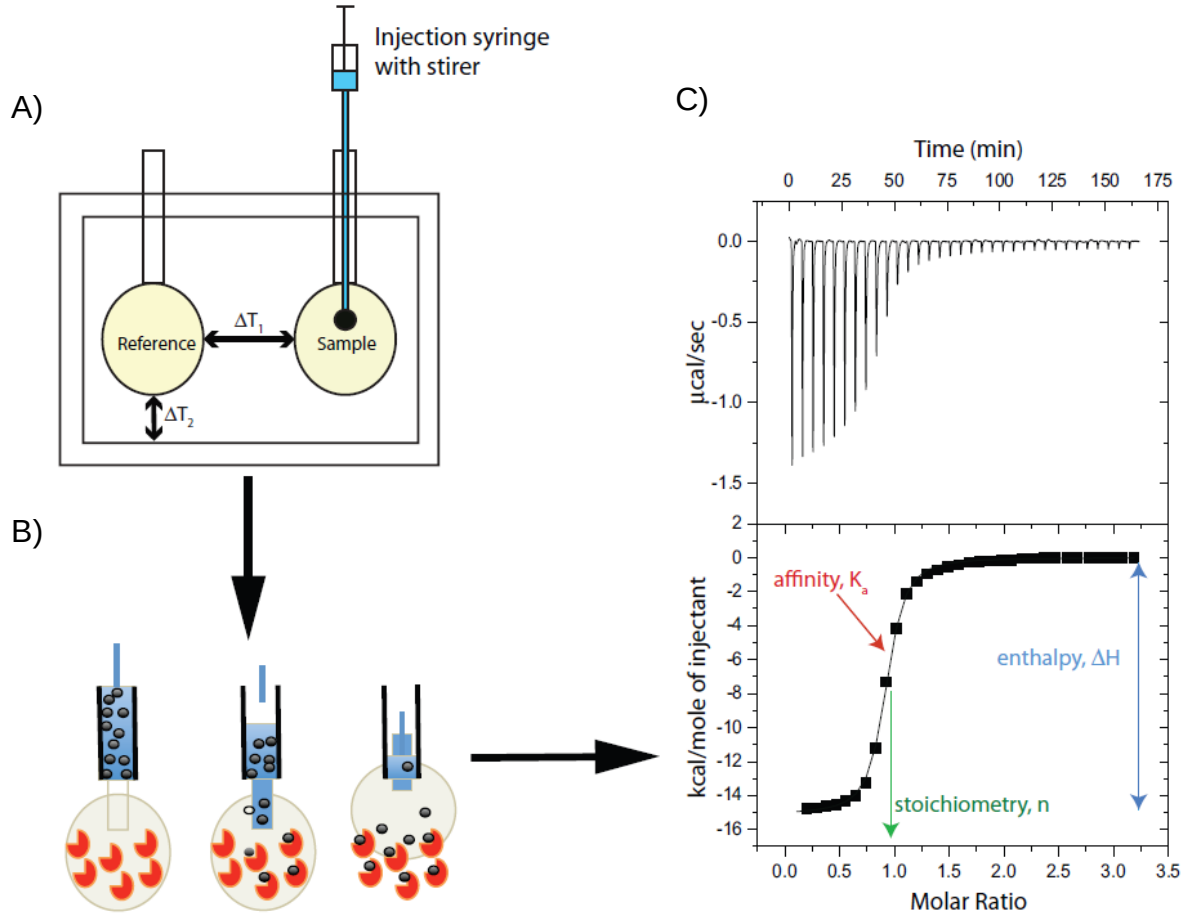

Figure 8. Diagram of an ITC instrument. A) The temperature difference between the sample cell and the reference cell is represented by ΔT_1. ΔT_2 represents the temperature difference between the cell and the adiabatic jacket. These two values are supposed to be zero during an experiment. B) Illustration of binding occurring as the ligand is gradually injected into the ITC cell that contains the aptamer. C) An ITC thermogram showing the interaction occurring between the cocaine-binding aptamer and its corresponding target ligand. It provides thermodynamic binding parameters such as binding affinity (K_a), enthalpy (ΔH), and stoichiometry (n). (Figure taken from reference 23)

Fluorescence Spectrometry

Fluorescence spectrometry is a sensitive technique that helps us understand aptamer-small molecule interactions. The basis of this technique is the emission of photons from a substance following excitation from light absorption.[24] These molecules emit lower energies of light (longer wavelengths) compared to the absorbed light due to vibrational energy levels. This process is called the Stokes' shift and is caused by a loss of energy in radioactive decay. This can be illustrated in a Jablonski diagram seen in Figure 9. A molecule is first seen at the ground state (S_0) and when it can absorb a photon of sufficient energy, an electron moves to singlet excited states (S_1 or S_2) of higher energy, where it contains energy equal to the absorbed photon.[24]

Photoluminescence is used to describe the process when an electron emits a photon when going through relaxation to return to the ground state. There are two types of photoluminescence: fluorescence and phosphorescence.[24] When an electron returns to the ground state from a singlet excited state, it emits energy in the form of photons which is referred to as fluorescence (Figure 9). The decay time is from the order of 10^{-10} s to 10^{-7} s. Phosphorescence is when an electron transitions from the singlet excited state to a triplet state (T_1) through intersystem crossing and then returns to the ground state. Because of a change in the electron spin, the phosphorescence time can be from 10^{-6} s to seconds.[24]

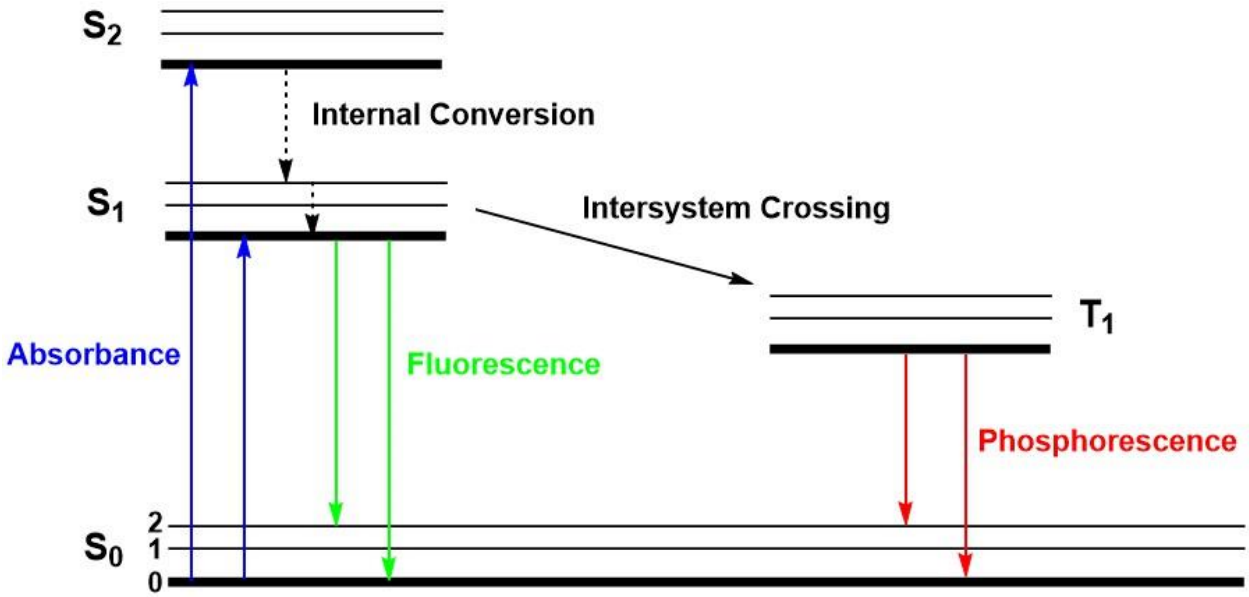

Figure 9. Schematic representation of the Jablonski Diagram.

The fluorescence of a sample is measured using a fluorescence spectrometer. Figure 10 shows a diagram of a typical fluorescence spectrometer. This instrument involves a sample cell that is excited by a xenon lamp at a known excitation wavelength, where the excitation incident light (λ_{ex}) passes through an excitation slit.[25] The fluorescence emissions are measured at 90° even though emissions from the sample are emitted in every direction. Polarizers can be used when the measurement of polarized fluorescence is of interest. Fluorescence emissions (λ_{em}) are detected and measured using the detector. Fluorescence intensities are then recorded from the generated spectrum (Figure 10). There are two types of fluorescence when it comes to aptamer-ligand binding studies: intrinsic and extrinsic. Extrinsic fluorescence involves the addition of a

fluorescent or quencher label to an aptamer which may affect its structure.[25] Intrinsic fluorescence is when a ligand has inherent fluorescent properties which can allow us to analyze the binding interaction between aptamer and ligand. One common method is to observe if there is ligand fluorescence quenching which can allow us to quantify the binding affinity of the aptamer for its ligand. A limitation of this technique is that the ligand chosen for a study must be intrinsically fluorescent.[25] This means that only ligands that naturally emit fluorescence can be used in this study, limiting the choice of ligands to those with inherent fluorescence.

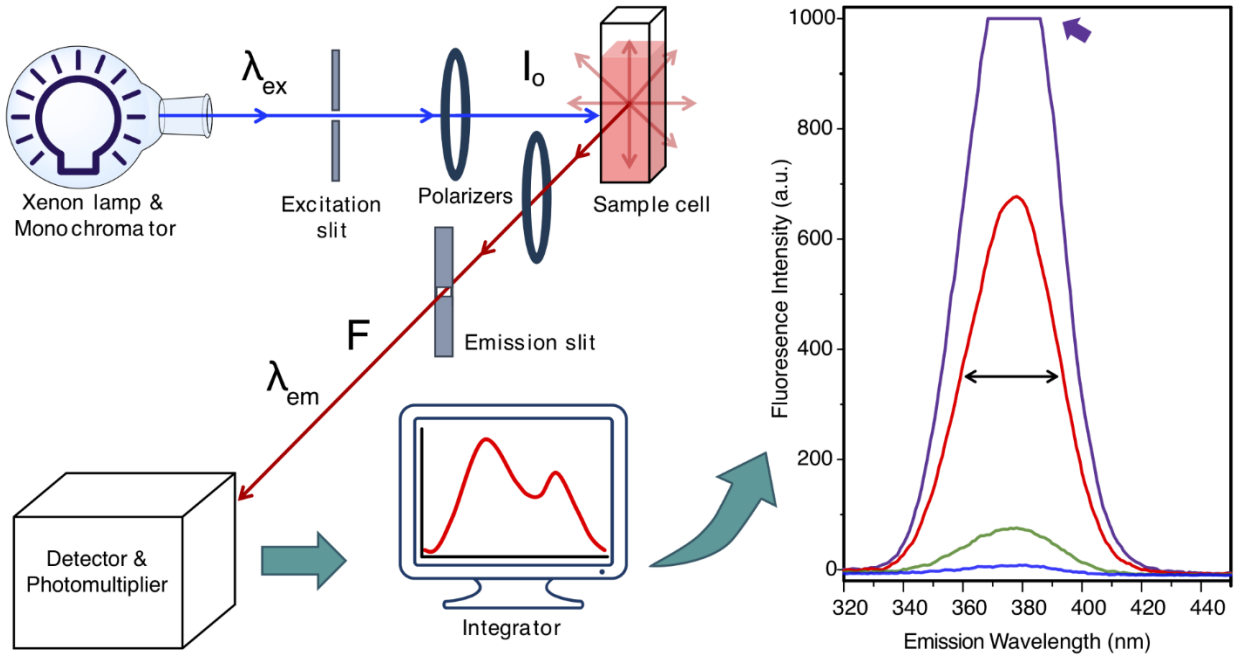

Figure 10. Diagram of a fluorescence spectrometer. Going from left to right, a sample cell is excited by a xenon lamp at a known excitation wavelength (λ_{ex}, blue line). The excitation incident light (I_o) passes through an excitation slit. The fluorescence emission (λ_{em}, red line) is measured at 90°even though emissions from the sample are emitted in every direction (F). A polarizer is utilized when polarized fluorescence is measured. The spectra on the right shows how detected emission photons are multiplied and integrated in relation to received emission wavelengths. (Figure taken from reference 25)

Nuclear Magnetic Resonance Spectroscopy

Nuclear Magnetic Resonance (NMR) spectroscopy is a method that can be employed to determine the three-dimensional structure of an aptamer both in the free state and ligand-bound state. In addition, NMR spectroscopy can be used to reveal the location of ligand-binding sites on an aptamer, investigate structural changes in an aptamer or its regions upon ligand binding and to assess dynamics and stability of an aptamer.[26] In solution state NMR spectroscopy, the sample of interest is subjected to a strong magnetic field, allowing nuclei such as ^{1}H, ^{13}C, ^{15}N,

and ^{31}P to have a magnetic spin number ½. Nuclei will emit resonance signals at specific frequencies which vary based on their chemical composition and surrounding molecular environment. Furthermore, NMR is viewed as a non-destructive method that enables several experiments to be carried out on the same sample across different conditions. This can include temperature, ligand concentration and buffer conditions.[26] Nevertheless, by tracing peaks of imino protons in 1D ^{1}H experiments, information about ligand binding and aptamer stability can be obtained. Imino protons are valuable because their signals are found downfield at higher ppm values, such as seen in Figure 11, which are distinctly isolated from signals of other protons that are found in nucleic acids. Imino proton signals generally only appear when they are involved in hydrogen bonds such as seen in base-pairing. The position of these signals on an NMR spectrum depends on its chemical identity and surrounding environment.[26] Imino protons can be found in both Watson-Crick and Non-Watson-Crick base-pairs. The signals from Watson-Crick base-pairs are the most downfield where they appear around 12-14 ppm. Guanine imino proton signals appear around 12-13 ppm and thymine or uracil imino proton signals appear around 13-14 ppm. Non-Watson-Crick base-pairs generally appear upfield of the signals from the Watson-Crick base-pairs around 10-12 ppm. Information such as structural elements of an aptamer both in the free and bound state can be obtained from an NMR spectrum after assignment of the imino resonances. Structures can include but are not limited to loops, stem lengths, and bulges. Assignments of peaks to individual bases can be done by analyzing a 2D NOESY experiment.[26]

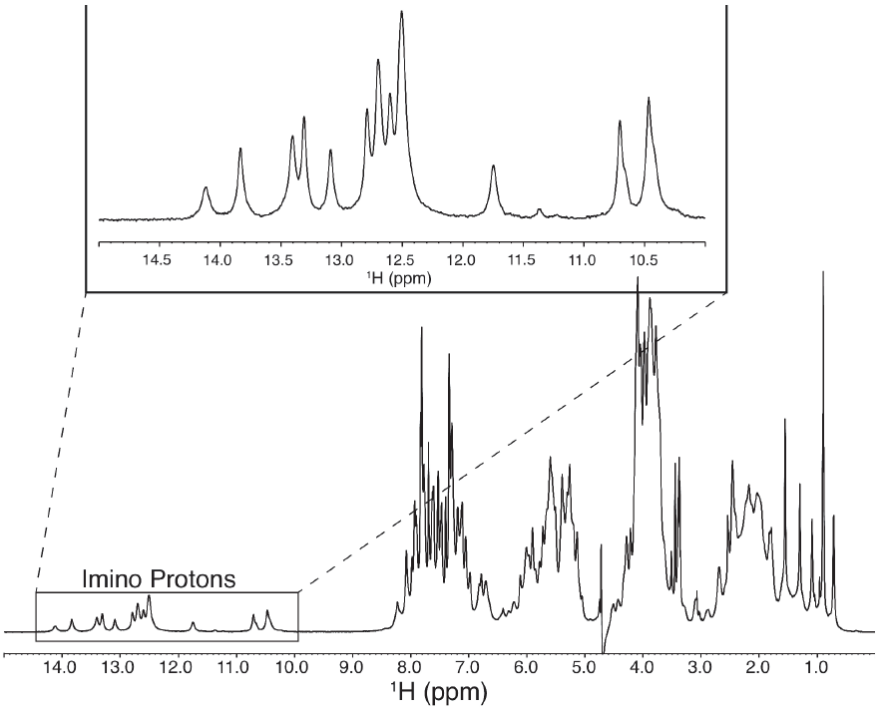

Figure 11. 1D ^{1}H-NMR spectrum of cocaine titrated into the cocaine-binding aptamer. The inset highlights the region that emphasizes the imino proton signals. The spectrum shows that cocaine is bound with the cocaine-binding aptamer. (Figure taken from reference 26)

Thesis Project

Previous work in the Johnson lab has investigated non-structure-switching aptamers as a function of NaCl concentration, such as with MN4, and have observed that as NaCl concentration is increased, the binding affinity of the aptamer for its ligand, quinine, decreases. However, binding studies have yet to be done with structure-switching aptamers as a function of NaCl concentration. The goal of this project is to analyze if this relationship is consistent and observe if structure-switching aptamers have a parallel relationship with non-structure-switching aptamers as a function of NaCl concentration. One assumption is that at low NaCl concentrations, binding affinity is favored because reduced shielding of charges would allow electrostatic interactions between the aptamer and ligand to occur more effectively. Also, at high NaCl concentrations, folding is favoured because increased shielding of charges would enhance aptamer folding upon ligand binding. Therefore, we would want to see how these two forces balance out each other during this study. The binding interaction between MN19 and quinine was

studied as a function of NaCl concentration, and this project was accomplished using isothermal titration calorimetry.

In E-AB biosensors, it was discussed that with MN19, the platform relies on a redox-reporter-ligand competition mechanism where methylene blue binds to the aptamer and then gets displaced upon the addition of ligand. The goal of this project is to see if other aptamers bind methylene blue and if so, measure the binding affinity to quantify the binding. Additionally, investigating other aptamers that bind to methylene blue can provide insight on any similarities between structural motifs. This can help one understand what is required for the aptamer to bind effectively to methylene blue. This part of the project was accomplished using fluorescence spectrometry.

Chapter 2. Analyzing the Binding Affinity of Structure-Switching Aptamers as a Function of NaCl Concentration Using Isothermal Titration Calorimetry

Introduction

Many intermolecular forces contribute to the aptamer and target binding such as Van der Waals, hydrogen bonding and electrostatic interactions.[27] The focus of this project was to examine the contribution of electrostatic forces towards aptamer and ligand binding. High ion concentrations produce a shielding effect between charged molecules present in solution. This effect was investigated by altering the NaCl content and tracking the changes in binding affinity. The high salt content would be expected to disrupt the electrostatic interaction between the phosphate backbone on the aptamer and the ligand. A study done by Hianik *et al.* has shown that increasing NaCl concentrations weakened binding between aptamers and thrombin and that this was likely because of the shielding effect of the Na^+ ions.[28] Another study done by Schmidt *et al.* which also involved multiple aptamers has shown that the binding got weaker for all aptamers toward their target when NaCl concentrations were increased.[29] In a study done by Reinstein *et al.*, they concluded that the affinity of MN4, a variant of the cocaine-binding aptamer, for quinine, increases when NaCl concentration decreases.[15] The reason why quinine was chosen as the ligand instead of cocaine is because it was identified that the cocaine-binding aptamer binds quinine approximately 30-fold tighter. Thus, since the function of non-structure-switching aptamers has been studied under changing NaCl concentrations, binding studies were done with structure-switching aptamers chosen for my research to see if this relationship is consistent.

Structure-switching aptamers are unfolded or loosely folded when in the free-state and only become fully structured when bound to their corresponding target ligand.[13,16] With structure-switching aptamers, it can be anticipated that at low NaCl concentrations, binding affinity is favoured as there is less shielding of charges, allowing electrostatic interactions to take place. At high NaCl concentrations, folding should be favoured as high shielding of charges would occur due to the high ion content, allowing the aptamer to fold more easily by overcoming repulsion between like charges.

Therefore, the long-term objective of this project is to see how these two factors balance each other out in structure-switching aptamers binding their ligand as a function of NaCl concentration. This long-term objective was achieved alongside various short-term objectives. One of the short-term objectives was to analyze the binding affinity of the MN19 aptamer when binding quinine under NaCl concentrations of 140 mM-2000 mM. MN19 is another variant of the cocaine-binding aptamer, and it differs from MN4 because it's 3 base-pairs shorter in its stem 1 and as a result is loosely folded in the free state (Figure 6).[16] One of our previous lab members has conducted unpublished studies using the DaMut3 aptamer, a structure-switching aptamer, binding dopamine. The aptamer has a high affinity for dopamine at a NaCl concentration of 10 mM. When the NaCl concentration is increased to 31.6 mM, the affinity of DaMut3 for dopamine decreases. However, when the NaCl concentration is increased up until 1000 mM, the binding affinity starts increasing again as seen in Figure 13. The reasoning behind this may be that at low NaCl concentrations, binding affinity is favoured because reduced shielding of charges allows the aptamer to bind dopamine more effectively through electrostatic interactions. At high NaCl concentrations, folding of the aptamer is favoured upon the binding of dopamine because increased shielding of charges reduces repulsion between like charges, facilitating the folding process. Charges on the aptamer phosphate backbone are expected to be shielded, allowing the aptamer to come together and folding to be favoured. This is why we can see high binding affinities at the lowest and highest NaCl concentrations. Thus, we aim to observe if there is a similar relationship with the MN19 aptamer when binding quinine at varying NaCl concentrations.

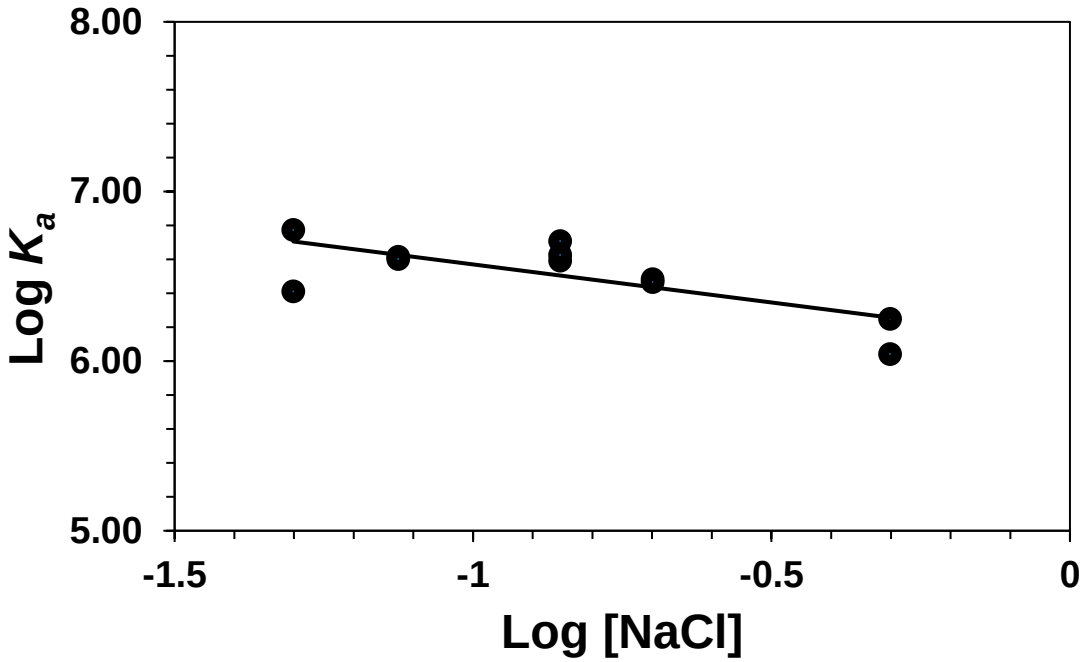

Figure 12. Plot of Log K_a vs. Log [NaCl] for the MN4 aptamer binding quinine under NaCl concentrations of 50 mM to 500 mM. The data was collected through isothermal titration calorimetry. The graph indicates that when NaCl concentration is increased, the binding affinity of the MN4 aptamer for quinine decreases. The data was collected by Reinstein *et al.*

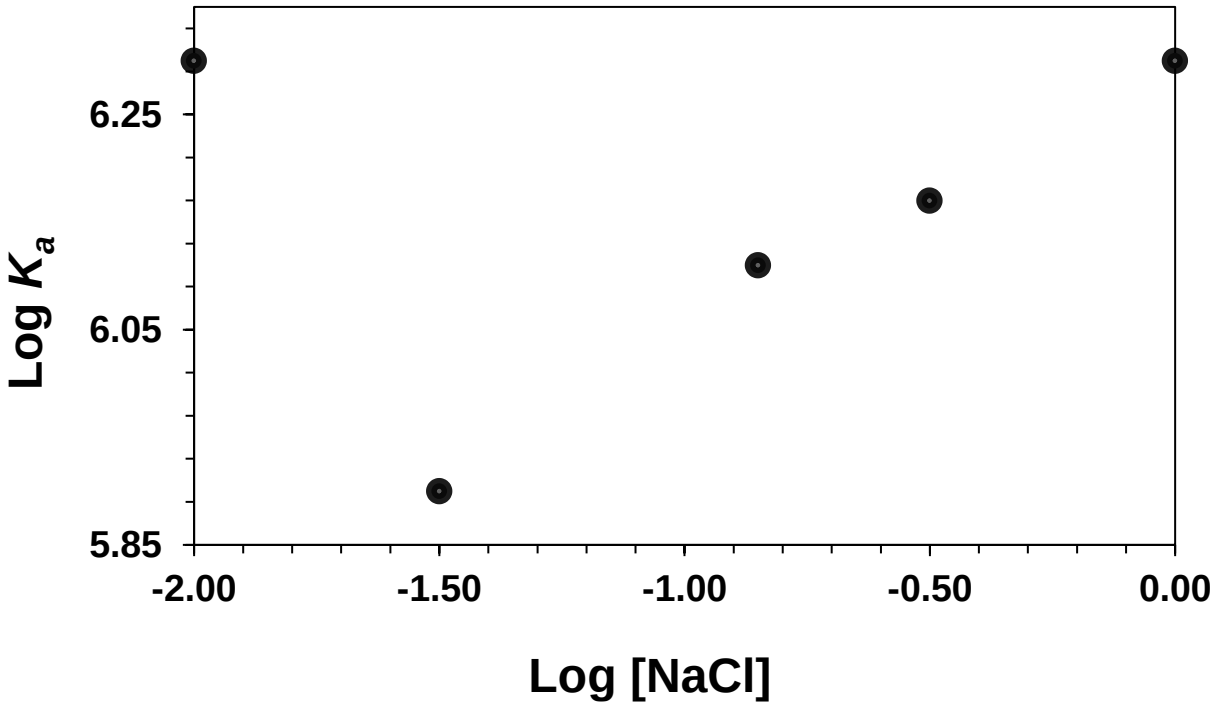

Figure 13. Plot of Log K_a vs. Log [NaCl] for the DaMut3 aptamer binding dopamine under NaCl concentrations of 10 mM to 1000 mM. The data was collected through isothermal titration calorimetry. The graph indicates that the DaMut3 aptamer has a high binding affinity for dopamine at 10 mM NaCl. When NaCl concentration is increased to 31.6 mM, the binding affinity of the aptamer for dopamine decreases. As the NaCl concentration is increased up until 1000 mM, the binding affinity starts increasing again. The data was collected by Matthew Bowman.

Materials and Methods

Materials

Quinine was obtained from Sigma Aldrich and salts and buffer reagents were obtained from BioShop. MN19 was obtained from Integrated DNA Technologies (IDT), which came as a lyophilized powder.

Aptamer Preparation

MN19 samples were first dissolved in Milli-Q water. In a 5 mL, 3 kDa concentrator, the samples were then exchanged three times against 1 M NaCl solution and six times against Milli-Q water. This was done to remove any leftover products from the synthesis process. The concentrations of the aptamers were determined using a Cary Varian UV-Vis spectrometer at an optical density (OD) reading of a wavelength of 260 nm with the corresponding extinction coefficient provided by IDT, 304 200 M^{-1} cm^{-1}.

Ligand Preparation

Quinine samples were dissolved in buffers used for experiments. The concentration of quinine was measured using a Cary Varian UV-Vis spectrometer at an OD reading of a wavelength of 331 nm with the corresponding extinction coefficient, 4244 M^{-1} cm^{-1}.

ITC Experiments

Firstly, aptamer and ligand samples were prepared in Phosphate-Buffered Saline (PBS) buffer (X mM NaCl, 10 mM $Na_xH_yPO_4$ buffer, pH of 7.4) where X represents varying concentrations of NaCl. Aptamer samples were prepared at a concentration of 0.04 mM and ligand samples were prepared at a concentration of 0.624 mM. Heating and cooling of the aptamer was also performed to achieve fast annealing by placing it in boiling water for 1 minute and then placing it on ice for 5 minutes; this was done to favour intramolecular folding. Samples were loaded into the MicroCal VP-ITC instrument, with the aptamer being placed in the sample cell, and ligand being placed in the syringe. All ITC experiments were conducted at 20 ℃ where the experiments were set to 35 injections of 8 µL spaced every 300 s. The first injection was set to 2 µL to account for diffusion from the syringe during equilibration.

Data processing and analysis was then performed on the thermogram generated by the Origin 5.0 Software. Manual integration was done, and the heat of dilution was corrected so that the data can be fit to an appropriate binding model. The fitted thermogram provides us with the stoichiometry of the interaction (n), enthalpy (ΔH) and entropy (ΔS). Most importantly, equilibrium binding constants K_a or K_d are given, which represents the binding affinity. Using K_a values obtained for the binding interaction done at each NaCl concentration, the log of the K_a values can be taken and plotted against the log of the NaCl concentration. The slope obtained from the line of best fit would give the value of $-Z\varphi$, where Z represents the apparent charge on the bound ligand and φ represents the fraction of Na^+ bound per nucleic acid phosphate.[15] This value can be used to determine the contribution of electrostatics to the free energy of binding by inputting it into Equation 1:

Contribution of Electrostatics to the Free Energy of Binding

$$\Delta G_{elec} = Z\varphi RT \ln [Na^+] \quad (1)$$

Where ΔG_{elec} is the contribution of electrostatics to the free energy of binding, Na^+ is the NaCl concentration of 140 mM NaCl, T is the temperature measured in Kelvin and R is the ideal gas constant.

Knowing the binding affinity of the aptamer for its ligand at 140 mM NaCl, the overall binding free energy can be determined with Equation 2:

Overall Binding Free Energy

$$\Delta G = RT \ln [K_d] \quad (2)$$

Where ΔG is the overall binding free energy, R is the ideal gas constant, T is the temperature measured in Kelvin and K_d is the binding affinity.

Using the contribution of electrostatics to the free energy of binding and the overall binding free energy, the representation for the contribution of electrostatics of the overall free energy of the aptamer binding its ligand at 140 mM NaCl can be determined.[15] Therefore, it can be identified whether altering NaCl concentration has an impact on the binding affinity of each structure-switching aptamer with its ligand.

Results and Discussion

Data was collected and processed through isothermal titration calorimetry for MN19 binding quinine under NaCl concentrations of 140 mM to 1000 mM. Unfortunately, experiments using NaCl concentrations of less than 140 mM were not included apart of the study. This is because of the two-site binding observed with MN19 binding quinine as seen in Figure 14 with 50 mM NaCl.[14] This prevents the analysis of the binding affinity of the aptamer at lower NaCl concentrations. Having the experimental model to be consistent is important and if our model suddenly develops two-site binding, it would be much more difficult to compare those data points with data points collected at NaCl concentrations where the aptamer has one-site binding. This can lead to bias in the results as lower NaCl concentrations would not be included apart of the study. Therefore, it is crucial to work with structure-switching aptamers that do not have two-site binding at specific NaCl concentrations.

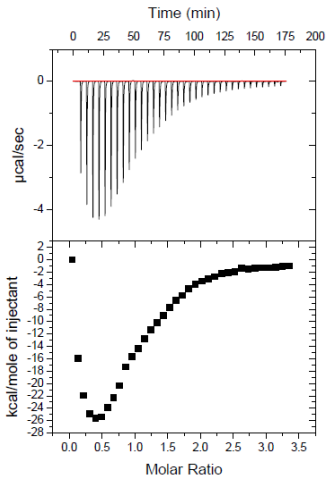

Figure 14. Representative ITC Thermogram showing the interaction of 0.04 mM of MN19 with 0.624 mM of quinine at a NaCl concentration of 50 mM. The thermogram indicates that two-site binding occurs for MN19 binding quinine at this NaCl concentration.

A plot was then made of log K_a vs. log [NaCl], and it showed the trend of the binding affinity of the MN19 aptamer for quinine at varying NaCl concentrations (Figure 16). The results suggested that the affinity of the aptamer for its ligand decreases when increasing the concentrations of NaCl. The Na^+ ions may be shielding the charges that are involved in electrostatic interactions between the aptamer and ligand. Therefore, by increasing the NaCl content in the solution where the binding interaction takes place, more shielding occurs and disrupts the electrostatic interactions. By disrupting these interactions, the binding affinity of the aptamer for the ligand becomes weaker.

This can also be compared to the results seen with the MN4 aptamer (Figure 17). The enthalpy for MN4 binding quinine was determined for a range of NaCl concentrations from 50 to 500 mM. As mentioned before, as NaCl concentration decreased, the binding affinity of the aptamer for quinine increased. A similar trend was observed with MN19 binding quinine which shows that there may be a parallel relationship between non-structure-switching and structure-switching aptamers when studied as a function of NaCl concentration.

The contribution of electrostatic interactions seems to be less for MN19 binding quinine than for MN4 binding quinine at 140 mM NaCl. From the plot of log K_a vs. log [NaCl] for MN4 binding quinine seen in Figure 12, the slope gives the value of $-Z\varphi$. This value was determined to be -0.45. This can then be inputted into the equation $\Delta G_{elec} = Z\varphi RT \ln [Na^+]$ to give the

contribution of electrostatics to the free energy of binding. This value for MN4 binding quinine was −0.51 kcal/mol at 140 mM NaCl. With the determined binding affinity of MN4 binding quinine at 140 mM NaCl, 0.23 μM, the overall binding free energy can then be determined which is -8.90 kcal/mol. These values show the contribution of electrostatics represents 6 % of the overall free energy of MN4 binding quinine at 140 mM NaCl.

The slope obtained from the plot of log K_a vs. log [NaCl] for MN19 binding quinine gives a value of -0.10 (Figure 16). Using this value, the contribution of electrostatics for the free energy of binding was calculated as -0.11 kcal/mol at 140 mM NaCl. With the binding affinity obtained for MN19 binding quinine at 140 mM NaCl, 3.47 μM, the overall free energy was determined to be -7.32 kcal/mol. This shows that the contribution of electrostatics represents 1.50 % of MN19 binding quinine at 140 mM NaCl. Therefore, we see that the contribution of electrostatics is less for MN19 binding quinine than MN4 binding quinine at 140 mM NaCl.

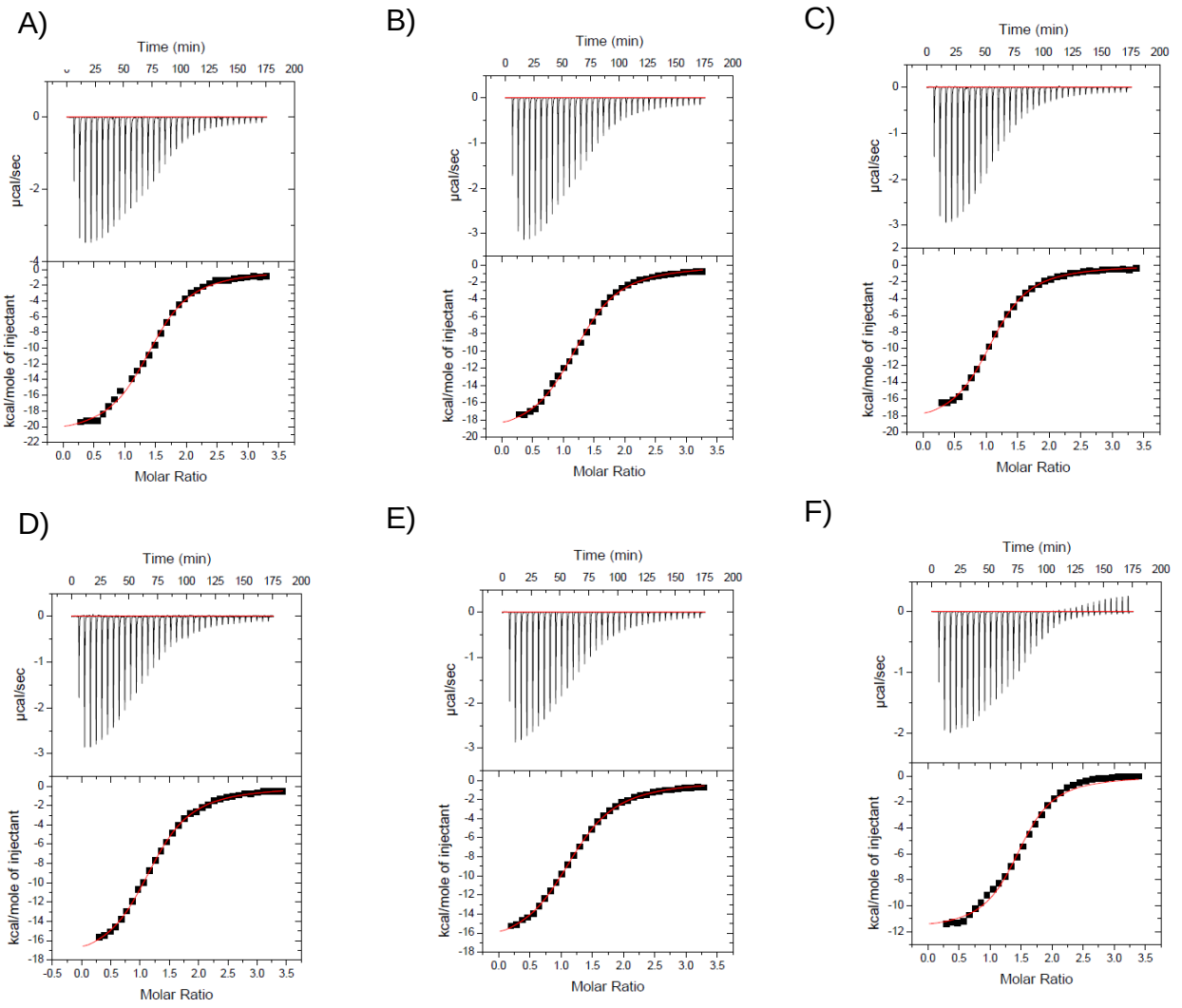

Figure 15. Representative ITC Thermograms showing the interaction of 0.04 mM of MN19 with 0.624 mM of quinine at a NaCl concentration of A) 140 mM, B) 250 mM, C) 355 mM, D) 500 mM, E) 1000 mM and F) 2000 mM. The sigmoidal curve indicates one-site binding with a K_d of A) 3.47 µM, B) 4.30 µM, C) 3.74 µM, D) 4.87 µM, E) 5.30 µM and F) 2.34 µM.

Table 1. Overall summary of the thermodynamic results of MN19 binding quinine at varying NaCl concentrations with a one-site binding model. The experiments were conducted in X mM NaCl, 10 mM $Na_xH_yPO_4$ buffer at pH 7.4, where X represents the varying concentrations of NaCl at 20°C. The error was determined through standard deviation of data collected from multiple experiments performed at each NaCl concentration. However, for the experiment conducted at 2000 mM NaCl, the error was determined through the fit of the curve as only one experiment was done.

NaCl Concentration (mM)	Number of Experiments	Average K_a (μM^{-1})	Average ΔH (kcal/mol)	Average -TΔS (kcal/mol)
140	3	0.23 ± 0.05	-23 ± 2	16 ± 2
250	2	0.20 ± 0.05	-21 ± 2	14 ± 2
355	3	0.21 ± 0.05	-19.1 ± 0.3	11.9 ± 0.3
500	2	0.18 ± 0.03	-22 ± 5	15 ± 5
1000	2	0.186 ± 0.004	-17.0 ± 0.8	9.9 ± 0.8
2000	1	0.43 ± 0.04	-11.8 ± 0.2	4.3

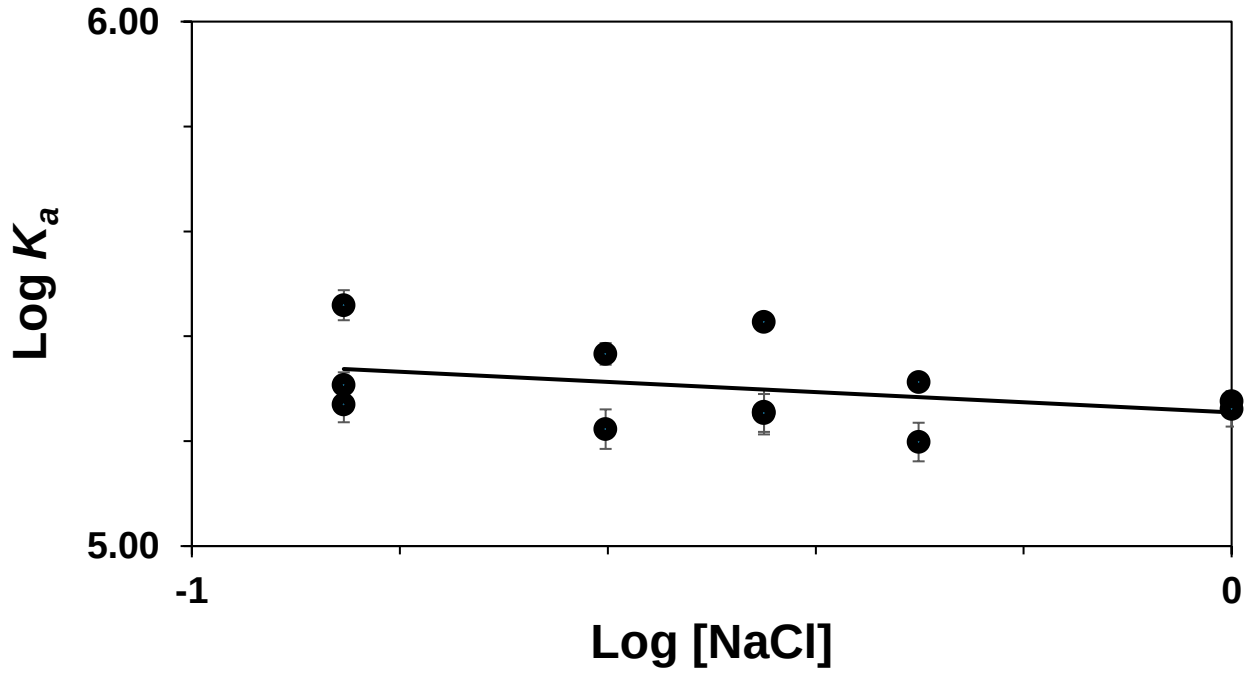

Figure 16. Plot of Log K_a vs. Log [NaCl] for the MN19 aptamer binding quinine under NaCl concentrations of 140 mM to 1000 mM. The data was collected through isothermal titration calorimetry. The graph indicates that the binding affinity of the MN19 aptamer for quinine decreases as the NaCl concentration increases.

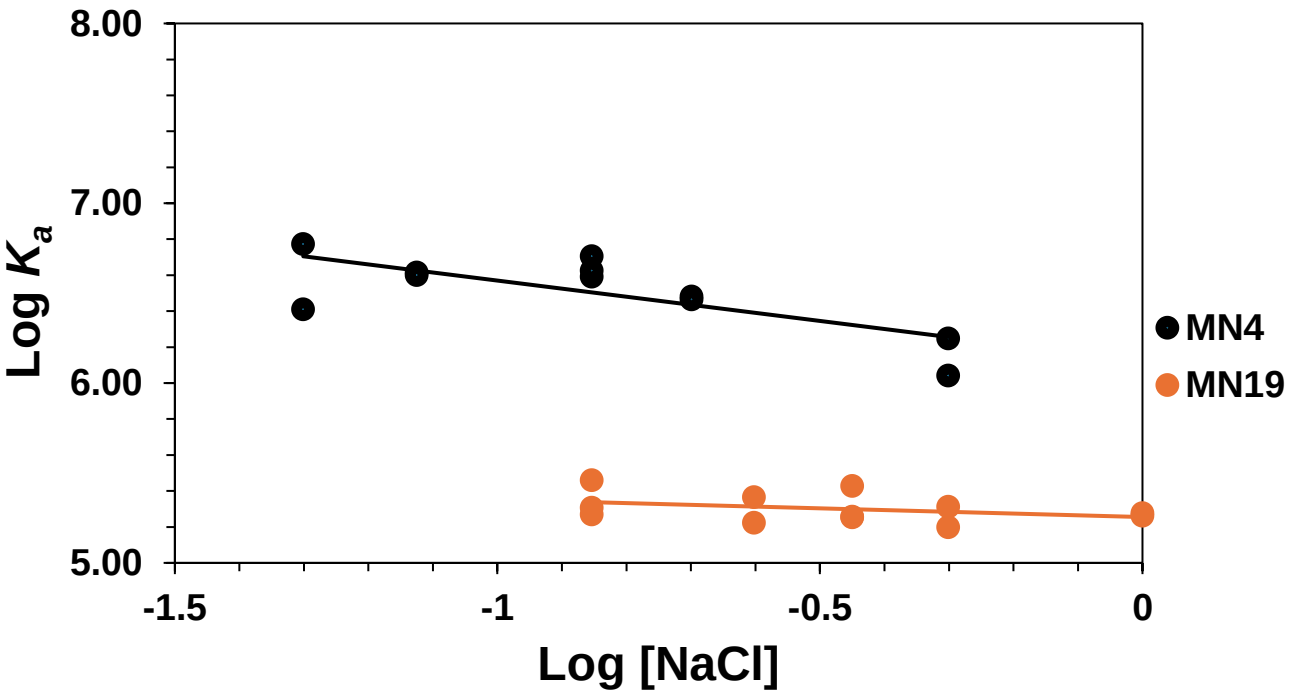

Figure 17. Plot of Log K_a vs. Log [NaCl] comparison for the MN4 aptamer binding quinine under NaCl concentrations of 50 mM to 500 mM and the MN19 aptamer binding quinine under NaCl concentrations of 140 mM to 1000 mM. The data was collected through isothermal titration calorimetry. The graph indicates that there is a smaller decrease in the binding affinity of the MN19 aptamer binding quinine than MN4 binding quinine as NaCl concentration is increased.

Another experiment was conducted for MN19 binding quinine at 2000 mM NaCl. At this concentration, the binding affinity of MN19 for quinine increases again. This behaviour is similar to the one seen with the DaMut3 aptamer when binding dopamine (Figure 13). The affinity decreases from 140 mM NaCl up until 1000 mM NaCl. The binding affinity then starts to increase again when the NaCl concentration is increased to 2000 mM (Figure 18). One explanation for this may be that at higher NaCl concentrations, folding is favoured of the structure-switching aptamer when binding its ligand which may be seen with the MN19 and DaMut3 aptamers and can explain the increase in binding affinity when NaCl concentration is increased. However, only one data point was collected at 2000 mM NaCl when MN19 binds quinine and therefore, more data points are needed to confirm if the binding affinity does increase again when the NaCl concentration increases.

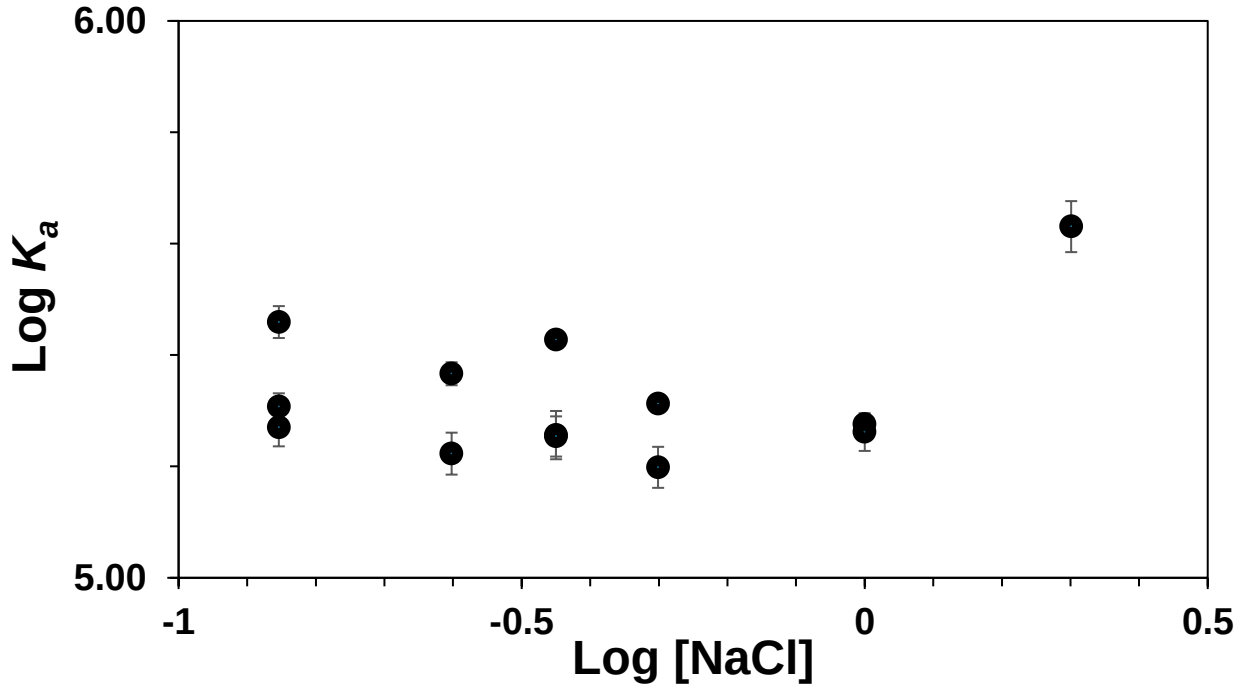

Figure 18. Plot of Log K_a vs. Log [NaCl] for the MN19 aptamer binding quinine under NaCl concentrations of 140 mM to 2000 mM. The data was collected through isothermal titration calorimetry. The graph indicates that the binding affinity of MN19 for quinine decreases up until 1000 mM NaCl. The binding affinity increases again when the NaCl concentration is increased to 2000 mM. However, it should be noted that one data point was only obtained at 2000 mM NaCl with ITC.

Conclusions

It was shown how the overall trend of the binding affinity of MN19 binding quinine decreases when increasing the NaCl concentration from 140 mM to 1000 mM. A similar trend was seen with the MN4 aptamer when binding quinine as the binding affinity decreases when increasing the NaCl concentration from 50 to 500 mM. Experiments for MN19 binding quinine at NaCl concentrations below 140 mM could not be analyzed as the aptamer develops a two-site binding model and we want to keep our study consistent by keeping it to a one-site model to easily compare binding affinities. The contribution of electrostatics at 140 mM NaCl was less for MN19 binding quinine as a value of 1.50 % was determined compared to MN4 binding quinine with a determined value of 6 %. Furthermore, when increasing the NaCl concentration to 2000 mM, the binding affinity increased again. This trend was similar to the one seen with the DaMut3 aptamer when binding dopamine, where the binding affinity starts increasing again when increasing the NaCl concentration from 31.6 mM to 1000 mM. However, since only one

data point was collected, more data points are needed to confirm if the binding affinity of MN19 for quinine increases again at 2000 mM NaCl.

Chapter 3. Characterizing the Interactions of Methylene Blue with Different Aptamers Using Fluorescence Spectrometry

Introduction

When it comes to aptamer applications, E-AB biosensors have become a promising tool for detecting and quantifying targets. This can be in undiluted complex matrices, such as plasma, serum and other bodily fluids, and can be used in the body.[20] The sensing platform involves a redox-reporter, methylene blue, covalently attached to an aptamer which is anchored to a gold electrode surface through thiol chemistry. The electrochemical signal produced from this platform is from a binding-induced conformational change of the aptamer when ligand is added. However, it was found that with the MN19 aptamer, the mechanism of which the signal is generated is due to a redox-reporter-ligand competition.[5] The aptamer undergoes a conformational change because of methylene blue binding at or near the ligand binding site on the MN19 aptamer as it's covalently attached to its 3' end. Methylene blue then gets displaced from the binding site upon ligand addition. This changes the distance of methylene blue from the electrode surface, leading to a change in electron transfer rates (Figure 7).

The long-term objective of this project is to see what other secondary structures methylene blue binds to on different aptamers. The long-term objective was achieved with various short-term objectives including comparative analyses of the binding affinities of methylene blue interacting with various aptamers such as Caff209, a variant of the caffeine-binding aptamer, HMX38, a methotrexate-binding aptamer, TRP94-2bp, a truncated version of the tryptophan-binding aptamer, among others. This goal was accomplished by measuring the intrinsic fluorescence properties of methylene blue using a fluorescence spectrometer.[30] A change in the fluorescence intensity of methylene blue indicates binding between methylene blue and the aptamer. Previous studies were done with methylene blue and the MN19 aptamer.[20] A fixed concentration of a methylene blue solution was excited at a wavelength of 620 nm. The relative mean fluorescence intensity was measured as a function of MN19 concentration at 683 nm. Results showed that there was a decrease in the fluorescence intensity upon addition of the

MN19 aptamer.[20] Therefore, we want to see if there are changes in the fluorescence intensity of methylene blue when working with other aptamers.

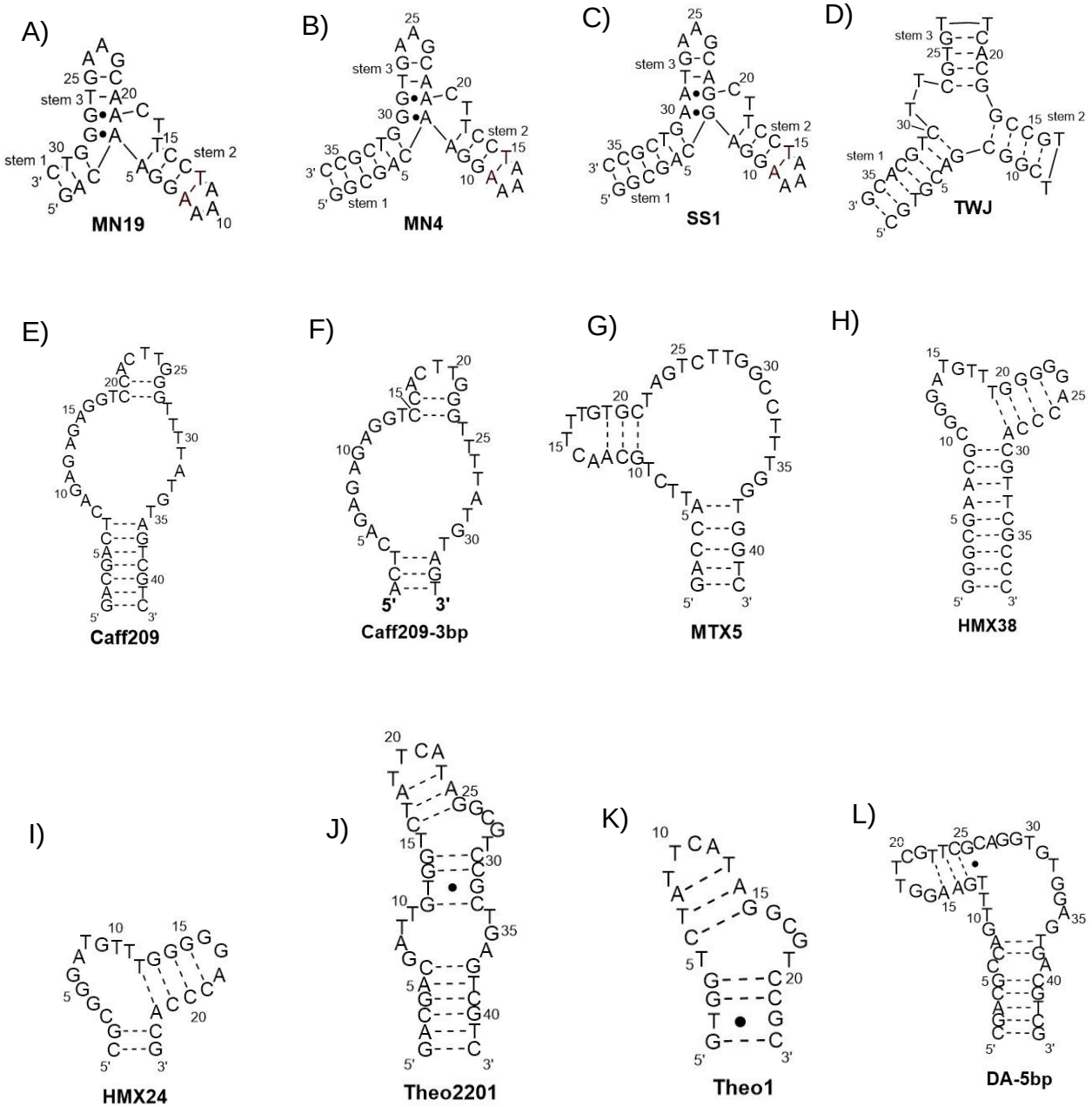

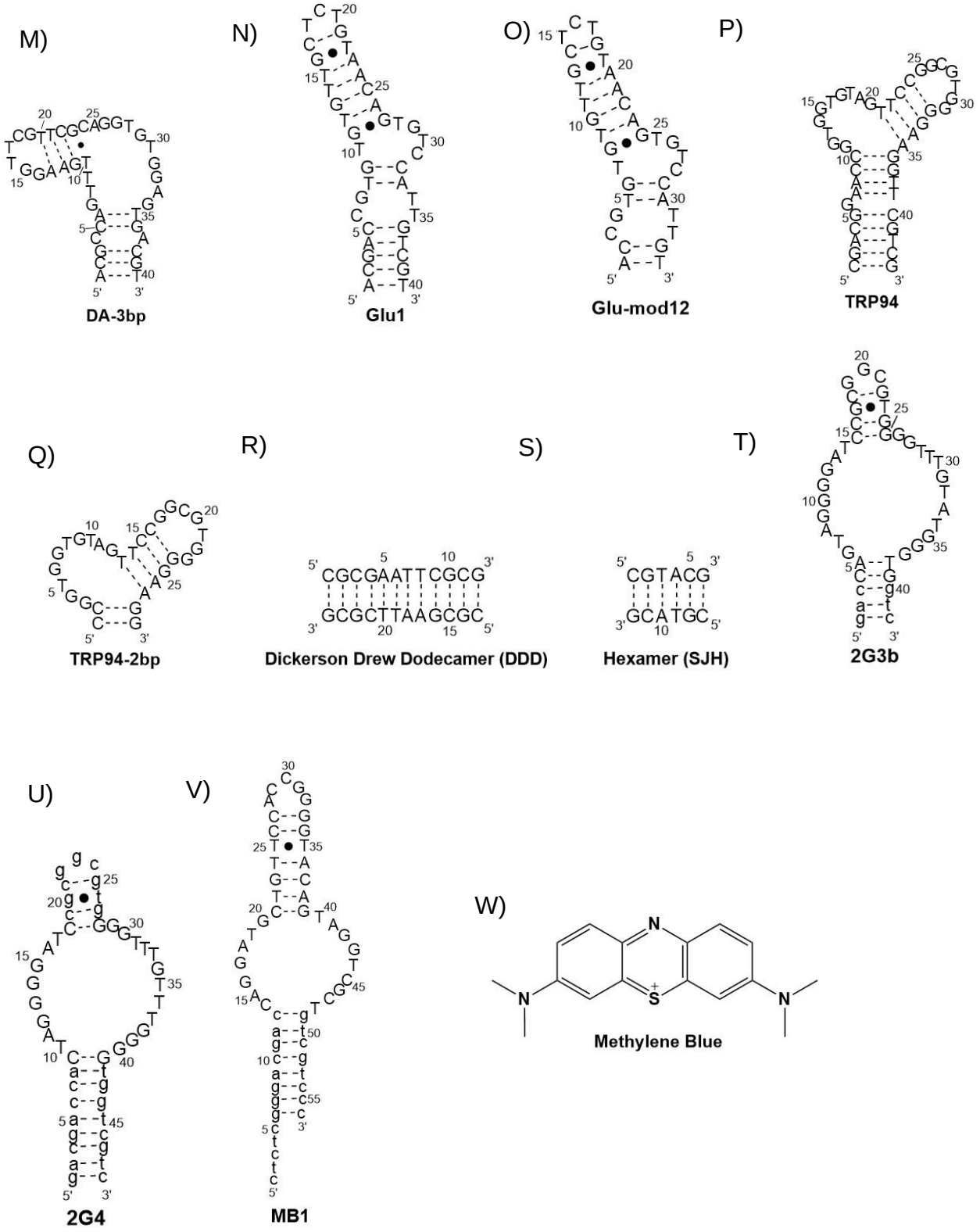

Figure 19. Predicted secondary structures of aptamers, duplex DNA sequences and methylene blue used for fluorescence experiments. The secondary structures show A) MN19, a variant of the cocaine-binding aptamer; B)

MN4, a variant of the cocaine-binding aptamer; C) SS1, a variant of the MN4 aptamer; D) TWJ, a generic three-way junction structure; E) Caff209, a variant of the caffeine-binding aptamer; F) Caff209-3bp, a truncation of the Caff209 aptamer; G) MTX5, a methotrexate-binding aptamer; H) HMX38, another version of the methotrexate-binding aptamer; I) HMX24, a truncation of the HMX38 aptamer; J) Theo2201, a theophylline-binding aptamer; K) Theo1, a truncation of the Theo2201 aptamer; L) DA-5bp, a dopamine-binding aptamer; M) DA-3bp, a truncation of the DA-5bp aptamer; N) Glu1, a glucose-binding aptamer; O) Glu-mod12, a modification of the Glu1 aptamer; P) TRP94, a tryptophan-binding aptamer; Q) TRP94-2bp, a truncation of the TRP94 aptamer; R) Dickerson Drew Dodecamer (DDD), a duplex DNA sequence; S) Hexamer (SJH), a duplex DNA sequence; T) 2G3b, a variant of the second-generation cocaine-binding aptamer; U) 2G4, a variant of the second-generation cocaine-binding aptamer; V) MB1, a methylene blue-binding aptamer and W) methylene blue (MB) redox-reporter.

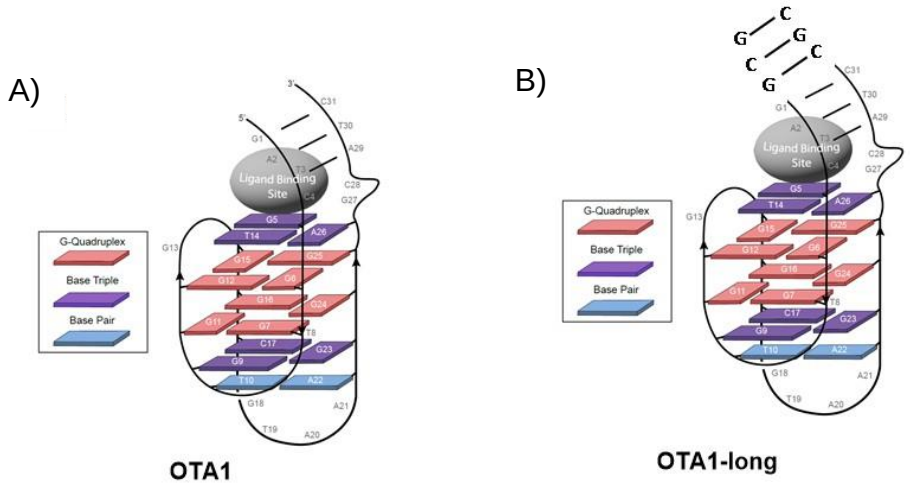

Figure 20. Structures of the A) OTA1, an ochratoxin A-binding aptamer and B) OTA1-long, an elongation of the OTA1 aptamer.

Materials and Methods

Materials

Methylene blue was obtained from Sigma Aldrich and salts and buffer reagents were obtained from BioShop. Aptamers were obtained from IDT, which came as a lyophilized powder.

Aptamer Preparation

Aptamer samples were first dissolved in Milli-Q water. In a 5 mL, 3 kDa concentrator, the samples were then exchanged three times against 1 M NaCl solution and six times against Milli-Q water. This was done to remove any leftover products from the synthesis process. The concentrations of the aptamers were determined using a Cary Varian UV-Vis spectrometer at an OD reading of a wavelength of 260 nm with the corresponding extinction coefficient provided by IDT.

Ligand Preparation

Methylene blue samples were dissolved in buffers used for experiments. The concentration of methylene blue was measured using a Cary Varian UV-Vis spectrometer at an OD reading of a wavelength of 665 nm with the corresponding extinction coefficient, 74 100 M^{-1} cm^{-1}.

Fluorescence Experiments

To begin, aptamer and methylene blue samples were prepared in PBS buffer (137 mM NaCl, 2.7 mM KCl, 10 mM Na_xH_yPO4, pH of 7.4). Aptamer samples were prepared at a concentration of (100 ± 3) µM and methylene blue samples were prepared at a concentration of (60 ± 1) nM. Data was collected using a Cary Eclipse fluorescence spectrometer. A blank PBS sample was first excited at 620 nm while the steady-state fluorescence was measured at an emission wavelength range of 630-800 nm as a negative control. A methylene blue sample was then excited, and its steady-state fluorescence was measured. Aptamer samples were then titrated into the methylene blue sample and aliquots were increased incrementally to an aptamer concentration of ~6 µM as methylene blue emissions were recorded. Data was then analyzed using a direct plot obtained from OriginPro 8.1, where the obtained emission intensities were normalized and plotted as a function of aptamer concentration. OriginPro 8.1 was used to determine the K_d by fitting the data to our published nonlinear regression function as seen in Equation 3:

Nonlinear Regression Function

$$\frac{F}{F_0} = F_1 + (F_2 - F_1)\frac{K_d^n}{(K_d^n + x^n)} \quad (3)$$

Where F and F_0 represents the fluorescence intensities of methylene blue with and without aptamer present, F_2 and F_1 denote the vertical and horizontal asymptotes, n represents the number of binding sites and K_d represents the binding affinity.[31]

A titration plot was also obtained from the software as another method to analyze the data. This would show that binding occurs between an aptamer and ligand if the data plotted looks sigmoidal. The plot was constructed by plotting the normalized fluorescence intensities of methylene blue at 683 nm as a function of the log of the concentration of aptamer titrated into

methylene blue. The midpoint of the titration plot was obtained from OriginPro 8.1 to calculate the K_d by taking the inverse log of the obtained midpoint. This value was then compared to the K_d obtained from the direct plot.

NMR Experiments

1D ^{1}H-NMR experiments were performed on a 700 MHz Bruker NMR spectrometer. Excitation sculpting was used to suppress the water signal. This method employs a gentle, low-power 180 degrees pulse that inverts and preserves all resonances while specifically reducing the intensity of the water peak. Experiments were conducted at 5°C in buffers where conditions are mentioned in the figure captions of the NMR spectra. The change in spectra was monitored as a function of ligand titration. After addition of ligand, the 1D NMR spectra of the bound state of the aptamer was compared to its free state. The data was then processed and analyzed using TOPSPIN 3.5 (Bruker).

Results and Discussion

Analysis through Direct Plots

Firstly, a negative control was performed by titrating PBS buffer into the methylene blue sample. As seen in Figure 21, a minute decrease in the fluorescence intensity is observed for methylene blue. This observation is expected as there is no DNA or aptamer sample titrated into the sample cell containing methylene blue for it to bind and cause changes in its fluorescence intensity. The very small change in the intensity can be due to dilution of the sample with increasing volume of the PBS buffer. The data was fit to a linear function to obtain an average slope of $(-5 \times 10^{-3} \pm 1 \times 10^{-3})$ μL^{-1}. This indicates that a minimal change is observed in the fluorescence intensity of methylene blue with increasing aliquots of PBS buffer.

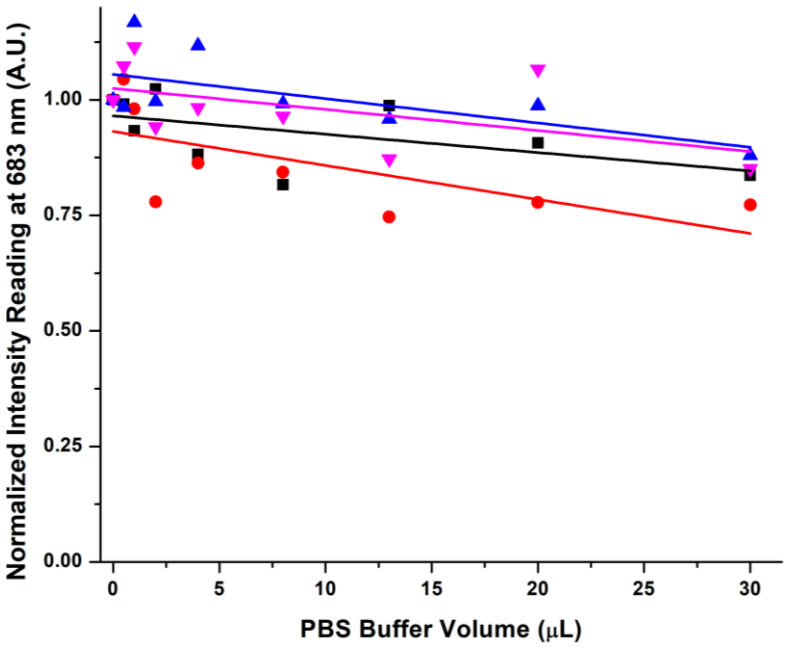

Figure 21. Normalized fluorescence intensity of methylene blue at λ_{em}= 683 nm as a function of volume of PBS buffer titrated into methylene blue. Titration of PBS buffer was used as a negative control and graphs indicate that a very small decrease in fluorescence intensity is observed which can be due to dilution of the methylene blue sample with increasing volume of PBS buffer. The data was fit to a linear function to obtain an average slope value of (-5 x 10^{-3} ± 1 x 10^{-3}) μL^{-1}. The different colors and symbols represent different runs of the PBS buffer titration into methylene blue experiment. The error was determined through standard deviation using data collected from 4 experiments.

A positive control was also conducted of the MN19 aptamer into methylene blue. Data collected from experiments were plotted and fit to a nonlinear binding function and an average K_d value of (0.14 ± 0.04) μM was calculated. This indicates that the aptamer binds tightly to methylene blue (Figure 22).

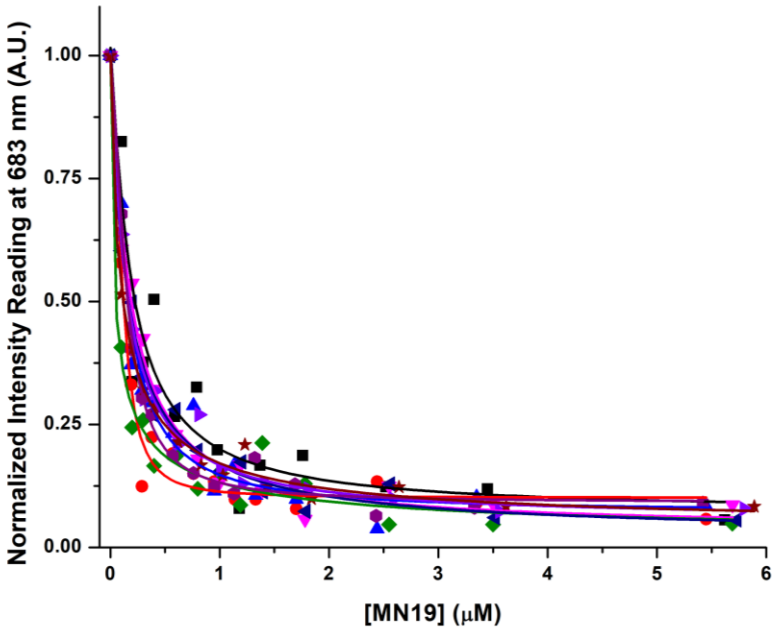

Figure 22. Normalized fluorescence intensity of methylene blue at λ_{em}= 683 nm as a function of concentration of the MN19 aptamer titrated into methylene blue. Titration of the MN19 aptamer was used as a positive control and graphs show the fluorescence decay of methylene blue with increasing concentration of the MN19 aptamer. The data was fit to a nonlinear binding function to obtain an average K_d value of (0.14 ± 0.04) μM. The different colors and symbols represent different runs of the MN19 titration into methylene blue experiment. The error was determined through standard deviation using data collected from 7 experiments.

When MN4, another variant of the cocaine-binding aptamer, was titrated into methylene blue, the aptamer appears to bind tighter than MN19 and an average K_d value of (0.017 ± 0.002) μM was obtained (Figure 23). The experiment was optimized to obtain a more well-defined curve, so that an accurate K_d value was obtained. This was done by working at half the concentration of methylene blue normally used and going to a 2:1 molar ratio. This explains why the x-axis for this plot has lower concentration values for the aptamer than the other plots constructed for this study. Another aptamer that was used was the SS1 aptamer, a variant of the MN4 aptamer. It differs from MN4 by having its two G-A base-pairs interchanged at the central three-way junction. When titrating the SS1 aptamer into methylene blue, the aptamer appears to bind methylene blue with an average K_d value of (2 ± 1) μM (Figure 24). This indicates that the aptamer binds weaker than both MN19 and MN4 to methylene blue. A generic three-way junction DNA structure (TWJ) was also used and when titrated into methylene blue, it binds tightly with an average K_d value of (0.461 ± 0.008) μM (Figure 25). The value obtained indicates a slightly lower binding affinity than MN19 yet binds tightly to methylene blue.

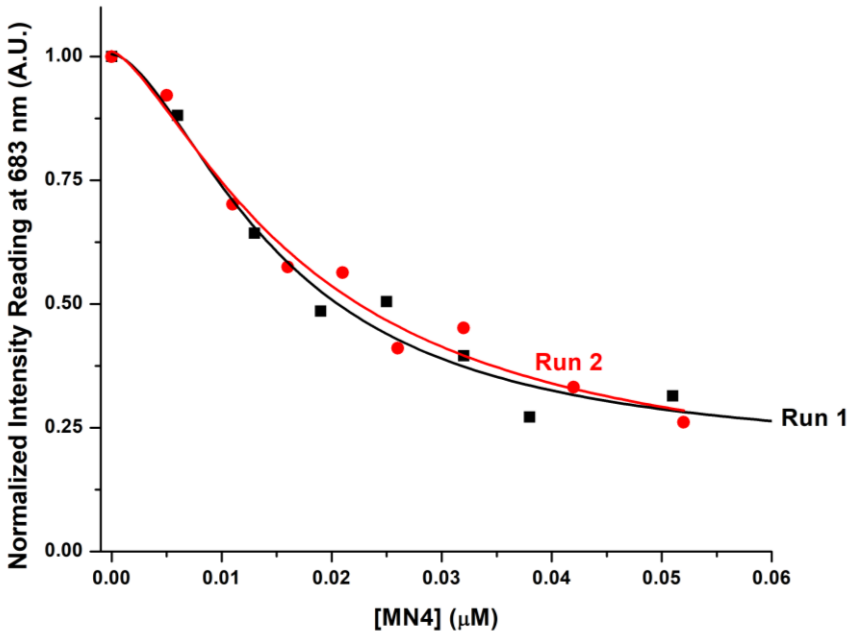

Figure 23. Normalized fluorescence intensity of methylene blue at λ_{em}= 683 nm as a function of concentration of the MN4 aptamer titrated into methylene blue. The graphs show the fluorescence decay of methylene blue with increasing concentration of the MN4 aptamer. This experiment was done in duplicates and the data was fit to a nonlinear binding function to obtain an average K_d value of (0.017 ± 0.002) μM. The error was determined through standard deviation using data collected from 2 experiments.

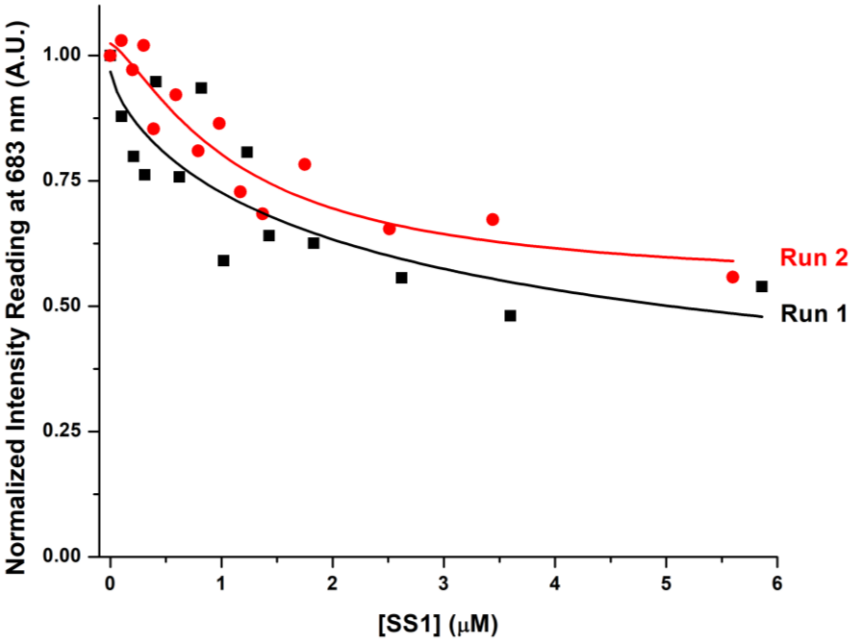

Figure 24. Normalized fluorescence intensity of methylene blue at λ_{em}= 683 nm as a function of concentration of the SS1 aptamer titrated into methylene blue. The graphs show the fluorescence decay of methylene blue with increasing concentration of the SS1 aptamer. This experiment was done in duplicates and the data was fit to a nonlinear binding function to obtain an average K_d value of (2 ± 1) μM. The error was determined through standard deviation using data collected from 2 experiments.

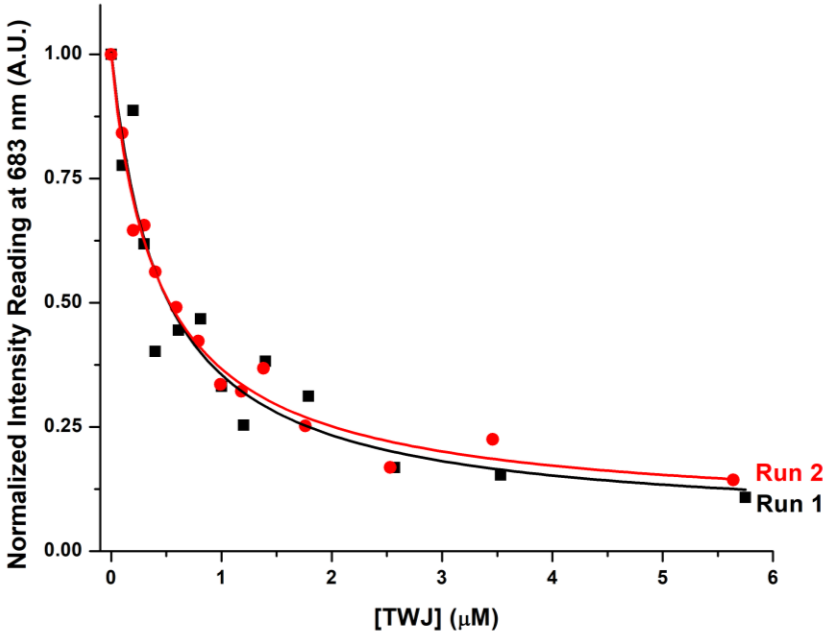

Figure 25. Normalized fluorescence intensity of methylene blue at λ_{em}= 683 nm as a function of concentration of the TWJ aptamer titrated into methylene blue. The graphs show the fluorescence decay of methylene blue with increasing concentration of the TWJ aptamer. This experiment was done in duplicates and the data was fit to a nonlinear binding function to obtain an average K_d value of (0.461 ± 0.008) μM. The error was determined through standard deviation using data collected from 2 experiments.

Caff209, a variant of the caffeine-binding aptamer,[32] was titrated into methylene blue. Figure 26 indicates that the aptamer binds tightly with an average K_d value of (0.6 ± 0.4) μM. The truncated version of the Caff209 aptamer, Caff209-3bp, was also titrated into methylene blue and Figure 27 shows a fluorescence decay which indicates binding of the aptamer to methylene blue. The data was fit to obtain an average K_d value of (4 ± 2) μM which shows that the truncation in the stem of the Caff209 structure leads to a weaker binding affinity.

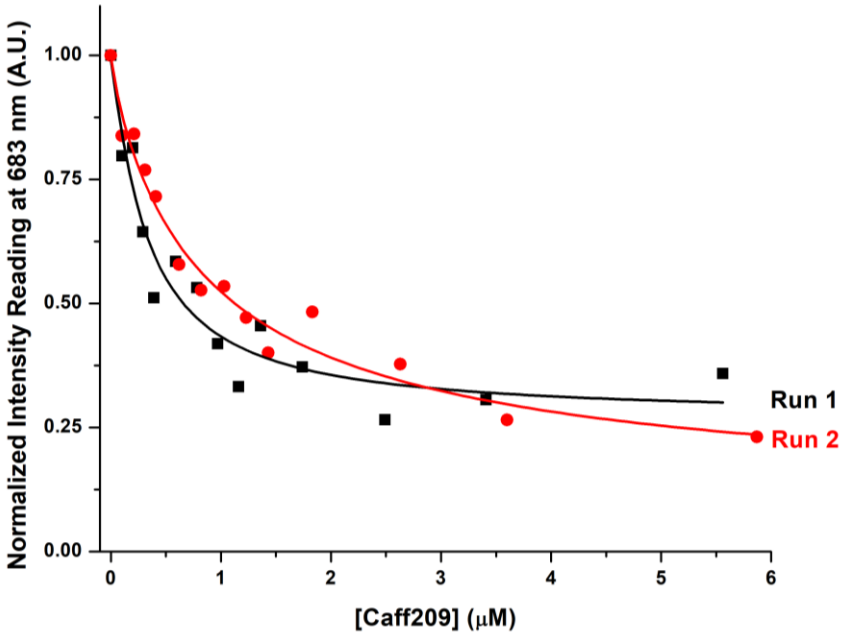

Figure 26. Normalized fluorescence intensity of methylene blue at λ_{em}= 683 nm as a function of concentration of the Caff209 aptamer titrated into methylene blue. The graphs show the fluorescence decay of methylene blue with increasing concentration of the Caff209 aptamer. This experiment was done in duplicates and the data was fit to a nonlinear binding function to obtain an average K_d value of (0.6 ± 0.4) μM. The error was determined through standard deviation using data collected from 2 experiments.

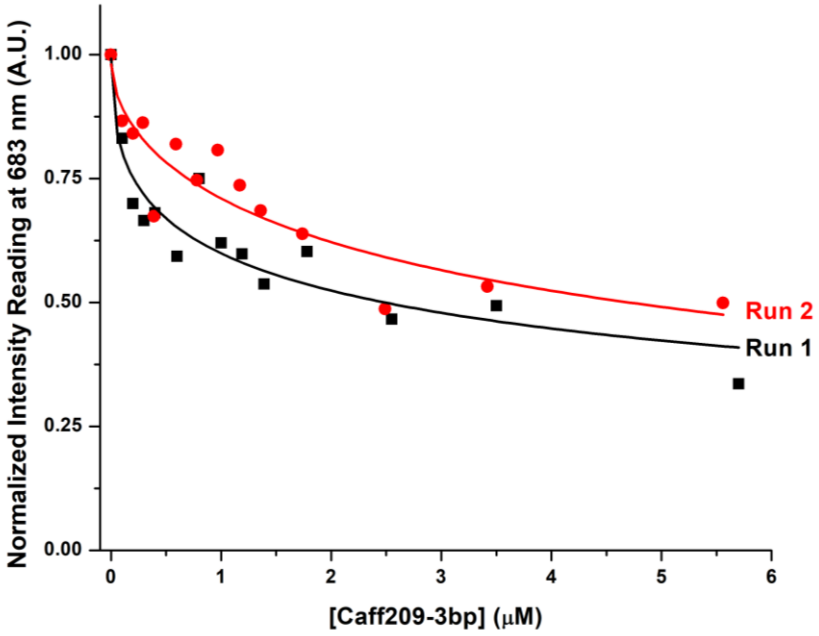

Figure 27. Normalized fluorescence intensity of methylene blue at λ_{em}= 683 nm as a function of concentration of the Caff209-3bp aptamer titrated into methylene blue. The graphs show the fluorescence decay of methylene blue with increasing concentration of the Caff209-3bp aptamer. This experiment was done in duplicates and the data was fit to a nonlinear binding function to obtain an average K_d value of (4 ± 2) μM. The error was determined through standard deviation using data collected from 2 experiments.

Figure 28 shows the fluorescence decay of methylene blue with increasing concentration of MTX5, a methotrexate-binding aptamer.[33] The graph indicates that the aptamer binds tightly, and the data was fit to obtain an average K_d value of (0.44 ± 0.02) µM. Another version of the methotrexate-binding aptamer, HMX38, was also used for the study.[34] A fluorescence decay was shown of methylene blue with increasing concentration of the aptamer; it binds tightly to methylene blue with an average K_d value of (0.5 ± 0.2) µM (Figure 29). The truncated version of HMX38, HMX24, also binds tightly to methylene blue with an average K_d value of (0.6 ± 0.2) µM (Figure 30). The truncated version of the HMX38 aptamer also exhibits a lower binding affinity as seen with the truncated version of the Caff209 aptamer.

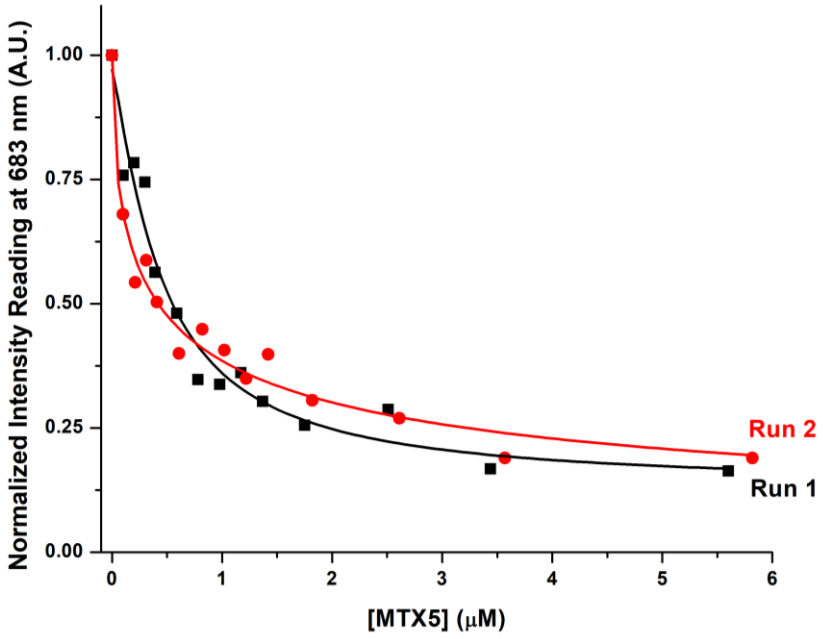

Figure 28. Normalized fluorescence intensity of methylene blue at λ_{em}= 683 nm as a function of concentration of the MTX5 aptamer titrated into methylene blue. The graphs show the fluorescence decay of methylene blue with increasing concentration of the MTX5 aptamer. This experiment was done in duplicates and the data was fit to a nonlinear binding function to obtain an average K_d value of (0.44 ± 0.02) µM. The error was determined through standard deviation using data collected from 2 experiments.

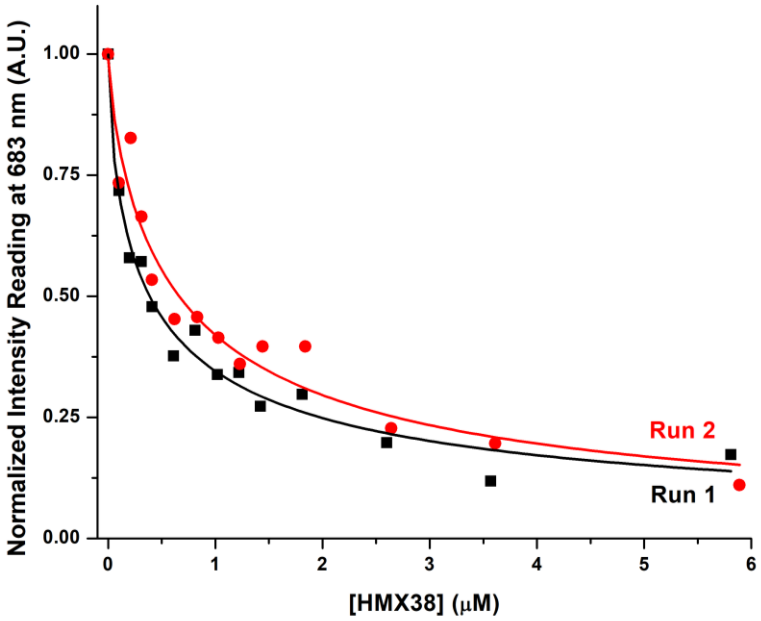

Figure 29. Normalized fluorescence intensity of methylene blue at λ_{em}= 683 nm as a function of concentration of the HMX38 aptamer titrated into methylene blue. The graphs show the fluorescence decay of methylene blue with increasing concentration of the HMX38 aptamer. This experiment was done in duplicates and the data was fit to a nonlinear binding function to obtain an average K_d value of (0.5 ± 0.2) μM. The error was determined through standard deviation using data collected from 2 experiments.

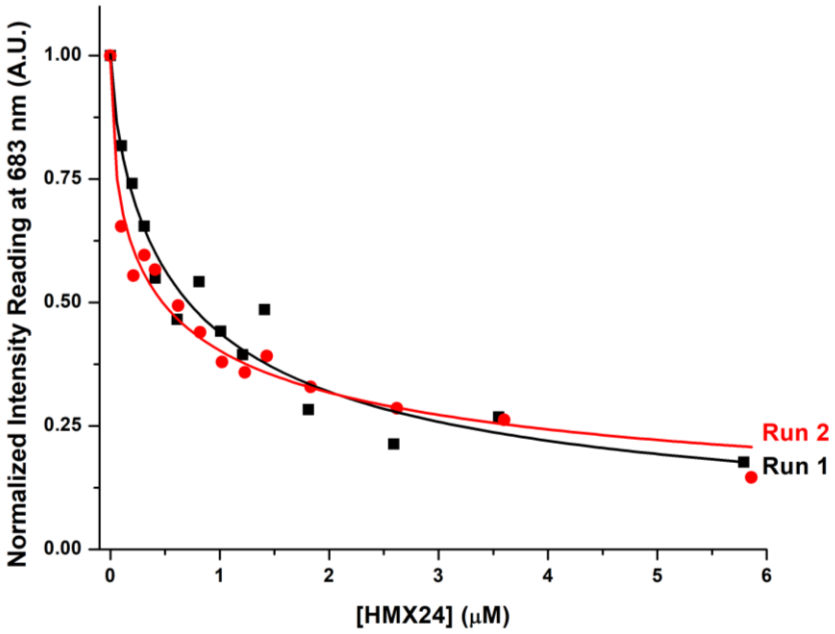

Figure 30. Normalized fluorescence intensity of methylene blue at λ_{em}= 683 nm as a function of concentration of the HMX24 aptamer titrated into methylene blue. The graphs show the fluorescence decay of methylene blue with increasing concentration of the HMX24 aptamer. This experiment was done in duplicates and the data was fit to a nonlinear binding function to obtain an average K_d value of (0.6 ± 0.2) μM. The error was determined through standard deviation using data collected from 2 experiments.

A theophylline-binding aptamer, Theo2201, was also used for this study.[35] Figure 31 shows a fluorescence decay as the aptamer was titrated into methylene blue and an average K_d value of (0.99 ± 0.06) µM was calculated. This shows that Theo2201 binds tightly to methylene blue. The truncated version of this aptamer, Theo1, also binds to methylene blue with an average K_d value of (1.3 ± 0.2) µM observed with the fluorescence decay shown on the graph (Figure 32). When comparing both aptamers, the truncated version also exhibits a lower binding affinity yet both aptamers bind to methylene blue.

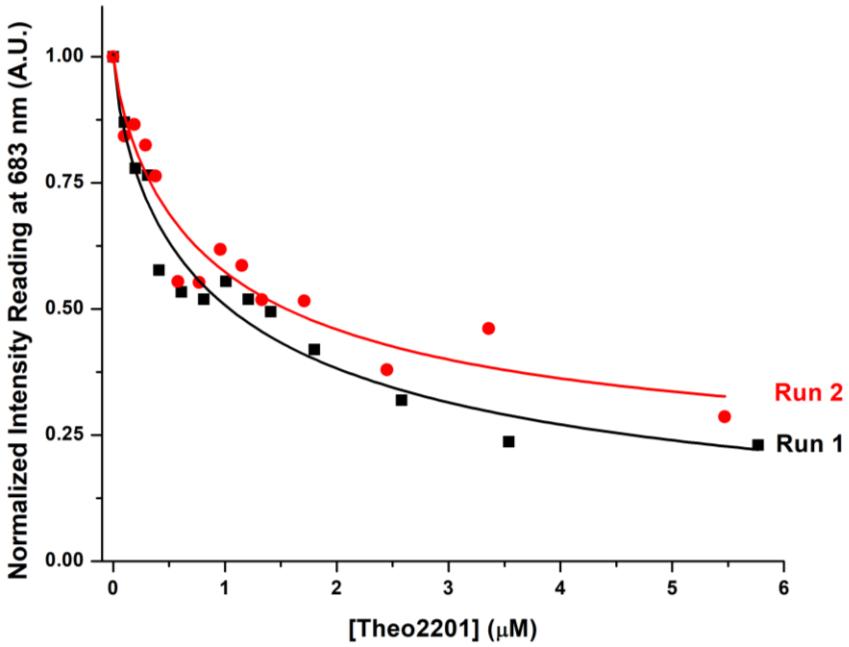

Figure 31. Normalized fluorescence intensity of methylene blue at λ_{em}= 683 nm as a function of concentration of the Theo2201 aptamer titrated into methylene blue. The graphs show the fluorescence decay of methylene blue with increasing concentration of the Theo2201 aptamer. This experiment was done in duplicates and the data was fit to a nonlinear binding function to obtain an average K_d value of (0.99 ± 0.06) µM. The error was determined through standard deviation using data collected from 2 experiments.

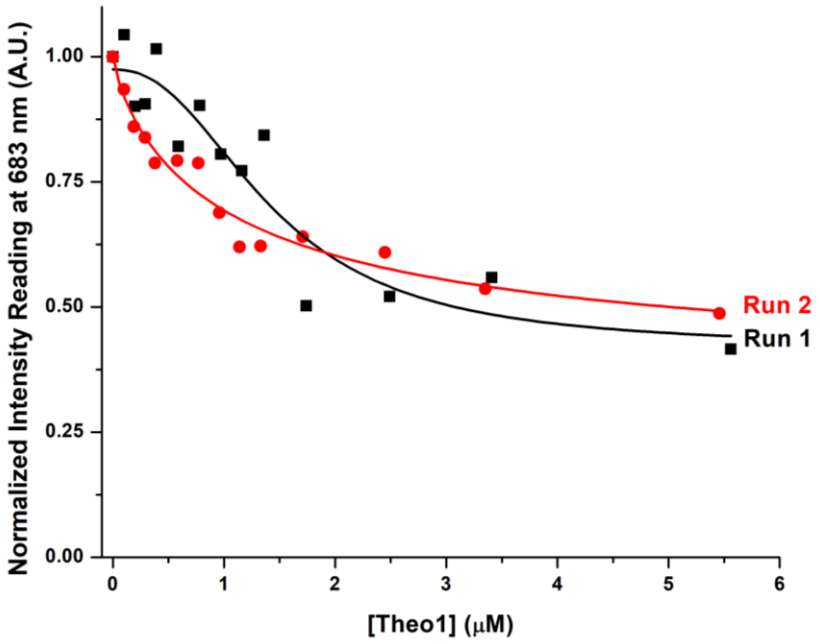

Figure 32. Normalized fluorescence intensity of methylene blue at λ_{em}= 683 nm as a function of concentration of the Theo1 aptamer titrated into methylene blue. The graphs show the fluorescence decay of methylene blue with increasing concentration of the Theo1 aptamer. This experiment was done in duplicates and the data was fit to a nonlinear binding function to obtain an average K_d value of (1.3 ± 0.2) μM. The error was determined through standard deviation using data collected from 2 experiments.

TRP94, a tryptophan-binding aptamer,[33] was titrated into methylene blue, and Figure 33 shows a fluorescence decay which indicates that the aptamer binds to methylene blue with an average K_d value of (1.4 ± 0.5) μM. The graph indicating the truncated version of the TRP94 aptamer, TRP94-2bp, also shows a fluorescence decay of methylene blue with increasing concentrations and it binds tightly with an average K_d value of (0.4 ± 0.3) μM (Figure 34). In this case, the truncated version binds tighter than the parent version of the tryptophan-binding aptamer. This demonstrates that the stem region of the parent aptamer does not play a significant role in the binding affinity towards methylene blue. This shows that methylene blue may be interacting with a different region on the aptamer.

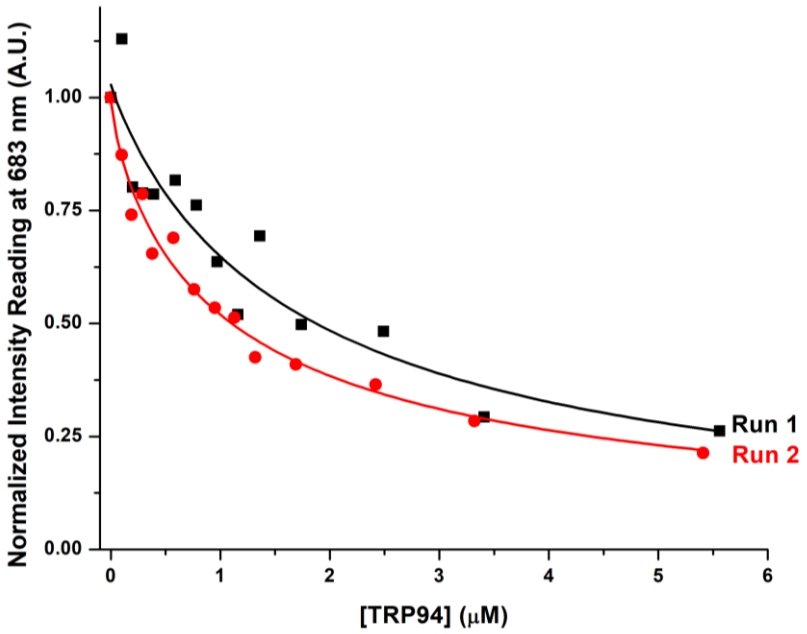

Figure 33. Normalized fluorescence intensity of methylene blue at λ_{em}= 683 nm as a function of concentration of the TRP94 aptamer titrated into methylene blue. The graphs show the fluorescence decay of methylene blue with increasing concentration of the TRP94 aptamer. This experiment was done in duplicates and the data was fit to a nonlinear binding function to obtain an average K_d value of (1.4 ± 0.5) μM. The error was determined through standard deviation using data collected from 2 experiments.

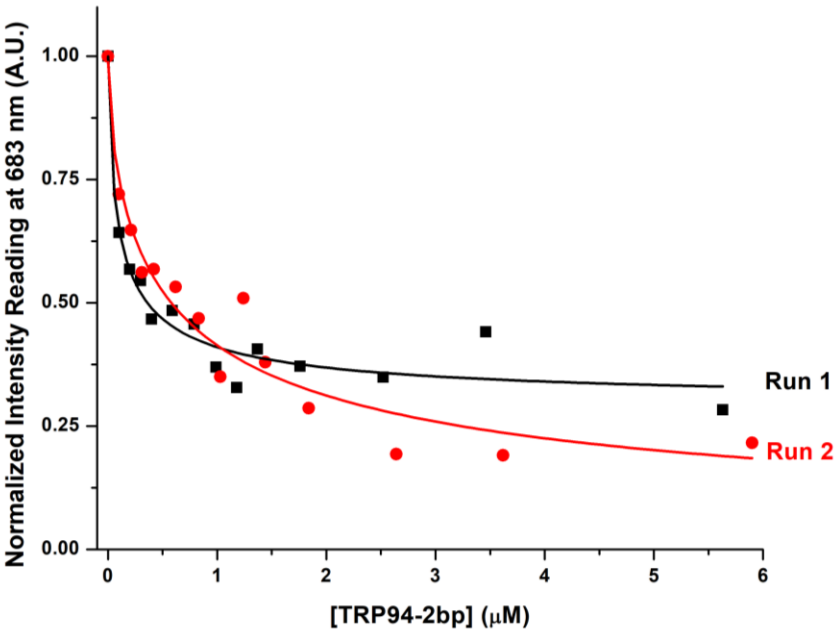

Figure 34. Normalized fluorescence intensity of methylene blue at λ_{em}= 683 nm as a function of concentration of the TRP94-2bp aptamer titrated into methylene blue. The graphs show the fluorescence decay of methylene blue with increasing concentration of the TRP94-2bp aptamer. This experiment was done in duplicates and the data was fit to a nonlinear binding function to obtain an average K_d value of (0.4 ± 0.3) μM. The error was determined through standard deviation using data collected from 2 experiments.

A dopamine-binding aptamer, DA-5bp,[36] was titrated into methylene blue, and Figure 35 shows a fluorescence decay with increasing concentration of the aptamer. The aptamer binds to methylene blue with an average K_d value of (1.3 ± 0.4) µM. The truncated version, DA-3bp, also binds to methylene blue with an average K_d value of (1.2 ± 0.4) µM as a fluorescence decay was also observed on the plotted graph (Figure 36). When comparing the binding affinities of both aptamers to methylene blue, the truncated version binds tighter to methylene blue as DA-3bp has a slightly higher binding affinity than DA-5bp. This also indicates how a longer stem region doesn't significantly contribute to stronger binding with the dopamine-binding aptamer.

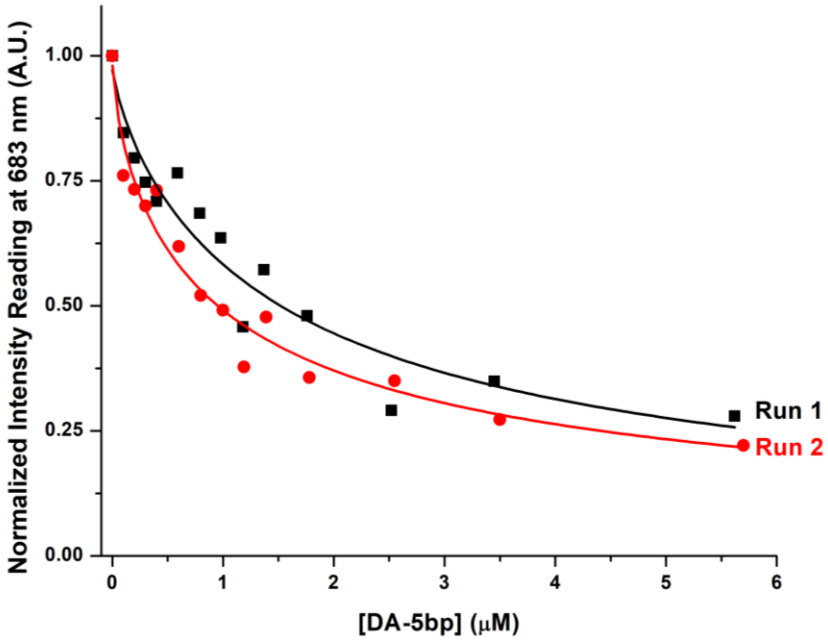

Figure 35. Normalized fluorescence intensity of methylene blue at λ_{em}= 683 nm as a function of concentration of the DA-5bp aptamer titrated into methylene blue. The graphs show the fluorescence decay of methylene blue with increasing concentration of the DA-5bp aptamer. This experiment was done in duplicates and the data was fit to a nonlinear binding function to obtain an average K_d value of (1.3 ± 0.4) µM. The error was determined through standard deviation using data collected from 2 experiments.

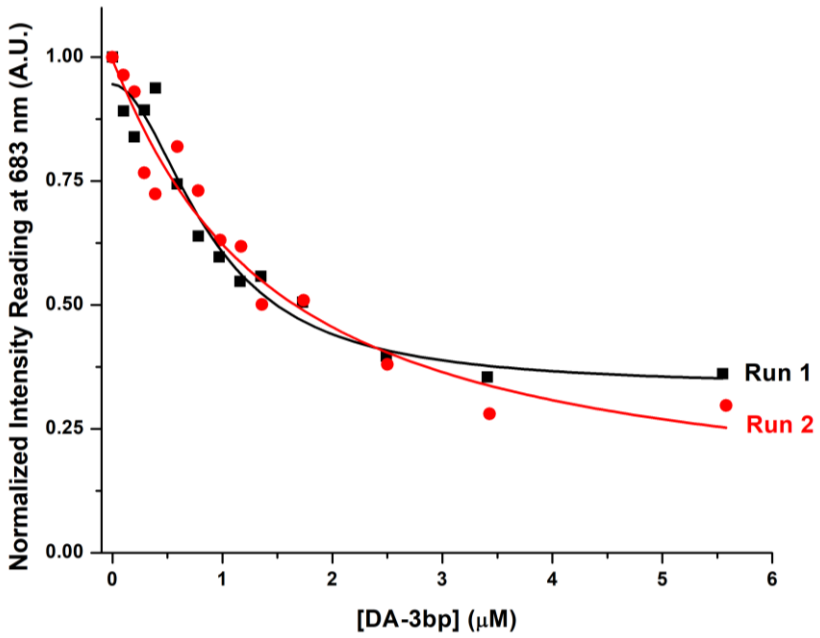

Figure 36. Normalized fluorescence intensity of methylene blue at λ_{em}= 683 nm as a function of concentration of the DA-3bp aptamer titrated into methylene blue. The graphs show the fluorescence decay of methylene blue with increasing concentration of the DA-3bp aptamer. This experiment was done in duplicates and the data was fit to a nonlinear binding function to obtain an average K_d value of (1.2 ± 0.4) μM. The error was determined through standard deviation using data collected from 2 experiments.

A glucose-binding aptamer, Glu1,[36] was incorporated into this study. Figure 37 shows fluorescence decay with increasing concentration of the Glu1 aptamer. The data was fit to obtain an average K_d value of (1.1 ± 0.3) μM which shows that this aptamer also binds to methylene blue. The modified version of the aptamer, Glu-mod12, showed binding with methylene blue with an average K_d value of (2 ± 1) μM (Figure 38). The modified version of the glucose-binding aptamer binds weaker than the parent aptamer but both aptamers exhibit binding with methylene blue.

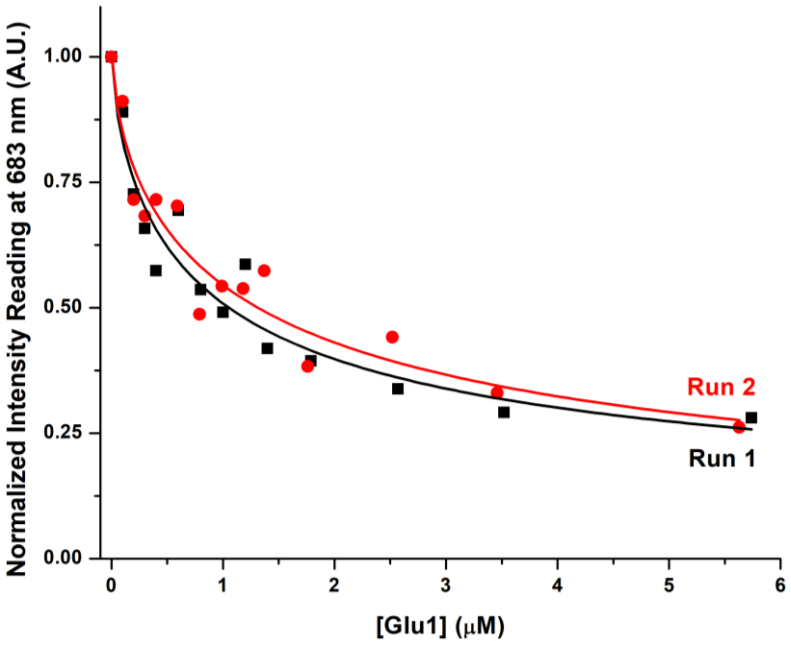

Figure 37. Normalized fluorescence intensity of methylene blue at λ_{em}= 683 nm as a function of concentration of the Glu1 aptamer titrated into methylene blue. The graphs show the fluorescence decay of methylene blue with increasing concentration of the Glu1 aptamer. This experiment was done in duplicates and the data was fit to a nonlinear binding function to obtain an average K_d value of (1.1 ± 0.3) μM. The error was determined through standard deviation using data collected from 2 experiments.

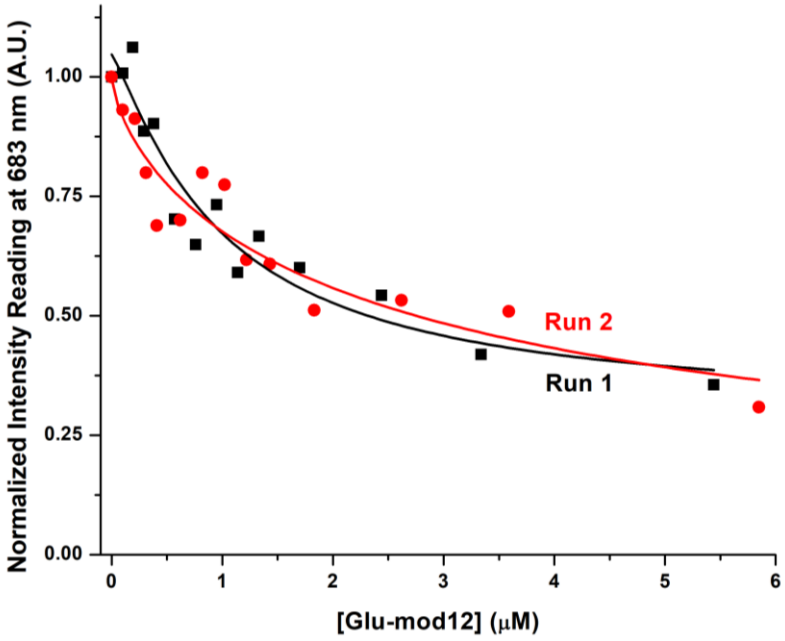

Figure 38. Normalized fluorescence intensity of methylene blue at λ_{em}= 683 nm as a function of concentration of the Glu-mod12 aptamer titrated into methylene blue. The graphs show the fluorescence decay of methylene blue with increasing concentration of the Glu-mod12 aptamer. This experiment was done in duplicates and the data was fit to a nonlinear binding function to obtain an average K_d value of (2 ± 1) μM. The error was determined through standard deviation using data collected from 2 experiments.

OTA1-long, is the elongated version of the ochratoxin A-binding aptamer. When titrating this aptamer into methylene blue, the fluorescence intensity decreases which shows that the aptamer binds tightly with a K_d value of (0.5 ± 0.5) µM (Figure 39). Experimental conditions were optimized by working at half the concentration of methylene blue normally used and performing titrations until a 2:1 molar ratio to obtain a well-defined curve for an accurate K_d value. However, duplicate experiments still need to be performed. The parent aptamer of ochratoxin A, OTA1,[37] also binds tightly to methylene blue, indicated by the decay in fluorescence, with an average K_d value of (0.13 ± 0.04) µM (Figure 40). In this case, the shorter version of the ochratoxin A-binding aptamer binds tighter to methylene blue.

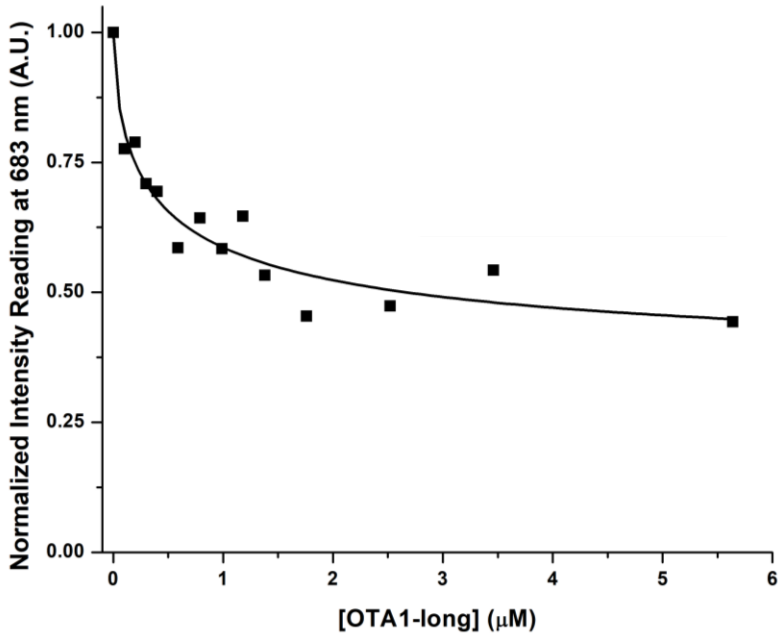

Figure 39. Normalized fluorescence intensity of methylene blue at λ_{em}= 683 nm as a function of concentration of the OTA1-long aptamer titrated into methylene blue. The graph shows the fluorescence decay of methylene blue with increasing concentration of the OTA1-long aptamer. The data was fit to a nonlinear binding function to obtain a K_d value of (0.5 ± 0.5) µM. This experiment was not completed in duplicates and therefore, the error was determined through the fit of the curve.

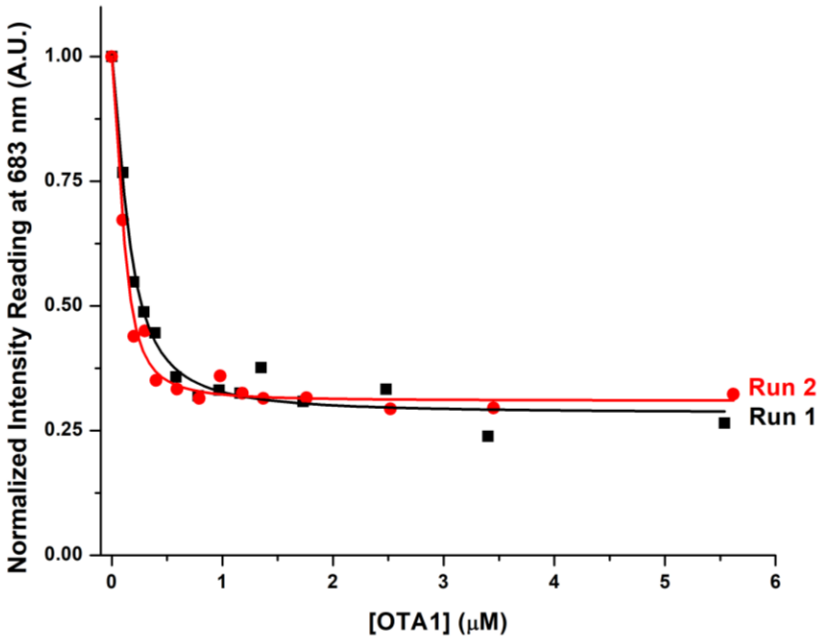

Figure 40. Normalized fluorescence intensity of methylene blue at λ_{em}= 683 nm as a function of concentration of the OTA1 aptamer titrated into methylene blue. The graphs show the fluorescence decay of methylene blue with increasing concentration of the OTA1 aptamer. This experiment was done in duplicates and the data was fit to a nonlinear binding function to obtain an average K_d value of (0.13 ± 0.04) μM. The error was determined through standard deviation using data collected from 2 experiments.

2G3b, a variant of the second-generation cocaine-binding aptamer,[38] was shown to bind tightly to methylene blue with a K_d value of (0.07 ± 0.05) μM (Figure 41). Experimental conditions were optimized to obtain a well-defined curve for an accurate K_d value. Additionally, this experiment was not conducted in duplicates. 2G4, another variant of the second-generation cocaine-binding aptamer, also binds tightly to methylene blue. The graph shows a fluorescence decay, and the data was fit to obtain an average K_d value of (0.22 ± 0.05) μM (Figure 42).

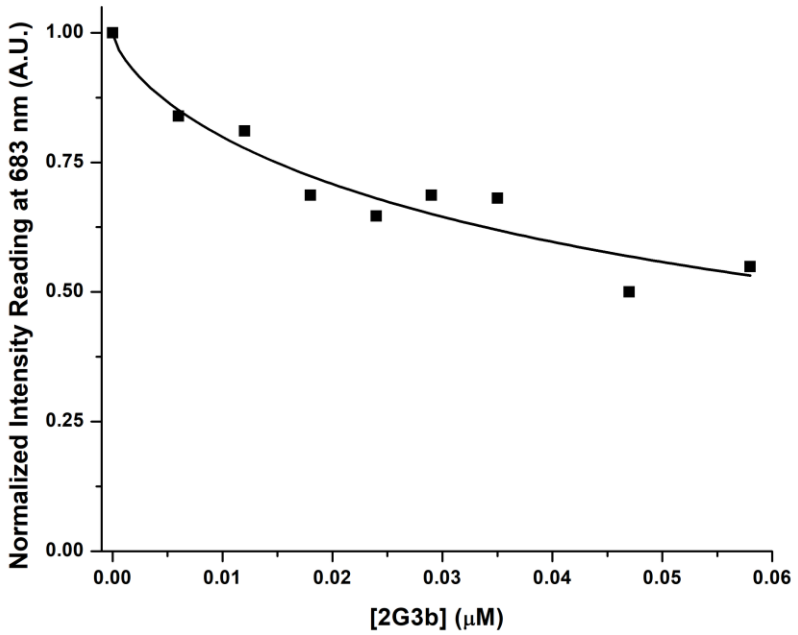

Figure 41. Normalized fluorescence intensity of methylene blue at λ_{em}= 683 nm as a function of concentration of the 2G3b aptamer titrated into methylene blue. The graph shows the fluorescence decay of methylene blue with increasing concentration of the 2G3b aptamer. The data was fit to a nonlinear binding function to obtain a K_d value of (0.07 ± 0.05) μM. This experiment was not completed in duplicates and therefore, the error was determined through the fit of the curve.

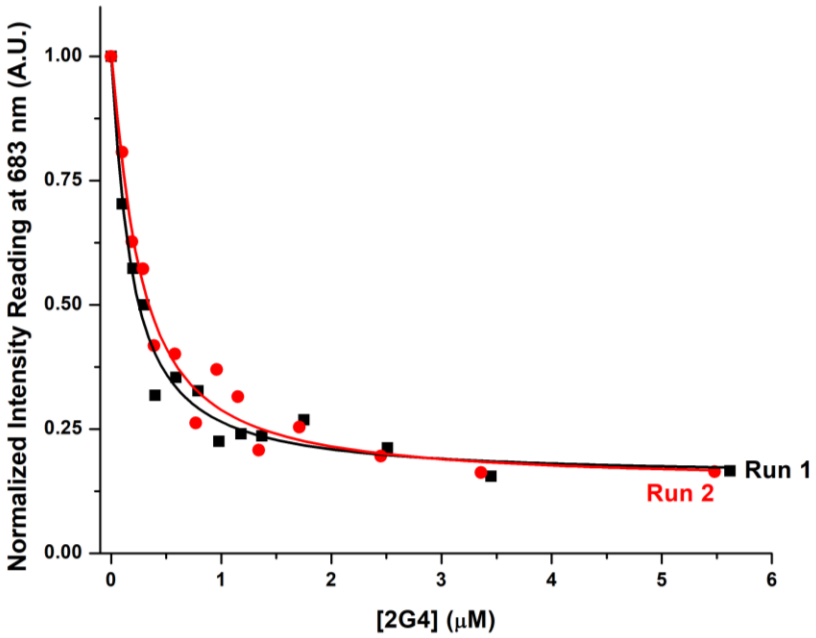

Figure 42. Normalized fluorescence intensity of methylene blue at λ_{em}= 683 nm as a function of concentration of the 2G4 aptamer titrated into methylene blue. The graphs show the fluorescence decay of methylene blue with increasing concentration of the 2G4 aptamer. This experiment was done in duplicates and the data was fit to a nonlinear binding function to obtain an average K_d value of (0.22 ± 0.05) μM. The error was determined through standard deviation using data collected from 2 experiments.

MB1, a methylene blue-binding aptamer,[39] binds tightly to methylene blue with an average K_d value of (0.013 ± 0.004) µM (Figure 43). The result is expected as this aptamer is presumed to be selected against methylene blue. This is consistent with the findings of Yang *et al.* who performed a Thioflavin T (ThT) dye displacement assay which included the methylene blue-binding aptamer and methylene blue and obtained a K_d value of 31 nM.[39] In the fluorescence experiment conducted to test for binding between methylene blue and MB1, the K_d value obtained was 13 nM (Figure 43). Experimental conditions were optimized by working at half the concentration of methylene blue normally used and performing titrations until a 2:1 molar ratio to obtain a well-defined curve for an accurate K_d value.

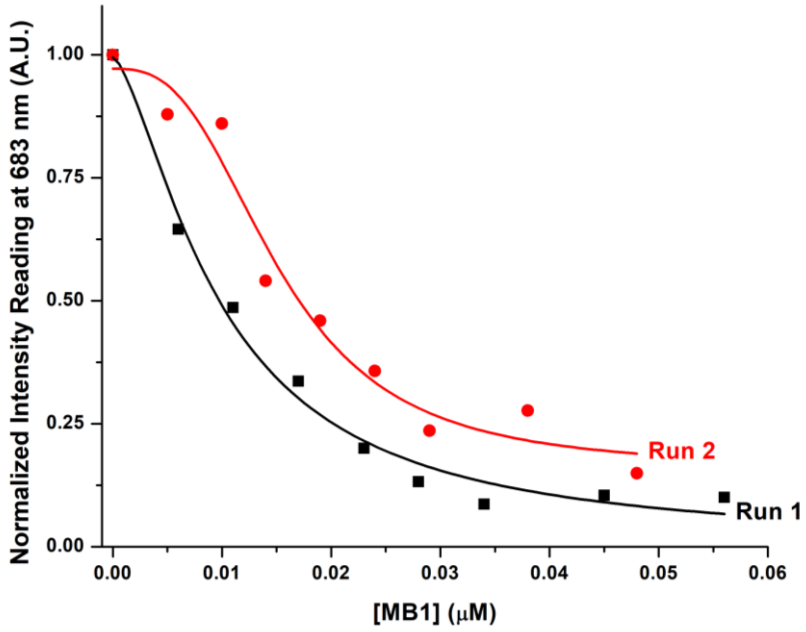

Figure 43. Normalized fluorescence intensity of methylene blue at λ_{em}= 683 nm as a function of concentration of the MB1 aptamer titrated into methylene blue. The graphs show the fluorescence decay of methylene blue with increasing concentration of the MB1 aptamer. This experiment was done in duplicates and the data was fit to a nonlinear binding function to obtain an average K_d value of (0.013 ± 0.004) µM. The error was determined through standard deviation using data collected from 2 experiments.

The Dickerson Drew Dodecamer (DDD), a well-studied duplex DNA sequence that consists of 12 base-pairs,[40] was titrated into a methylene blue sample. Figure 44 shows a small decrease in fluorescence intensity, and it appears that this sequence binds very weakly to methylene blue. The data could not be fit to a nonlinear binding function as the trend of the data plotted appears linear. This trend resembled the observations seen with the change in the fluorescence intensity in the PBS buffer titration experiment. The data was fit to a linear function

and an average slope value of ($-5.7 \times 10^{-2} \pm 0.8 \times 10^{-2}$) μM^{-1} was obtained. When comparing this value with the average slope obtained for the PBS buffer titration (Figure 21), ($-5 \times 10^{-3} \pm 1 \times 10^{-3}$) μL^{-1}, the value indicates a more negative slope. The more negative slope can be attributed to two key factors: the very weak binding occurring between DDD and methylene blue and the dilution of the methylene blue sample. The Hexamer (SJH), another duplex DNA sequence that consists of 6 base-pairs, was also titrated into methylene blue (Figure 45). Just like the DDD titration into methylene blue, the graph indicates that this sequence binds very weakly to methylene blue, and the data was fit to a linear function to obtain an average slope of ($-3.5 \times 10^{-2} \pm 0.9 \times 10^{-2}$) μM^{-1}. The slope obtained is more negative than the slope obtained for the negative control, and this can also be due to the two factors mentioned for the DDD titration into methylene blue. Overall, both duplex DNA sequences show a weak binding interaction with methylene blue.

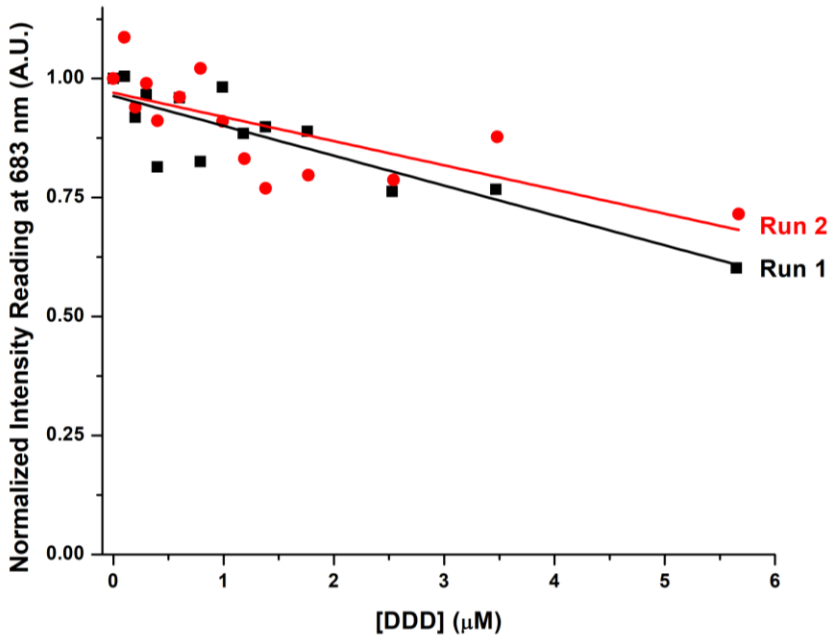

Figure 44. Normalized fluorescence intensity of methylene blue at λ_{em}= 683 nm as a function of concentration of the Dickerson Drew Dodecamer (DDD) duplex DNA sequence titrated into methylene blue. The graphs show the fluorescence decay of methylene blue with increasing concentration of DDD. This experiment was done in duplicates and the data was fit to a linear function to obtain an average slope of ($-5.7 \times 10^{-2} \pm 0.8 \times 10^{-2}$) μM^{-1}. The error was determined through standard deviation using data collected from 2 experiments.

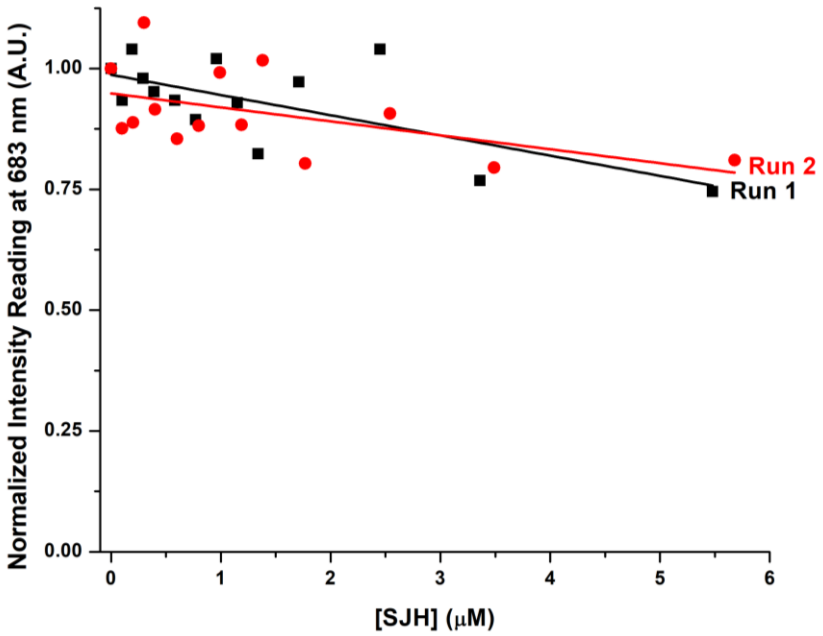

Figure 45. Normalized fluorescence intensity of methylene blue at λ_{em}= 683 nm as a function of concentration of the Hexamer (SJH) duplex DNA sequence titrated into methylene blue. The graphs show the fluorescence decay of methylene blue with increasing concentration of SJH. This experiment was done in duplicates and the data was fit to a linear function to obtain an average slope of $(-3.5 \times 10^{-2} \pm 0.9 \times 10^{-2})$ μM^{-1}. The error was determined through standard deviation using data collected from 2 experiments.

Overall, when conducting a direct plot analysis of the normalized fluorescence intensity of methylene blue at λ_{em}= 683 nm as a function of concentration of the aptamer or DNA titrated into methylene blue, the results suggest that methylene blue binds very weakly to duplex DNA. This was reflected in the plots constructed of the DDD and SJH titration into methylene blue as a minimal change in fluorescence intensity was seen compared to the decay curves seen with the aptamers. Methylene blue seems to bind tightly to aptamer structures containing a bulge or stem-loop. As seen in Figure 34, the tryptophan-binding aptamer had its stem truncated to two base-pairs and still binds tightly to methylene blue. This can indicate how methylene blue is likely binding other structures on aptamers and not the duplex DNA structure. Furthermore, a summary of all aptamer titrations completed with their associated K_d values is shown in Table 2. The table shows all the aptamers that bound tightly to methylene blue when compared to MN19 are in the range of 0-4 μM. The aptamers that bind tightly also contain either a stem-loop or bulge in their structures. However, both DDD and SJH were not fit to a nonlinear binding function but fit to a linear function where their corresponding slope values were compared with the negative control in Table 3.

Table 2. Summary of binding affinities obtained from a direct plot for all aptamers titrated into methylene blue. The data was fit to a nonlinear binding function where their associated K_d values were compared to MN19. The error was determined through standard deviation of each experiment. * denotes that the error was determined through the fit of the curve.

Binds weaker than MN19 (μM)	**Binds similar to MN19** (μM)	**Binds tighter than MN19** (μM)
2G4, (0.22 ± 0.05)	MN19, (0.14 ± 0.04)	*2G3b, (0.07 ± 0.05)
TRP94-2bp, (0.4 ± 0.3)	OTA1, (0.13 ± 0.04)	MN4, (0.017 ± 0.002)
MTX5, (0.44 ± 0.02)		MB1, (0.013 ± 0.004)
TWJ, (0.461 ± 0.008)		
HMX38, (0.5 ± 0.2)		
*OTA1-long, (0.5 ± 0.5)		
HMX24, (0.6 ± 0.2)		
Caff209, (0.6 ± 0.4)		
Theo2201, (0.99 ± 0.06)		
Glu1, (1.1 ± 0.3)		
DA-3bp, (1.2 ± 0.4)		
Theo1, (1.3 ± 0.2)		
DA-5bp, (1.3 ± 0.4)		
TRP94, (1.4 ± 0.5)		
Glu-mod12, (2 ± 1)		
SS1, (2 ± 1)		
Caff209-3bp, (4 ± 2)		

Table 3. Summary of slopes obtained from a direct plot for duplex DNA sequences titrated into methylene blue. The data was fit to a linear function where their associated slope values were compared to the PBS buffer titration. The error was determined through standard deviation of each experiment.

Sample	**Slope**
PBS Buffer	$(-5 \times 10^{-3} \pm 1 \times 10^{-3})$ μL^{-1}
DDD	$(-5.7 \times 10^{-2} \pm 0.8 \times 10^{-2})$ μM^{-1}
SJH	$(-3.5 \times 10^{-2} \pm 0.9 \times 10^{-2})$ μM^{-1}

Methylene blue was previously found to be a DNA intercalator, a molecule that reversibly intercalates with the double-strand helix of DNA through insertion between adjacent base-pairs and thereby, disrupting the structure of DNA.[41-42] However in this study, it was found that the duplex DNA sequences, DDD and SJH, binds very weakly to methylene blue. This shows that it may be a weakly binding intercalator. Another possibility is that methylene blue may be interacting with the aptamer through a π-π stacking mechanism. Aron A. Shoara *et al.* have previously showed that quinine and cocaine interact with the cocaine-binding aptamer in a

π-π stacking mechanism where one face of the aromatic ring in the ligand interacts with one or more bases from the aptamer.[31] When adding the cocaine-binding aptamer to both quinine and cocaine, the intrinsic fluorescence of the ligands was quenched. To support this stacking mechanism, the fluorescence of ethidium bromide, a known intercalator, was measured after titration of the cocaine-binding aptamer.[31] It was shown that the fluorescence intensity increased upon addition of the aptamer. With methylene blue, fluorescence intensity decreased upon addition of the aptamer like the addition of aptamer to quinine or cocaine. Therefore, it's possible that methylene blue may be interacting with the aptamer through a stacking manner where the aromatic ring from methylene blue interacts with one or more bases from the aptamer.

Analysis through Titration Plots

Another way the data can be interpreted is through the analysis of a titration plot. The plot is constructed by plotting the normalized fluorescence intensities of methylene blue at 683 nm as a function of the log of the concentration of aptamer or DNA titrated into methylene blue. When observing a sigmoidal shape, it can indicate binding is occurring between the aptamer and methylene blue. However, some of the data were successfully fit on a titration plot to yield a sigmoidal shape while others were not. As a result, some data sets could not have a midpoint adequately identified. Furthermore, the modelled behaviour that the titration plots exhibited was inconsistent between the duplicates acquired. For some data sets, the midpoint was identified, and the K_d was calculated. This is done by taking the inverse log of the midpoint identified. This value can then be used to compare with the K_d values obtained from the direct plot of normalized fluorescence intensity of methylene blue at λ_{em}= 683 nm as a function of the concentration of aptamer or DNA titrated into methylene blue. Ideally, the K_d values should be similar if not the same.

Firstly, when looking at the titration plots of the MN19 aptamer titrated into methylene blue, the average K_d value was calculated to be (0.29 ± 0.08) µM. This value is relatively close to the value obtained from the direct plot of the MN19 titration where the average K_d value was calculated to be (0.14 ± 0.04) µM. However, the average K_d value was determined based on titration plots that were able to fit a sigmoidal model (Figure 46). Other runs done with MN19 and graphed as a titration plot were excluded as the data did not conform to a sigmoidal model. Midpoints not apart of the range of the x-axis plotted were identified and therefore, their K_d

values were not calculated. This shows that a direct plot provides a clearer representation of the data as consistency is present between multiple runs. Therefore, a direct plot is a more effective way to analyze the data (Figure 22). Furthermore, the graphs which exhibit a sigmoidal-shaped modelled behaviour indicate that the MN19 aptamer binds to methylene blue (Figure 46).

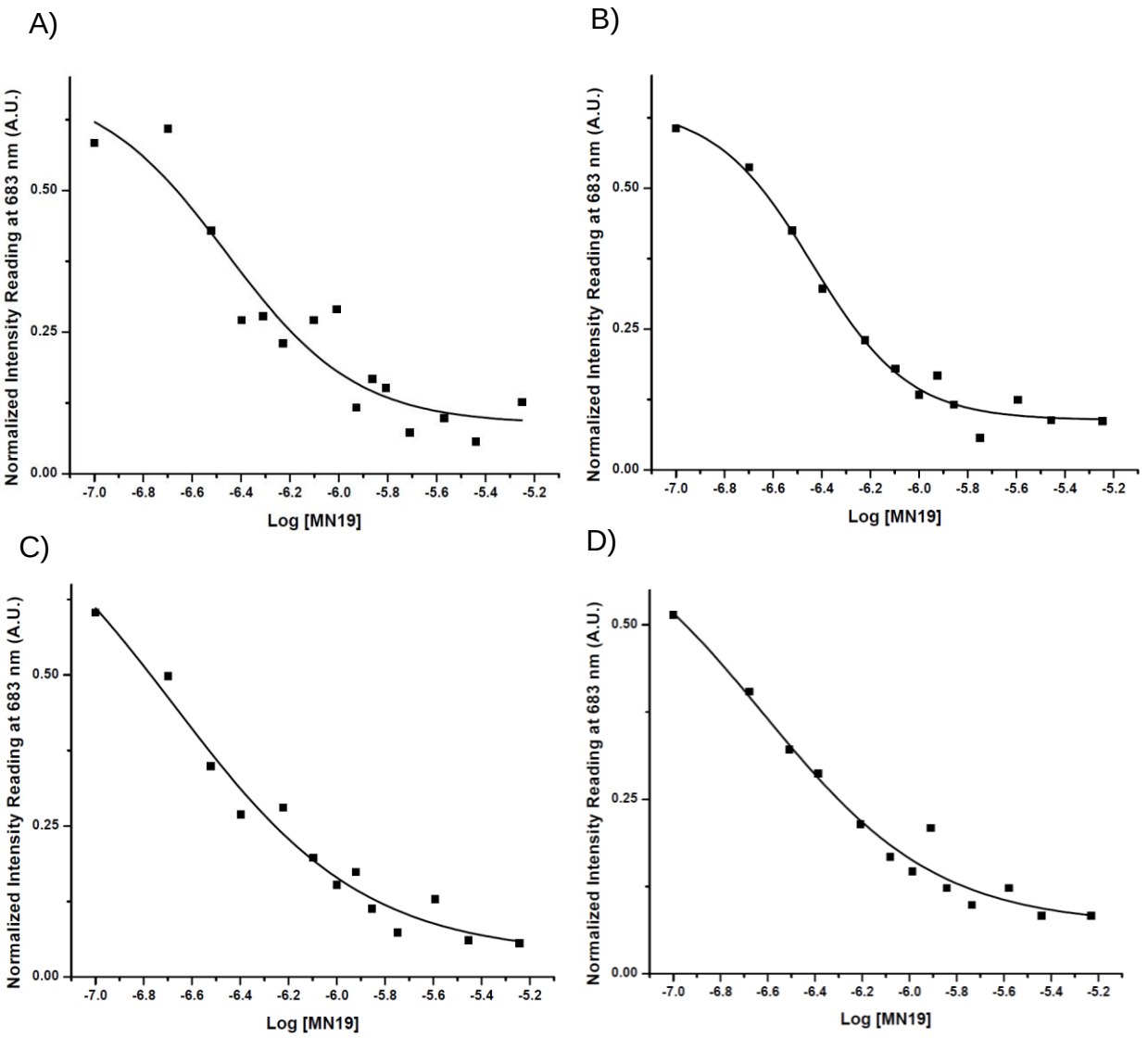

Figure 46. Normalized fluorescence intensity of methylene blue at λ_{em}= 683 nm versus log of concentration of the MN19 aptamer titrated into methylene blue. MN19 was used as a positive control before starting experiments with other aptamers. An attempt was made to fit the titration plots to a sigmoidal fit, however, some runs plotted on a titration plot yielded midpoint values that were not in the range of the x-axis plotted. Therefore, the values were not taken for calculation of K_d. Graphs that did yield midpoint values that were apart of the x-axis were used for the calculation of K_d. (A) and (B) have a sigmoidal-shaped modelled behaviour and (C) and (D) show a sigmoidal-shaped modelled behaviour less pronounced compared to (A) and (B). Overall, the modelled behaviours between the four graphs appear consistent. The midpoint of the titration plots was identified as A) -6.46, B) -6.44, C) -6.68 and D) -6.62 which enabled the calculation of K_d values of A) 0.35 µM, B) 0.36 µM, C) 0.21 µM and D) 0.24 µM which gives an average K_d value of (0.29 ± 0.08) µM. The error was determined through standard deviation using data collected from 4 experiments.

When looking at the titration plot of MN4 into methylene blue, the K_d value was calculated to be (0.01 ± 0.02) µM. The average K_d value from the direct plot was calculated to be (0.017 ± 0.002) µM. The values presented are nearly identical which shows how both plots represent a similar binding affinity of the aptamer for methylene blue. However, the data presented as a titration plot does not fit as well to obtain a sigmoidal-shaped modelled behaviour as the graph exhibits low sigmoidicity (Figure 47). It would be difficult to determine whether the MN4 aptamer binds to methylene blue just through a titration plot. Therefore, a direct plot would be considered a more effective method for analyzing binding and determining K_d values (Figure 23).

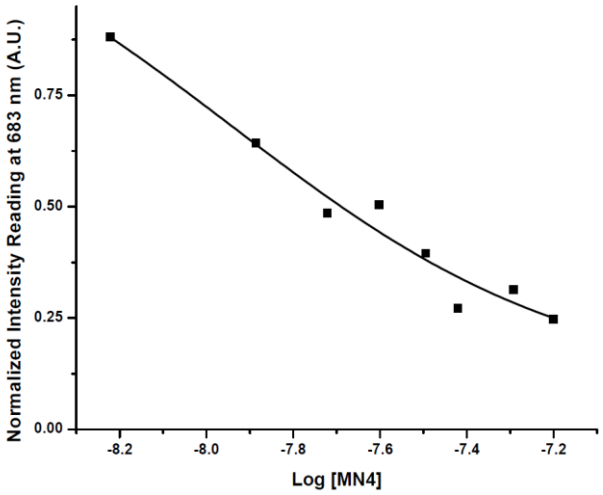

Figure 47. Normalized fluorescence intensity of methylene blue at λ_{em}= 683 nm versus log of concentration of the MN4 aptamer titrated into methylene blue. An attempt was made to fit the titration plot to a sigmoidal fit. The graph exhibits a sigmoidal-shaped modelled behaviour with low sigmoidicity. The midpoint was identified as -7.94 which enabled the calculation of a K_d value of (0.01 ± 0.02) µM. The error was determined through the fit of the curve.

In the SS1 aptamer titration plot, an average K_d value of (1.34 ± 0.09) µM was calculated. The average K_d value from the direct plot was calculated to be (2 ± 1) µM. The values are moderately close to each other which can indicate that both plots represent a moderately similar binding affinity of SS1 for methylene blue. However, it is also seen how the modelled behaviour between the duplicate experiments appears almost consistent. In Figure 48A, a sigmoidal-shaped modelled behaviour is observed, while in Figure 48B, it shows a sigmoidal-shaped curve with lower sigmoidicity compared to Figure 48A. It is difficult to determine if binding occurs based on the titration plots. Therefore, the direct plot method of analysis can be more effective in determining binding and binding affinities (Figure 24).

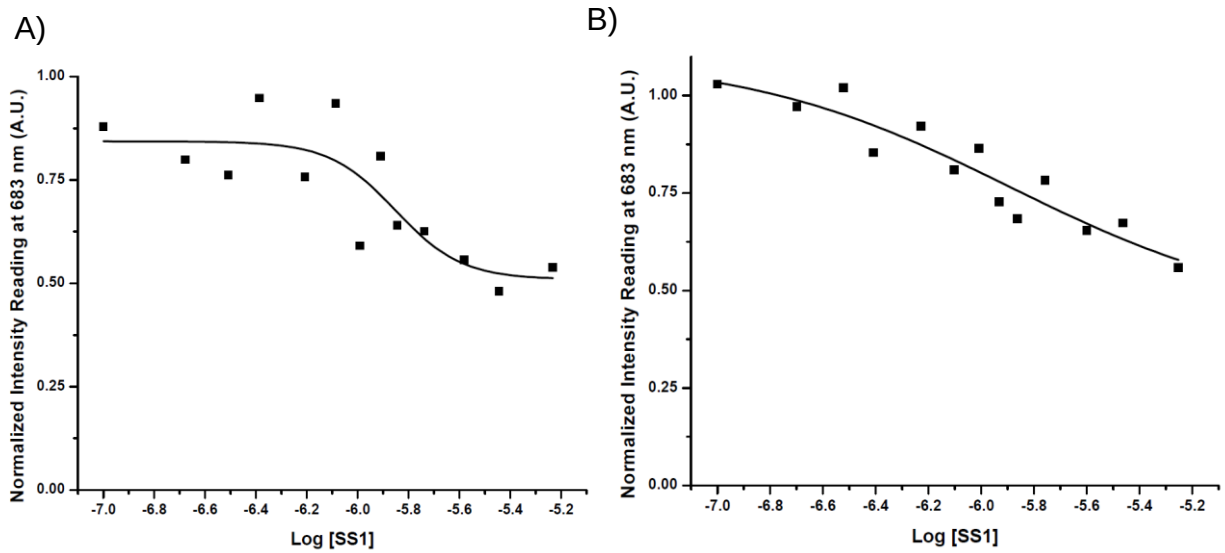

Figure 48. Normalized fluorescence intensity of methylene blue at λ_{em}= 683 nm versus log of concentration of the SS1 aptamer titrated into methylene blue. An attempt was made to fit the titration plots to a sigmoidal fit. (A) shows a sigmoidal-shaped curve. (B) shows a sigmoidal-shaped curve with lower sigmoidicity compared to (A). The modelled behaviours of both graphs appear almost consistent. The midpoint of the titration plots was identified as A) -5.85 and B) -5.89 which enabled the calculation of K_d values of A) 1.41 µM and B) 1.28 µM which gives an average K_d value of (1.34 ± 0.09) µM. The error was determined through standard deviation using data collected from 2 experiments.

In the TWJ titration plot, an average K_d value of (0.427 ± 0.009) µM was calculated. The average K_d value from the direct plot was calculated to be (0.461 ± 0.008) µM. The values presented are close to each other which shows how both plots represent a similar binding affinity of the aptamer for methylene blue. When the data was fit to a sigmoidal behaviour, the graphs for the duplicate experiments have a sigmoidal-shaped curve that have low sigmoidicity (Figure 49). The plots can indicate that binding is occurring between TWJ and methylene blue, however, to accurately quantify how tight or weak the binding is, a direct plot can be used to determine K_d values (Figure 25).

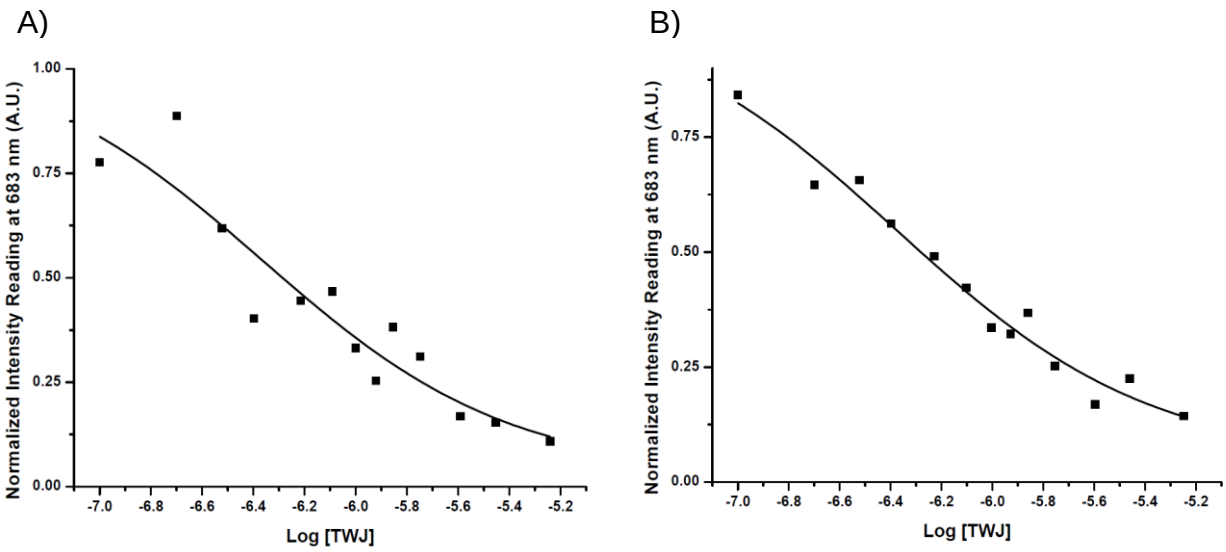

Figure 49. Normalized fluorescence intensity of methylene blue at λ_{em}= 683 nm versus log of concentration of TWJ titrated into methylene blue. An attempt was made to fit the titration plots to a sigmoidal fit. The graph for both (A) and (B) have a sigmoidal-shaped curve that have low sigmoidicity and therefore, the modelled behaviour of both graphs appears consistent. The midpoint of the titration plots was identified as A) -6.36 and B) -6.38 which enabled the calculation of K_d values of A) 0.43 µM and B) 0.42 µM which gives an average K_d value of (0.427 ± 0.009) µM. The error was determined through standard deviation using data collected from 2 experiments.

With the titration plot of Caff209, an average K_d value of (0.7 ± 0.3) µM was calculated. The average K_d value from the direct plot was calculated to be (0.6 ± 0.4) µM. The values are close to each other which shows that the two plots represent a similar binding affinity of Caff209 for methylene blue. The modelled behaviour for both plots appear consistent despite Figure 50B showing a sigmoidal-shaped curve less pronounced as Figure 50A. By looking at the plots, it can be determined that binding is occurring between Caff209 and methylene blue yet binding affinities can be analyzed more accurately using the direct plot (Figure 26).

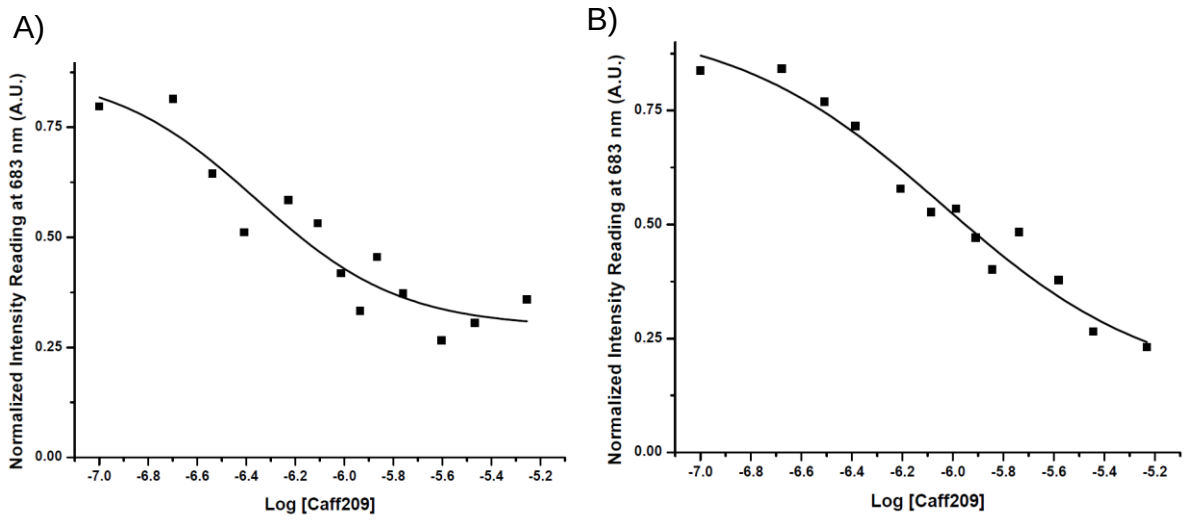

Figure 50. Normalized fluorescence intensity of methylene blue at λ_{em}= 683 nm versus log of concentration of the Caff209 aptamer titrated into methylene blue. An attempt was made to fit the titration plots to a sigmoidal fit. (A) shows a sigmoidal-shaped curve and (B) shows a sigmoidal-shaped curve less pronounced as (A). The modelled behaviour of both graphs appears consistent. The midpoint of the titration plots was identified as A) -6.36 and B) -6.04 which enabled the calculation of K_d values of A) 0.44 µM and B) 0.91 µM which gives an average K_d value of (0.7 ± 0.3) µM. The error was determined through standard deviation using data collected from 2 experiments.

The titration plot for the Caff209-3bp aptamer provided a K_d value of (1.6 ± 0.2) µM. The average K_d value from the direct plot was calculated to be (4 ± 2) µM. The values obtained are relatively far apart. This can be a result of how the K_d was calculated and obtained from the titration plot. Figure 51A shows a hyperbolic curve rather than a sigmoidal-shaped curve and the midpoint identified from this plot was 3.11 which is not a value within the range of the x-axis plotted. Therefore, this value was not taken for the calculation of K_d. Figure 51B shows a sigmoidal-shaped curve. The midpoint obtained from this plot gave the corresponding K_d value for this titration plot. Therefore, the K_d was solely based on one titration plot as a sigmoidal model could not be successfully fit for Figure 51A. The modelled behaviour between the duplicate experiments is not consistent and therefore, it can be difficult to accurately determine binding and binding affinities from a titration plot. Hence, a direct plot is a more accurate method of analysis (Figure 27).

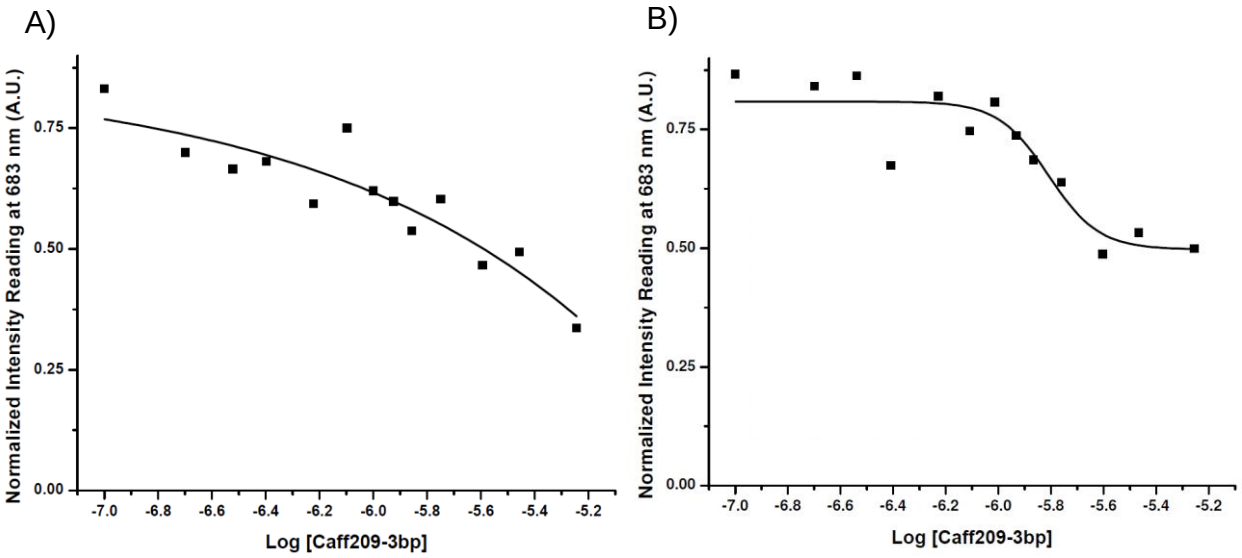

Figure 51. Normalized fluorescence intensity of methylene blue at λ_{em}= 683 nm versus log of concentration of the Caff209-3bp aptamer titrated into methylene blue. An attempt was made to fit the titration plots to a sigmoidal fit. (A) shows a hyperbolic curve rather than a sigmoidal-shaped curve and (B) shows a sigmoidal-shaped curve. The modelled behaviour between the duplicate experiments is not consistent. The midpoint of (A) was identified as 3.11 which is not a value within the range of the x-axis plotted. Therefore, this value was not taken for calculation of K_d. The midpoint of the titration plot for (B) was identified as -5.81 which enabled the calculation of a K_d value of (1.6 ± 0.2) µM. The error was determined through the fit of the curve.

Looking at the MTX5 titration plot, a K_d value of (0.55 ± 0.09) µM was calculated. The average K_d value from the direct plot was calculated to be (0.44 ± 0.02) µM. The obtained values are relatively close to each other which shows how the two plots represent a similar binding affinity of MTX5 for methylene blue. However, the K_d obtained from the titration plot is solely based on one experiment. Figure 52A shows a sigmoidal-shaped curve and Figure 52B appears linear rather than a sigmoidal-shaped curve therefore showing that the modelled behaviour between the duplicate experiments is not consistent. The midpoint of Figure 52B was identified as -5.69 which is close towards the end of the titration plot. Therefore, this value was not taken for the calculation of K_d. Figure 52A shows a sigmoidal model successfully fit and the midpoint was identified which led to the calculation of the K_d value. Thus, a direct plot can be used to accurately determine if binding is occurring between the MTX5 aptamer and methylene blue and to quantify the binding affinity (Figure 28).

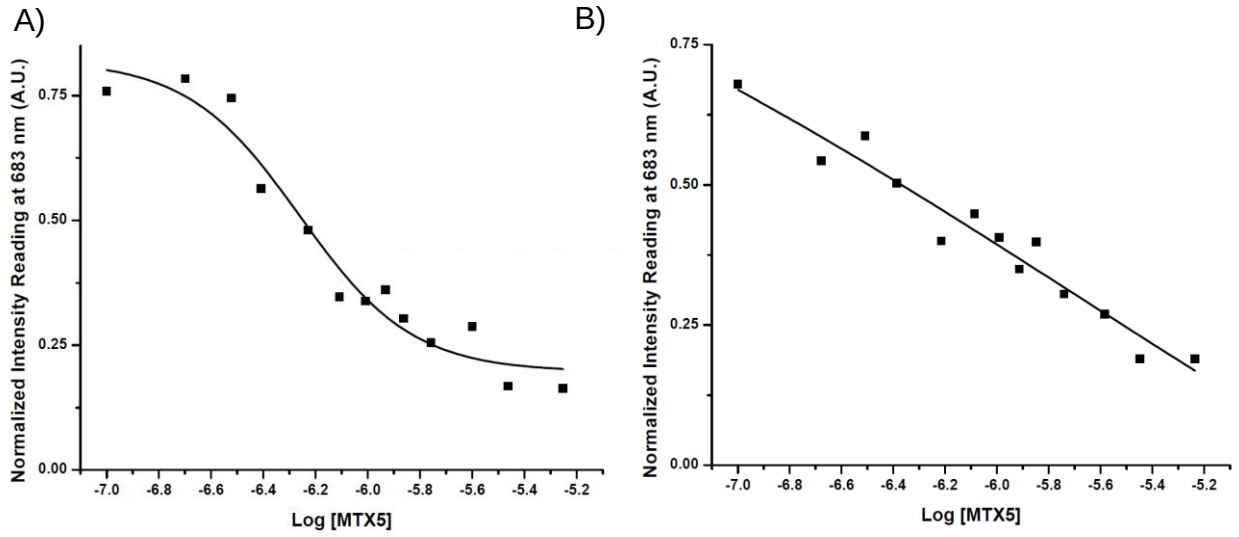

Figure 52. Normalized fluorescence intensity of methylene blue at λ_{em}= 683 nm versus log of concentration of the MTX5 aptamer titrated into methylene blue. An attempt was made to fit the titration plots to a sigmoidal fit. (A) shows a sigmoidal-shaped curve and (B) appears linear rather than a sigmoidal-shaped curve. The modelled behaviour between the duplicate experiments is not consistent. The midpoint of (B) was identified as -5.69 which is towards the end of the titration plot. Therefore, this value was not taken for calculation of K_d. The midpoint of (A) was identified as -6.26 and enabled the calculation of a K_d value of (0.55 ± 0.09) µM. The error was determined through the fit of the curve.

In the HMX38 titration plot, an average K_d value of (0.7 ± 0.5) µM was calculated. The average K_d value from the direct plot was calculated to be (0.5 ± 0.2) µM. The values are near each other which indicates the two plots presenting a similar binding affinity. However, it is important to recognize that the graphs for both Figure 53A and Figure 53B have a very low sigmoidicity despite the modelled behaviour of both graphs appearing consistent. It seems that the data presented on the titration plot does not fit as well to a sigmoidal model. It could be difficult to accurately determine whether binding is occurring just based off the titration plot and therefore, determine the binding affinity. Hence, a direct plot can be used to accurately determine if binding occurs and the binding affinity (Figure 29).

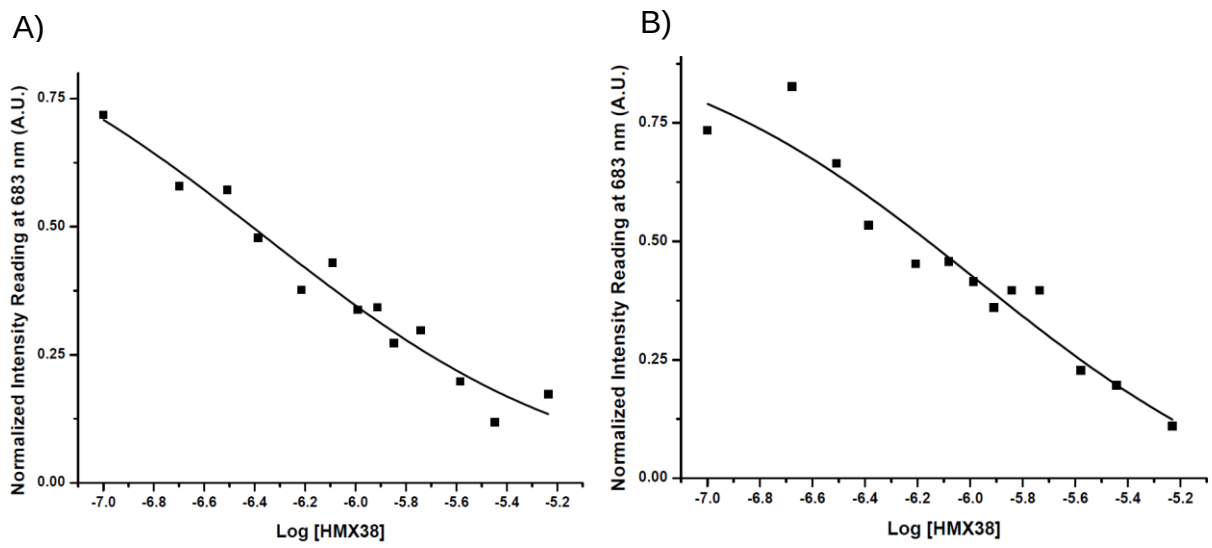

Figure 53. Normalized fluorescence intensity of methylene blue at λ_{em}= 683 nm versus log of concentration of the HMX38 aptamer titrated into methylene blue. An attempt was made to fit the titration plots to a sigmoidal fit. The graph for both (A) and (B) have a very low sigmoidicity, yet the modelled behaviour of both graphs appears consistent. The midpoint of the titration plots was identified as A) -6.37 and B) -5.97 which enabled the calculation of K_d values of A) 0.43 µM and B) 1.07 µM which gives an average K_d value of (0.7 ± 0.5) µM. The error was determined through standard deviation using data collected from 2 experiments.

In the HMX24 titration plot, a K_d value of (0.6 ± 0.9) µM was calculated. The average K_d value from the direct plot was calculated to be (0.6 ± 0.2) µM. The values obtained are the same which indicates that a direct plot and titration plot of the data provides the same binding affinity. However, the data may seem to not be accurately fit to a sigmoidal model and therefore, a titration plot would not be the primary method of analysis. Figure 54A has a sigmoidal-shaped curve with very low sigmoidicity and Figure 54B appears to be hyperbolic rather than a sigmoidal-shaped curve. Therefore, the modelled behaviour between the duplicate experiments is not consistent. The midpoint of Figure 54B was identified as -5.68 which is towards the end of the titration plot. Therefore, this value was not taken for the calculation of K_d. It seems that the midpoint identified is as if the x-axis were to be extended beyond the last titration so a sigmoidal-shaped modelled behaviour can be observed. Thus, experimental conditions can be optimized where titrations are still performed beyond the set parameters. Furthermore, the K_d obtained from the titration plot is solely just off of Figure 54A which shows how a direct plot of analysis can be a more reliable method of analysis to determine if binding is occurring and to quantify binding affinity (Figure 30).

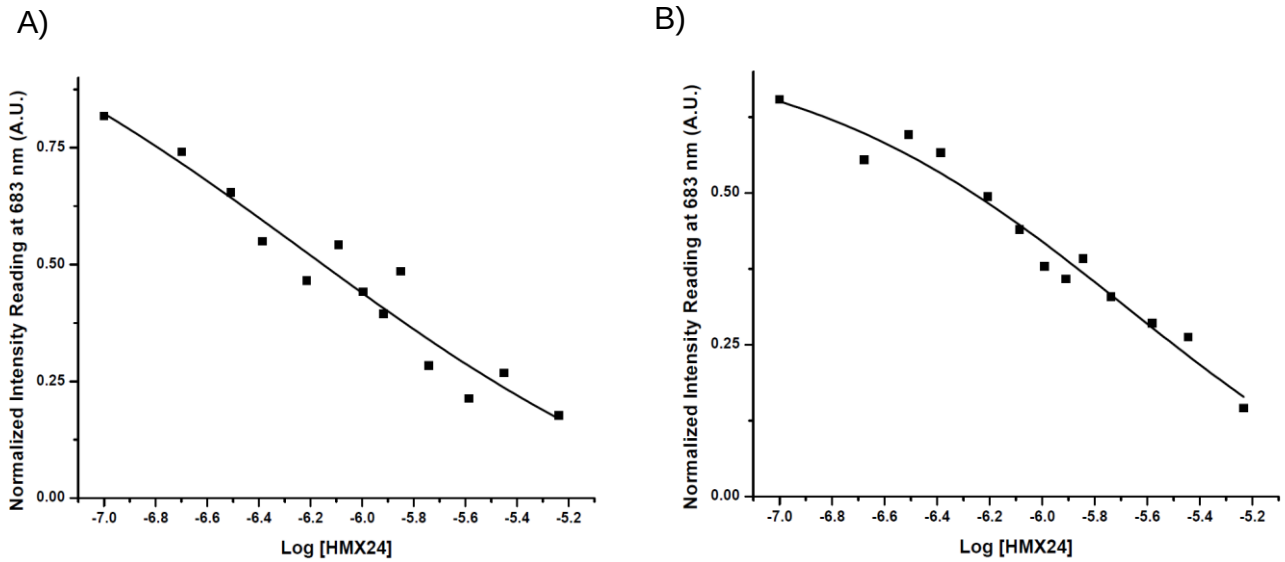

Figure 54. Normalized fluorescence intensity of methylene blue at λ_{em}= 683 nm versus log of concentration of the HMX24 aptamer titrated into methylene blue. An attempt was made to fit the titration plots to a sigmoidal fit. (A) has a sigmoidal-shaped curve with very low sigmoidicity and (B) appears to be hyperbolic rather than a sigmoidal-shaped curve. The modelled behaviour between the duplicate experiments is not consistent. The midpoint of (B) was identified as -5.68 which is towards the end of the titration plot. Therefore, this value was not taken for calculation of K_d. The midpoint of the titration plot for (A) was identified as -6.23 and enabled the calculation of a K_d value of (0.6 ± 0.9) µM. The error was determined through the fit of the curve.

A K_d value of (0.9 ± 0.7) µM was calculated for the Theo2201 titration plot. The average K_d value obtained for the direct plot was (0.99 ± 0.06) µM which shows how the two values are close to each other, and the two plots represent very similar binding affinities of the aptamer for methylene blue. However, it should be noted that the K_d obtained for the titration may be inaccurate despite being close to the value obtained from the direct plot. The data presented on the titration plot may not fit as well to a sigmoidal model. Figure 55A appears linear rather than a sigmoidal-shaped curve and Figure 55B shows a sigmoidal-shaped curve with low sigmoidicity which shows that the modelled behaviour between the duplicate experiments is not consistent. The midpoint of Figure 55A was identified as 7.69 which is not a value within the range of the x-axis plotted. Therefore, this value was not taken for the calculation of K_d. Hence, the K_d calculated from the titration plot is only based on one experiment. Thus, this suggests that the direct plot is a more effective method to accurately determine binding affinities between Theo2201 and methylene blue (Figure 31).

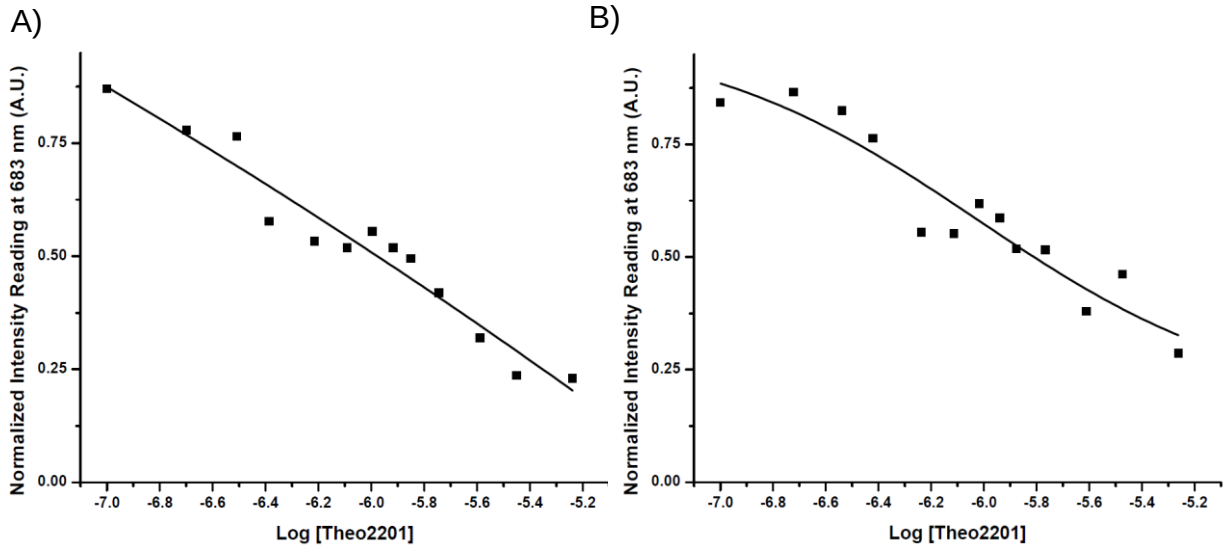

Figure 55. Normalized fluorescence intensity of methylene blue at λ_{em}= 683 nm versus log of concentration of the Theo2201 aptamer titrated into methylene blue. An attempt was made to fit the titration plots to a sigmoidal fit. (A) appears linear rather than a sigmoidal-shaped curve and (B) shows a sigmoidal-shaped curve with low sigmoidicity. The modelled behaviour between the duplicate experiments is not consistent. The midpoint of (A) was identified as 7.69 which is not a value within the range of the x-axis plotted. Therefore, this value was not taken for calculation of K_d. The midpoint of the titration plot for (B) was identified as -6.02 which enabled the calculation of a K_d value of (0.9 ± 0.7) µM. The error was determined through the fit of the curve.

An average K_d value of (1.3 ± 0.1) µM was calculated from the titration plot of Theo1. The average K_d value obtained from the direct plot was (1.3 ± 0.2) µM. The values are the same however, it should be noted that the obtained value from the titration plot can be inaccurate. The titration plot for Figure 56A appears to have a sigmoidal-shaped curve and Figure 56B shows a sigmoidal-shaped curve with very low sigmoidicity compared to Figure 56A. The modelled behaviour between the duplicate experiments is not consistent. Therefore, a titration plot may not be the best method to represent the binding affinity, yet a direct plot can used to accurately determine and quantify the binding affinity (Figure 32).

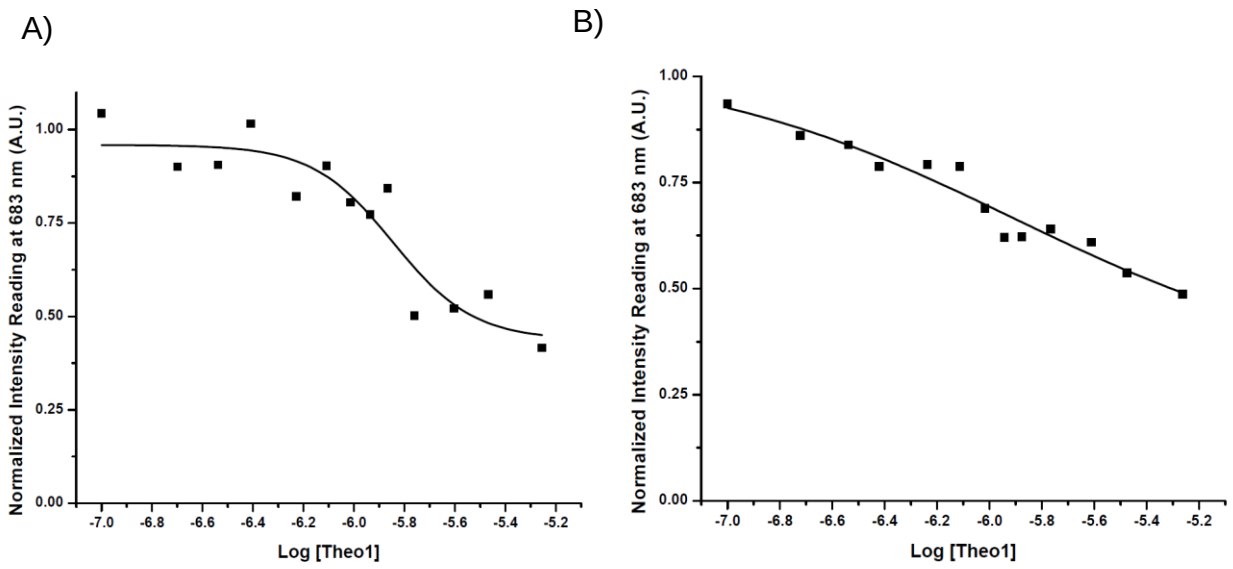

Figure 56. Normalized fluorescence intensity of methylene blue at λ_{em}= 683 nm versus log of concentration of the Theo1 aptamer titrated into methylene blue. An attempt was made to fit the titration plots to a sigmoidal fit. The titration plot for (A) appears to have a sigmoidal-shaped curve and (B) shows a sigmoidal-shaped curve with very low sigmoidicity compared to (A). The modelled behaviour between the duplicate experiments is not consistent. The midpoint of the titration plots was identified as A) -5.85 and B) -5.91 which enabled the calculation of K_d values of A) 1.43 µM and B) 1.24 µM which gives an average K_d value of (1.3 ± 0.1) µM. The error was determined through standard deviation using data collected from 2 experiments.

With the titration plot of the TRP94 aptamer, a K_d value of (1.2 ± 0.5) µM was calculated. When compared to the average K_d value obtained from the direct plot, (1.4 ± 0.5) µM, it shows that the values are nearly close to each other. However, the value obtained from the titration plot may also be inaccurate. The data presented on the titration plot may not be appropriate for a sigmoidal fit. Figure 57A appears hyperbolic rather than a sigmoidal-shaped curve where the midpoint identified, 10.46, is not a value within the range of the x-axis plotted. Therefore, this value was not taken for the calculation of K_d. Figure 57B shows a sigmoidal-shaped curve with low sigmoidicity which shows how the modelled behaviour between the duplicate experiments is not consistent. Although K_d values from the direct plot and titration plot are nearly the same, a direct plot can be used to accurately analyze binding affinity (Figure 33).

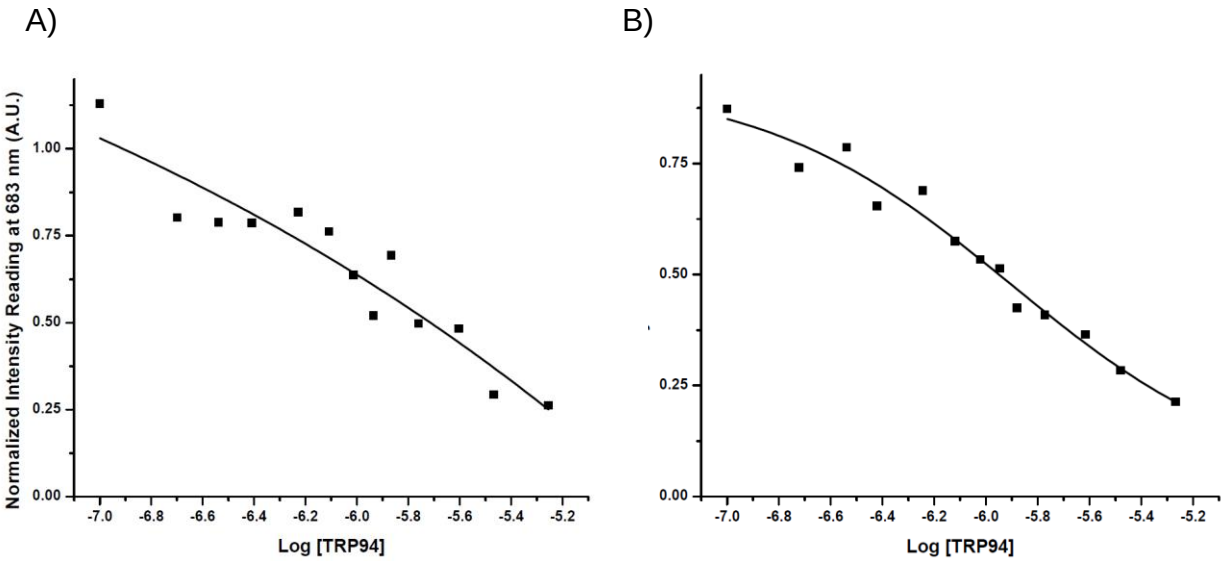

Figure 57. Normalized fluorescence intensity of methylene blue at λ_{em}= 683 nm versus log of concentration of the TRP94 aptamer titrated into methylene blue. An attempt was made to fit the titration plots to a sigmoidal fit. (A) appears hyperbolic rather than a sigmoidal-shaped curve and (B) shows a sigmoidal-shaped curve with low sigmoidicity. The modelled behaviour between the duplicate experiments is not consistent. The midpoint of (A) was identified as 10.46 which is not a value within the range of the x-axis plotted. Therefore, this value was not taken for calculation of K_d. The midpoint of (B) was identified as -5.90 which enabled the calculation of a K_d value of (1.2 ± 0.5) µM. The error was determined through the fit of the curve.

With the titration plot of the TRP94-2bp aptamer, an average K_d value of (0.7 ± 0.5) µM was calculated. The average K_d value obtained for the direct plot was (0.7 ± 0.5) µM. The values are the same which shows how the same binding affinity can be obtained from both the direct plot and titration plot. Both titration plots of the aptamer present a sigmoidal model although the sigmoidal shape looks less pronounced in Figure 58A compared to Figure 58B. The plots indicate that binding occurs between TRP94-2bp and methylene blue yet to accurately quantify how tight or weak the binding is, binding affinities can be analyzed from the direct plot (Figure 34).

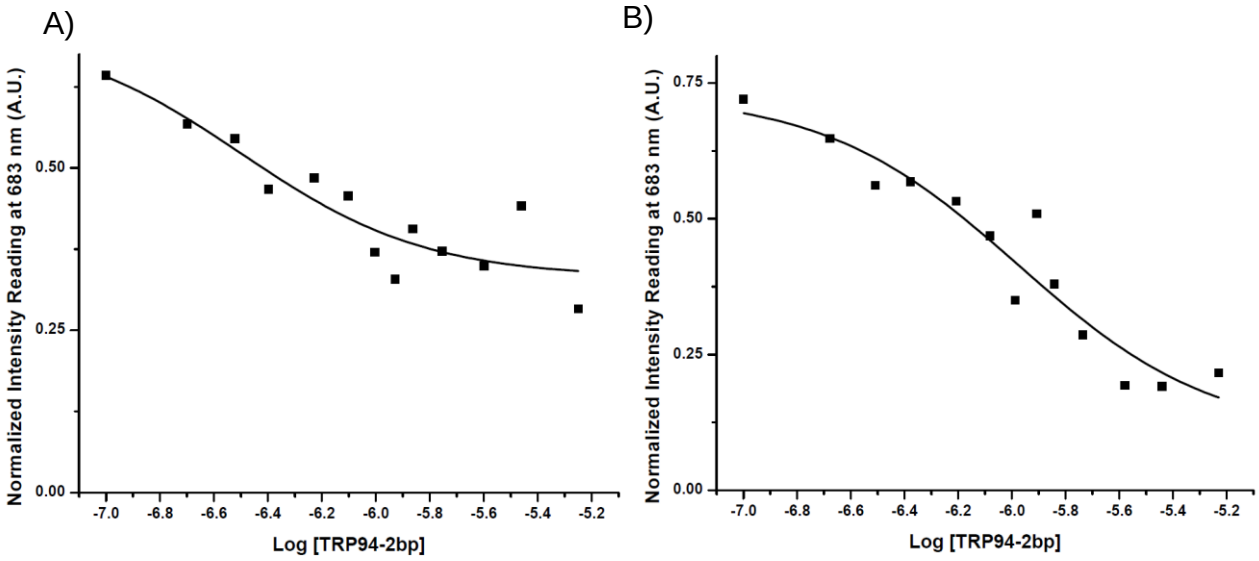

Figure 58. Normalized fluorescence intensity of methylene blue at λ_{em}= 683 nm versus log of concentration of the TRP94-2bp aptamer titrated into methylene blue. An attempt was made to fit the titration plots to a sigmoidal fit. The modelled behaviour of both runs have a sigmoidal-shaped curve. The modelled behaviour of both graphs appears consistent even though the sigmoidal shape looks less pronounced in (A) compared to (B). The midpoint of the titration plots was identified as A) -6.50 and B) -5.97 which enabled the calculation of K_d values of A) 0.32 µM and B) 1.06 µM which gives an average K_d value of (0.7 ± 0.5) µM. The error was determined through standard deviation using data collected from 2 experiments.

An average K_d value of (1.1 ± 0.2) µM was calculated from the titration plot of DA-5bp into methylene blue. This value is nearly the same as the average K_d value obtained from the direct plot which was (1.3 ± 0.4) µM. The modelled behaviour of both runs from the titration plot has a sigmoidal-shaped curve which makes them appear consistent (Figure 59). From the plot, it can be indicated that binding occurs between DA-5bp and methylene blue. Furthermore, to accurately quantify the binding affinity, the direct plot (Figure 35) would be a more appropriate method of analysis where the titration plot can be used to determine if binding occurs.

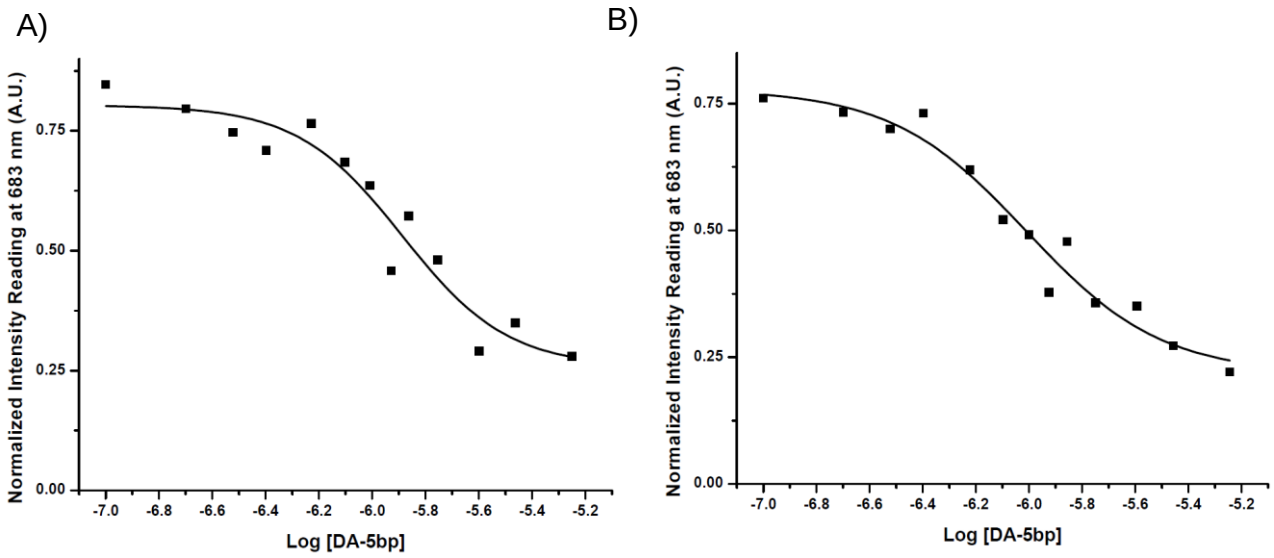

Figure 59. Normalized fluorescence intensity of methylene blue at λ_{em}= 683 nm versus log of concentration of the DA-5bp aptamer titrated into methylene blue. An attempt was made to fit the titration plots to a sigmoidal fit. The modelled behaviour of both runs have a sigmoidal-shaped curve which makes them appear consistent. The midpoint of the titration plots was identified as A) -5.89 and B) -6.01 which enabled the calculation of K_d values of A) 1.30 µM and B) 0.98 µM which gives an average K_d value of (1.1 ± 0.2) µM. The error was determined through standard deviation using data collected from 2 experiments.

An average K_d value of (1.2 ± 0.3) µM was calculated from the titration plot of DA-3bp into methylene blue. The average K_d value from the direct plot was shown to be (1.2 ± 0.4) µM. These values are the same which shows how the same binding affinity can be obtained from both the direct plot and titration plot. Figure 60A shows a sigmoidal-shaped curve and Figure 60B shows a sigmoidal-shaped curve less pronounced as Figure 60A. The modelled behaviour can indicate that binding occurs between DA-3bp and methylene blue. Hence, to accurately quantify the binding affinity, the direct plot (Figure 36) can be used where binding can be determined from the titration plot.

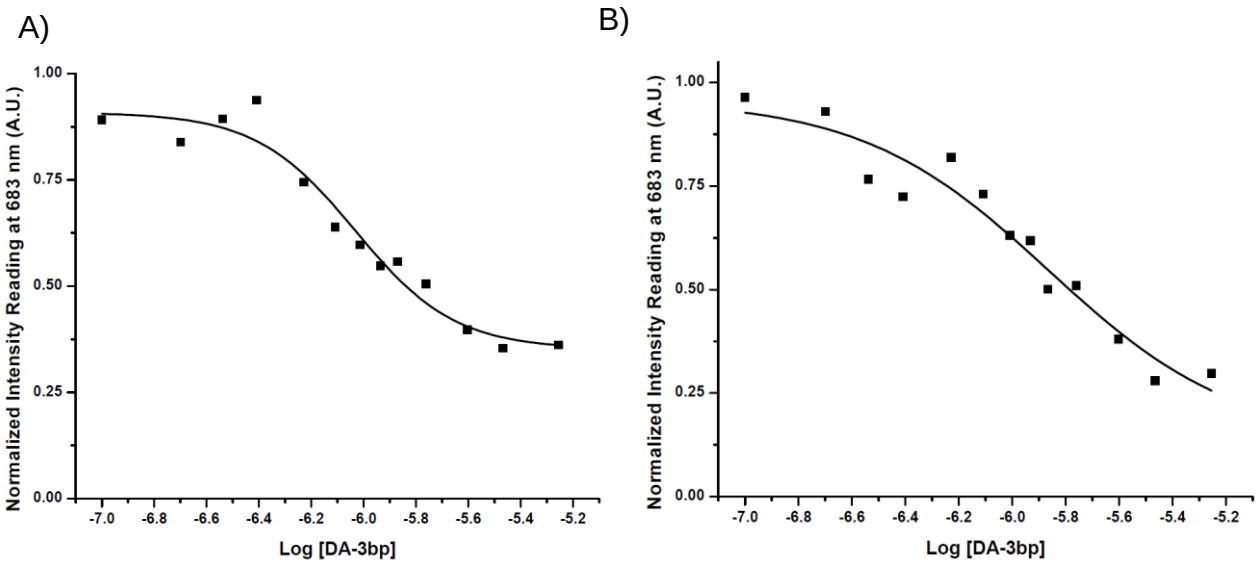

Figure 60. Normalized fluorescence intensity of methylene blue at λ_{em}= 683 nm versus log of concentration of the DA-3bp aptamer titrated into methylene blue. An attempt was made to fit the titration plots to a sigmoidal fit. (A) shows a sigmoidal-shaped curve and (B) shows a sigmoidal-shaped curve less pronounced as (A). The modelled behaviour of both graphs appears consistent. The midpoint of the titration plots was identified as A) -6.03 and B) -5.86 which enabled the calculation of K_d values of A) 0.93 µM and B) 1.37 µM which gives an average K_d value of (1.2 ± 0.3) µM. The error was determined through standard deviation using data collected from 2 experiments.

Looking at the Glu1 titration plot, a K_d value could not be calculated and compared to the direct plot. The data presented does not fit to a sigmoidal model as both runs of the Glu1 titration exhibit a linear modelled behaviour showing that the modelled behaviour of both graphs appear consistent. The midpoint of the titration plots was identified as -28.45 for Figure 61A and 14.60 for Figure 61B where both values do not fall under the range of the x-axis plotted. Therefore, K_d values could not be calculated from the midpoints obtained. Thus, this result suggests that a direct plot would be more suitable for analysis for the Glu1 titration experiment (Figure 37).

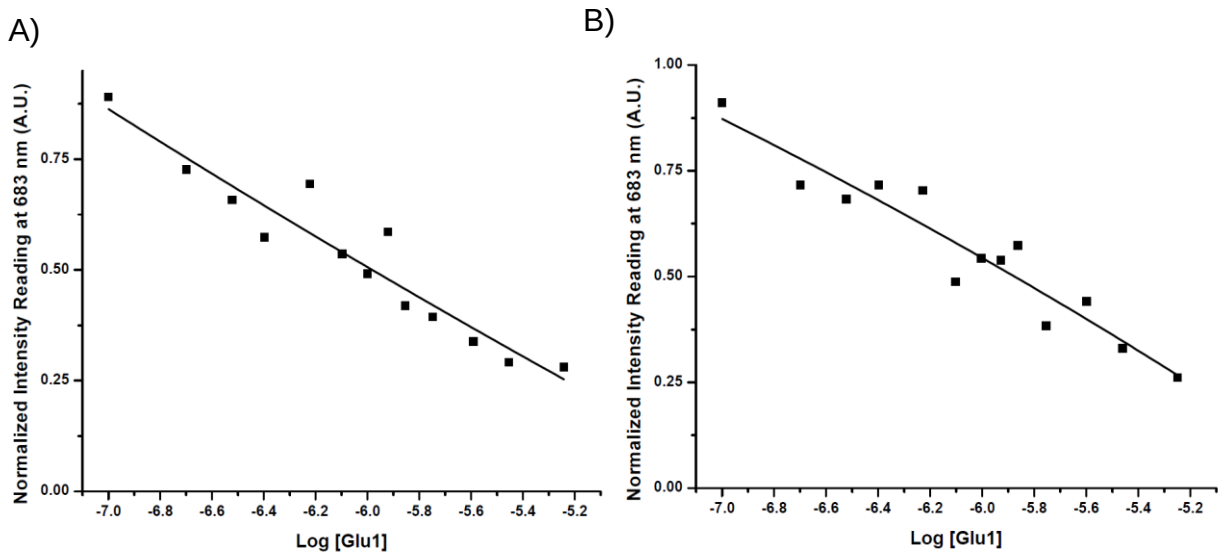

Figure 61. Normalized fluorescence intensity of methylene blue at λ_{em}= 683 nm versus log of concentration of the Glu1 aptamer titrated into methylene blue. An attempt was made to fit the titration plots to a sigmoidal fit however, both runs exhibit a linear modelled behaviour and therefore, the modelled behaviour of both graphs appear consistent. The midpoint of the titration plots was identified as A) -28.45 and B) 14.60 where both values do not fall under the range of the x-axis plotted. Therefore, K_d values could not be calculated from midpoints obtained.

When analyzing the Glu-mod12 titration plot, a K_d value of (1 ± 1) µM was calculated. For the direct plot analysis, an average K_d value of (2 ± 1) µM was obtained. These values are relatively close however, the K_d value obtained from the titration plot is solely based on one experiment. Figure 62A appears to have a sigmoidal-shaped curve with very low sigmoidicity. The K_d was still calculated from this plot, but Figure 62B did not have a K_d value calculated. A hyperbolic curve was shown rather than a sigmoidal-shaped curve making the modelled behaviour between the duplicate experiments appear inconsistent. The midpoint of the titration plot for Figure 62B was identified as 3.69 which is not a value within the range of the x-axis plotted. Therefore, this value was not taken for the calculation of K_d. Hence, the K_d was calculated just from Figure 62A. This result suggests that to accurately determine if binding occurs and to obtain the binding affinity, the direct plot is more effective (Figure 38).

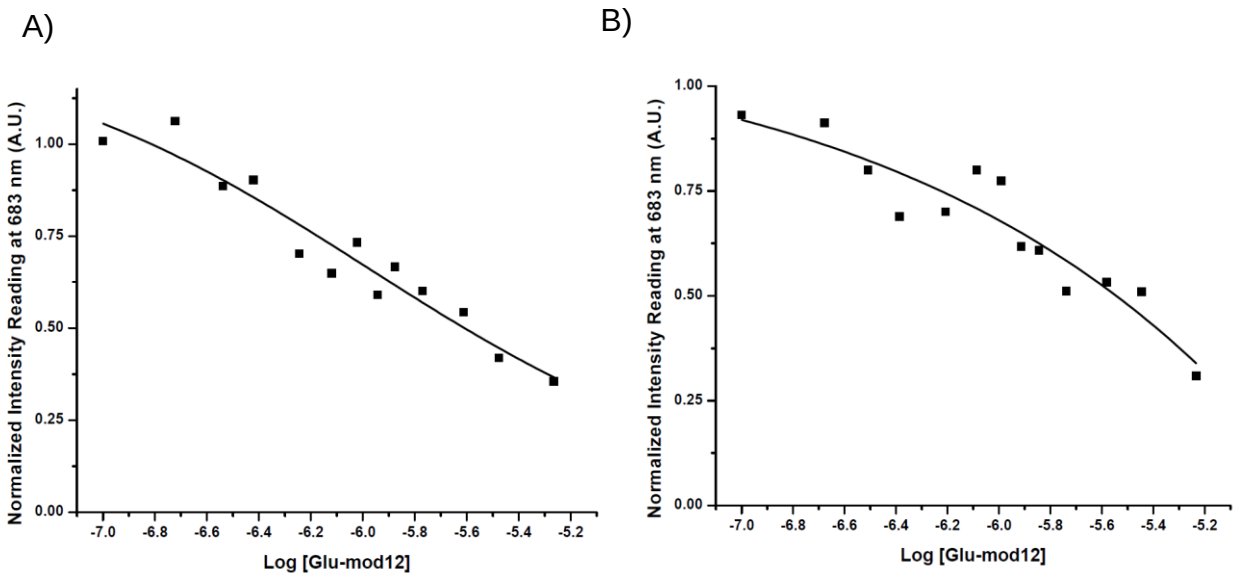

Figure 62. Normalized fluorescence intensity of methylene blue at λ_{em}= 683 nm versus log of concentration of the Glu-mod12 aptamer titrated into methylene blue. An attempt was made to fit the titration plots to a sigmoidal fit. (A) appears to have a sigmoidal-shaped curve with very low sigmoidicity and (B) shows a hyperbolic curve rather than a sigmoidal-shaped curve. The modelled behaviour between the duplicate experiments is not consistent. The midpoint of the titration plot for (B) was identified as 3.69 which is not a value within the range of the x-axis plotted. Therefore, this value was not taken for calculation of K_d. The midpoint of (A) was identified as -5.98 which enabled the calculation of a K_d value of (1 ± 1) µM. The error was determined through the fit of the curve.

In the OTA1-long titration plot, a K_d value of (0.7 ± 0.3) µM was calculated while for the direct plot, a K_d value of (0.5 ± 0.5) µM was calculated. This shows that the values obtained are relatively close to each other. The graph appears sigmoidal which can indicate that binding occurs between the aptamer and methylene blue (Figure 63). However, to accurately quantify the binding affinity, a direct plot can be used for analysis (Figure 39).

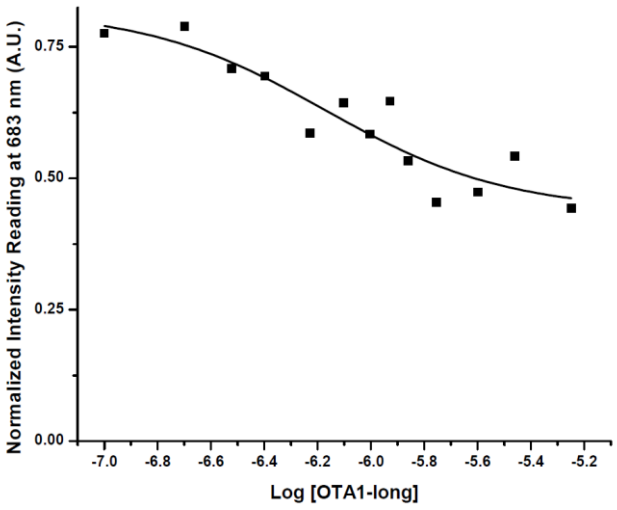

Figure 63. Normalized fluorescence intensity of methylene blue at λ_{em}= 683 nm versus log of concentration of the OTA1-long aptamer titrated into methylene blue. An attempt was made to fit the titration plot to a sigmoidal fit. The graph appears to exhibit a sigmoidal-shaped modelled behaviour where the midpoint was identified as -6.17 which enabled the calculation of a K_d value of (0.7 ± 0.3) µM. The error was determined through the fit of the curve.

In the OTA1 titration plot, a K_d value could not be calculated and compared to the direct plot. The data presented does not fit as well to a sigmoidal model as both runs of the OTA1 titration exhibit a hyperbolic model showing that the modelled behaviour of both graphs appear consistent. The midpoint of the titration plots was identified as -10.88 for Figure 64A and -9.74 for Figure 64B where both values do not fall under the range of the x-axis plotted. Therefore, K_d values could not be calculated from the midpoints obtained. It seems that the midpoints identified is as if the x-axis were to be extended before the start of the first titration so a sigmoidal-shaped modelled behaviour can be observed. Thus, experimental conditions such as aptamer concentration can be optimized so that a more accurate midpoint can be obtained. Overall, this result suggests that a direct plot (Figure 40) can be used to determine if binding occurs and analyze the binding affinity for the OTA1 titration experiment.

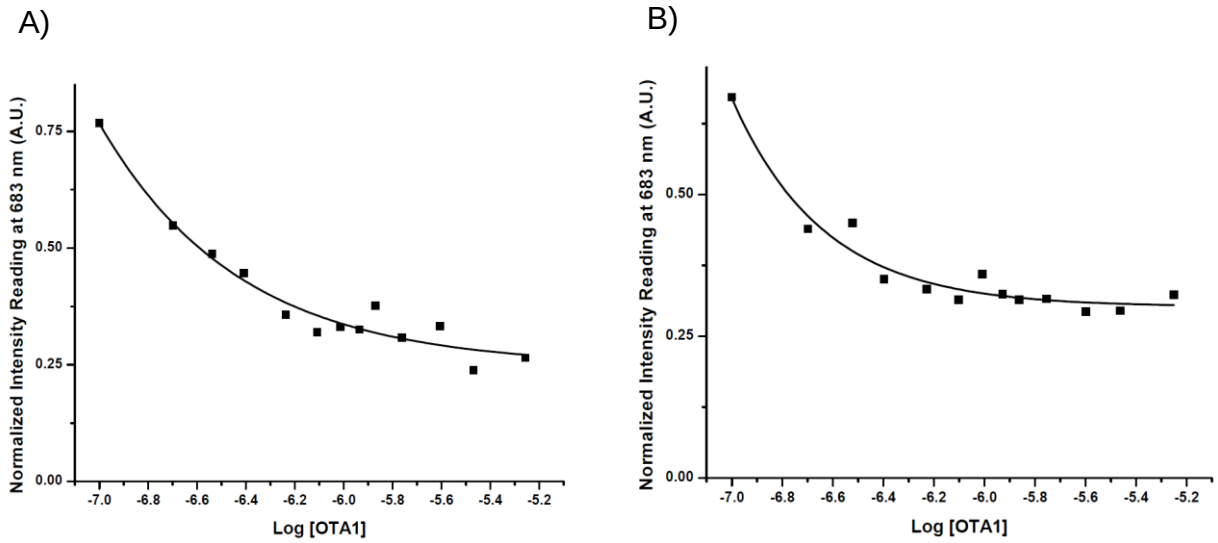

Figure 64. Normalized fluorescence intensity of methylene blue at λ_{em}= 683 nm versus log of concentration of the OTA1 aptamer titrated into methylene blue. An attempt was made to fit the titration plots to a sigmoidal fit, but both runs exhibit a hyperbolic modelled behaviour. Both modelled behaviours from the graphs appear consistent. The midpoint of the titration plots was identified as A) -10.88 and B) -9.74 where both values do not fall under the range of the x-axis plotted. Therefore, K_d values could not be calculated from midpoints obtained.

Looking at the 2G3b titration plot, a K_d value could not be calculated. The data presented does not fit as well to a sigmoidal model as the plot exhibits a hyperbolic curve (Figure 65). The midpoint was identified as -6.84 which is not a value within the range of the x-axis plotted. Therefore, this value was not taken for the calculation of K_d. It seems that the midpoint identified is as if the x-axis were to be extended beyond the last titration so a sigmoidal-shaped modelled behaviour can be observed. Thus, experimental conditions can be optimized where titrations are still performed beyond the set parameters. Hence, this result suggests that a direct plot would be a more accurate method for analysis (Figure 41).

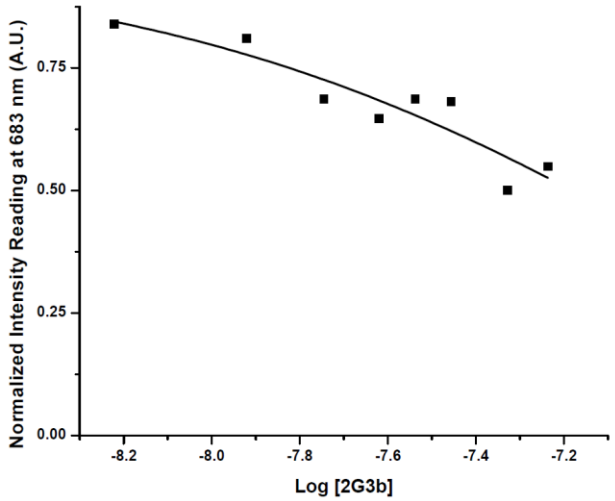

Figure 65. Normalized fluorescence intensity of methylene blue at λ_{em}= 683 nm versus log of concentration of the 2G3b aptamer titrated into methylene blue. An attempt was made to fit the titration plot to a sigmoidal fit however, the plot exhibits a hyperbolic curve rather than a sigmoidal-shaped modelled behaviour. The midpoint of the titration plot was identified as -6.84 which is not a value within the range of the x-axis plotted. Therefore, a K_d cannot be calculated with the midpoint obtained.

In the 2G4 titration plot, a K_d value of (0.2 ± 0.2) µM was calculated while an average K_d value of (0.22 ± 0.05) µM was obtained from the direct plot. These values are nearly the same which shows how both plots represent a very similar binding affinity of 2G4 for methylene blue. The titration plot shows a sigmoidal model with low sigmoidicity (Figure 66). Therefore, by looking at the graph, it can indicate that binding occurs between the aptamer and methylene blue however, to quantify how tight or weak the binding is, a direct plot (Figure 42) can be used.

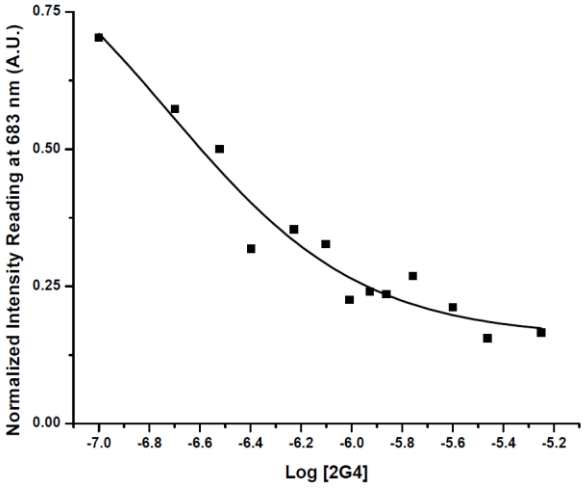

Figure 66. Normalized fluorescence intensity of methylene blue at λ_{em}= 683 nm versus log of concentration of the 2G4 aptamer titrated into methylene blue. An attempt was made to fit the titration plot to a sigmoidal fit. The graph appears to have a sigmoidal-shaped curve with low sigmoidicity where the midpoint was identified as -6.72 which enabled the calculation of a K_d value of (0.2 ± 0.2) µM. The error was determined through the fit of the curve.

In the MB1 titration plot, an average K_d value of (0.0153 ± 0.0005) µM was calculated. The average K_d value from the direct plot was calculated to be (0.013 ± 0.004) µM. These values are nearly the same which shows how the two plots represent a very similar binding affinity of the aptamer for methylene blue. The titration plot of both runs was successfully fit to a sigmoidal model which can indicate that binding is occurring between the MB1 aptamer and methylene blue (Figure 67). Furthermore, the binding affinity can be analyzed more accurately using a direct plot (Figure 43).

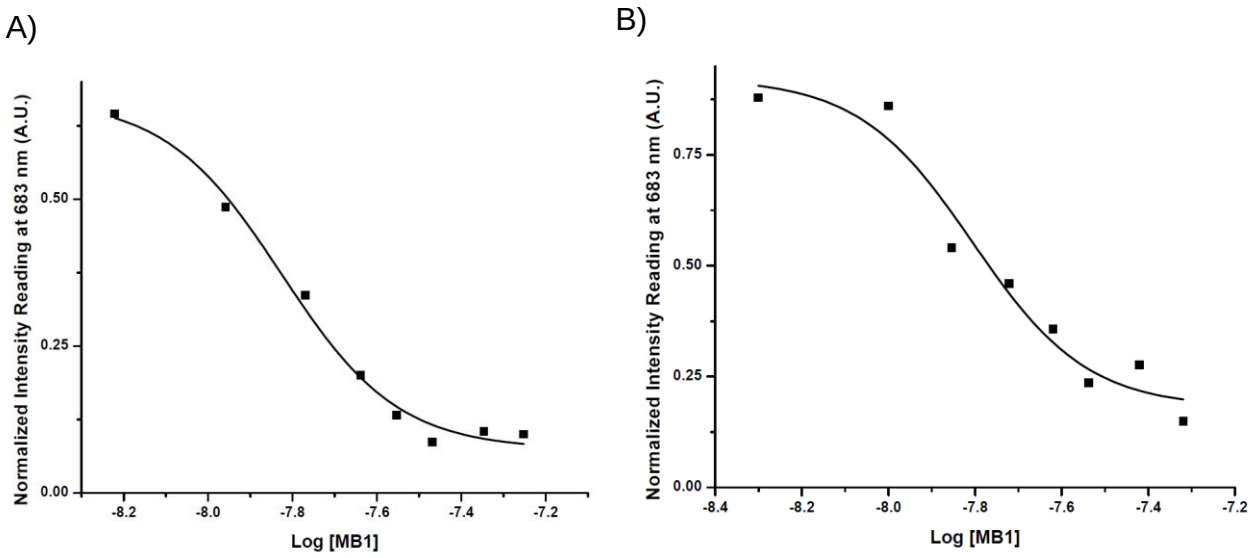

Figure 67. Normalized fluorescence intensity of methylene blue at λ_{em}= 683 nm versus log of concentration of the MB1 aptamer titrated into methylene blue. An attempt was made to fit the titration plots to a sigmoidal fit. The modelled behaviour of both runs have a sigmoidal-shaped curve which makes them appear consistent. The midpoint of the titration plots was identified as A) -7.83 and B) -7.80 which enabled the calculation of K_d values of A) 0.015 µM and B) 0.016 µM which gives an average K_d value of (0.0153 ± 0.0005) µM. The error was determined through standard deviation using data collected from 2 experiments.

For the DDD titration plot, a K_d value could not be calculated. Figure 68A appears to show a fit nearly horizontal at the beginning of the titration plot until the very end where it slightly starts to curve. The midpoint for Figure 68A was identified as -2.12 which is not a value within the range of the x-axis plotted. It seems that the midpoint identified is as if the x-axis were to be extended to observe a sigmoidal model. Hence, experimental conditions such as DNA concentration can be optimized to see if a sigmoidal model can be obtained. For Figure 68B, a sigmoidal fit was considered inappropriate to fit the data set and therefore, the graph does not show a specific modelled behaviour, and the K_d could not be calculated. The data is nearly horizontal which can indicate that there is almost no effect of DDD concentration titrated on

methylene blue fluorescence intensity which is almost like what is seen in Figure 68A. This result is like the direct plot analysis which indicates that methylene blue binds very weakly to DDD as a nonlinear binding function was not appropriate to fit the data, yet a linear function was successfully fit. Overall, to accurately determine if binding occurs, a direct plot is more effective (Figure 44).

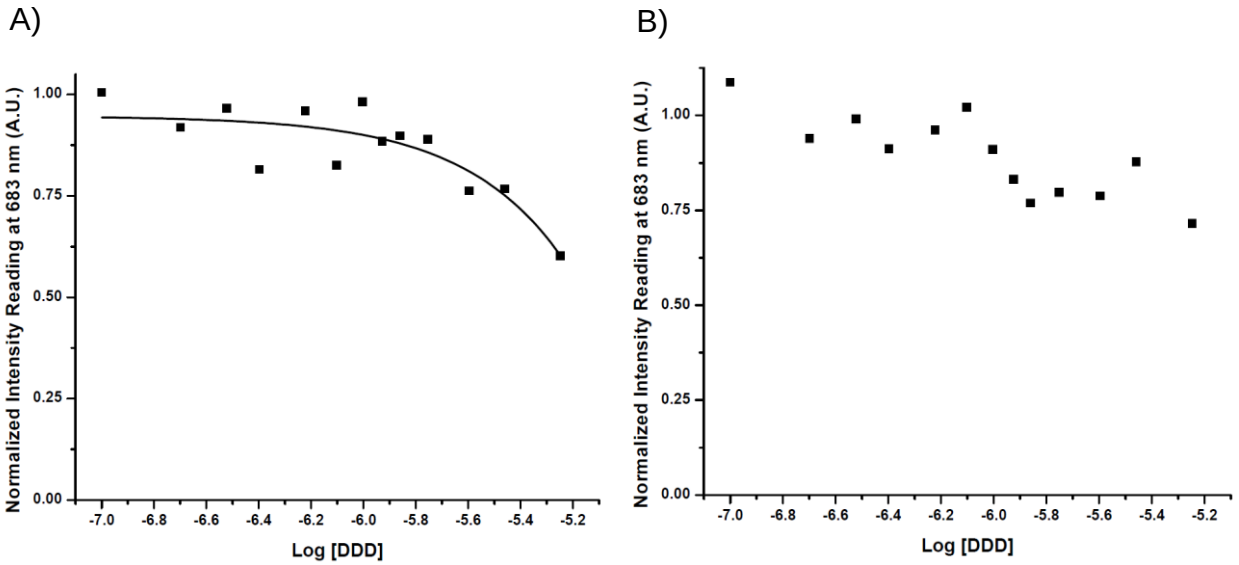

Figure 68. Normalized fluorescence intensity of methylene blue at λ_{em}= 683 nm versus log of concentration of the DDD duplex DNA sequence titrated into methylene blue. An attempt was made to fit the titration plot to a sigmoidal fit. (A) appears to present a fit that is nearly horizontal at the beginning of the titration plot until the very end where it slightly starts to curve. A sigmoidal fit was considered inappropriate to fit the data set for (B) and therefore, the graph does not show a specific modelled behaviour. The midpoint for (A) was identified as -2.12 which is not a value within the range of the x-axis plotted and the midpoint could not be identified for (B) as the data could not be fit. Therefore, K_d values cannot be calculated.

For the SJH titration plot, the data presented could not be fit to a sigmoidal model and therefore, there is no specific modelled behaviour observed. The data is nearly horizontal which can indicate that there is almost no effect of SJH concentration titrated on methylene blue fluorescence intensity (Figure 69). A midpoint could not be identified as the data could not be fit. Therefore, a K_d value could not be calculated. This result agrees with the result obtained from the direct plot analysis. The plot was fit to a linear function as a nonlinear binding function was not appropriate and it was shown that SJH binds very weakly to methylene blue (Figure 45). Nevertheless, to quantify the level of binding of SJH to methylene blue, a direct plot is a more accurate method of analysis.

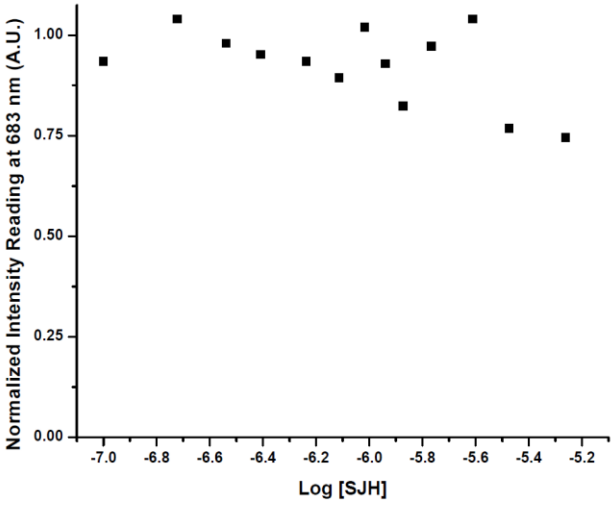

Figure 69. Normalized fluorescence intensity of methylene blue at λ_{em}= 683 nm versus log of concentration of the SJH duplex DNA sequence titrated into methylene blue. An attempt was made to fit the titration plot to a sigmoidal fit, yet a sigmoidal fit was considered inappropriate to fit this data set. The data appears almost horizontal which indicates that SJH binds very weakly to methylene blue.

Overall, it was shown that the K_d values obtained from the titration plot are relatively consistent and closely align with the K_d values obtained from the direct plot (Table 4). The results from the DDD and SJH titration demonstrated that they align with the results from the direct plot where the titration plot indicated that there is almost no effect of DNA titration on methylene blue fluorescence intensity and the direct plot indicated very weak binding. However, although there is consistency between the values, the values obtained from the titration plot may be inaccurate. It was shown that a sigmoidal fit did not fit as well for some of the data sets. It could not be determined whether binding occurred since an adequate sigmoidal curve was not generated, and midpoints could not be accurately identified to determine K_d. For some data sets, a sigmoidal model was fit and observed which indicated that there is binding between the aptamer and methylene blue. Therefore, it was determined that a direct plot would be more appropriate to accurately determine if binding occurred and to quantify the binding affinity in a consistent manner.

Table 4. Summary of binding affinities obtained from a titration plot for all aptamers titrated into methylene blue and successfully fit to a sigmoidal model. The K_d values were compared to the K_d values obtained from the direct plot. The error was determined through standard deviation of each experiment. * denotes that the error was determined through the fit of the curve.

Aptamer/DNA	**Direct Plot K_d values** (μM)	**Titration Plot K_d values** (μM)
2G4	(0.22 ± 0.05)	(0.2 ± 0.2)*
TRP94-2bp	(0.4 ± 0.3)	(0.7 ± 0.5)
MTX5	(0.44 ± 0.02)	(0.55 ± 0.09)*
TWJ	(0.461 ± 0.008)	(0.427 ± 0.009)
HMX38	(0.5 ± 0.2)	(0.7 ± 0.5)
HMX24	(0.6 ± 0.2)	(0.6 ± 0.9)*
Caff209	(0.6 ± 0.4)	(0.7 ± 0.3)
Theo2201	(0.99 ± 0.06)	(0.9 ± 0.7)*
Glu1	(1.1 ± 0.3)	N/A
DA-3bp	(1.2 ± 0.4)	(1.2 ± 0.3)
Theo1	(1.3 ± 0.2)	(1.3 ± 0.1)
DA-5bp	(1.3 ± 0.4)	(1.1 ± 0.2)
TRP94	(1.4 ± 0.5)	(1.2 ± 0.5)*
Glu-mod12	(2 ± 1)	(1 ± 1)*
SS1	(2 ± 1)	(1.34 ± 0.09)
Caff209-3bp	(4 ± 2)	(1.6 ± 0.2)*
MN19	(0.14 ± 0.04)	(0.29 ± 0.08)
OTA1-long	(0.5 ± 0.5)*	(0.7 ± 0.3)*
OTA1	(0.13 ± 0.04)	N/A
MN4	(0.017 ± 0.002)	(0.01 ± 0.02)*
MB1	(0.013 ± 0.004)	(0.0153 ± 0.0005)
2G3b	(0.07 ± 0.05)*	N/A
DDD	N/A	N/A
SJH	N/A	N/A

Analysis through NMR Spectroscopy

NMR was conducted of methylene blue titrated into the MB1 and RKEC1 aptamer and the DDD duplex DNA sequence. As discussed before, MB1 is an aptamer selected for methylene blue and it was shown through fluorescence experiments that MB1 binds very tightly to methylene blue (Figure 43). It was of interest to see if there is structure formation with ligand binding that may cause the aptamer to bind very tightly to methylene blue. Figure 70 shows some peaks in the free state which suggests that there is some base-pairing in the free state of the aptamer. This indicates that the aptamer has a partially preformed structure in the free state

which most likely is the stem region (Figure 70). New peaks start to appear at 0.20 equivalents of methylene blue around 14.3 and 13.0 ppm and at 0.50 equivalents, another peak appears at around 11.7 ppm. Peaks also start to shift to become resolved from one another at 0.50 equivalents of methylene blue around 12.5 ppm. This can indicate that there are more imino protons that may be involved in base-pairing upon addition of methylene blue which show that there may be slight structure formation with ligand binding.

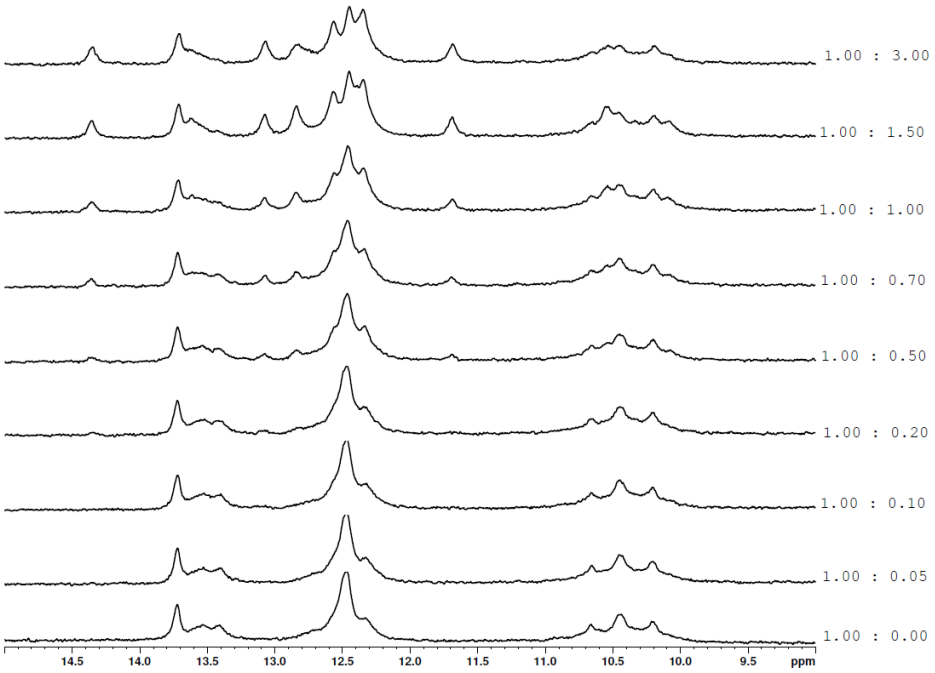

Figure 70. 1D ^{1}H-NMR spectra showing the imino proton resonances of the MB1 aptamer with methylene blue. All NMR data showed was collected in 10 mM $Na_xH_yPO_4$, 140 mM NaCl, pH 7.4 and 10% D_2O at 5°C. Data was collected by Yunus Kaiyum. The molar ratio of aptamer: ligand is noted to the right of each spectrum.

Methylene blue has been found to be a DNA intercalator, but it was found in this study that methylene blue binds very weakly to DDD through fluorescence (Figure 44). NMR was conducted as another method to see this observation. Figure 71 shows the duplex of DDD and upon titration of methylene blue, there is a reduction in the intensity of the peaks shown until 2.00 equivalents of methylene blue is added where the peaks are almost no longer present (Figure 71). This result is consistent with the finding that methylene blue intercalates duplex DNA as peaks are almost no longer present. This may be due to methylene blue disrupting base-pairing. The results suggest that the aptamer becomes more dynamic and loses rigidity in its structure. Overall, this result indicates that methylene blue interacts with duplex DNA. In

comparison to the NMR experiments, the fluorescence direct plot analysis would be a more accurate method when determining and quantifying the binding affinity. This is because fluorescence requires working concentrations of the DNA that are lower than the K_d value while NMR requires working concentrations that are higher than the K_d. Therefore, NMR can be used to determine if binding occurs between DDD and methylene blue but to determine and quantify the binding affinity, a fluorescence direct plot analysis can be used.

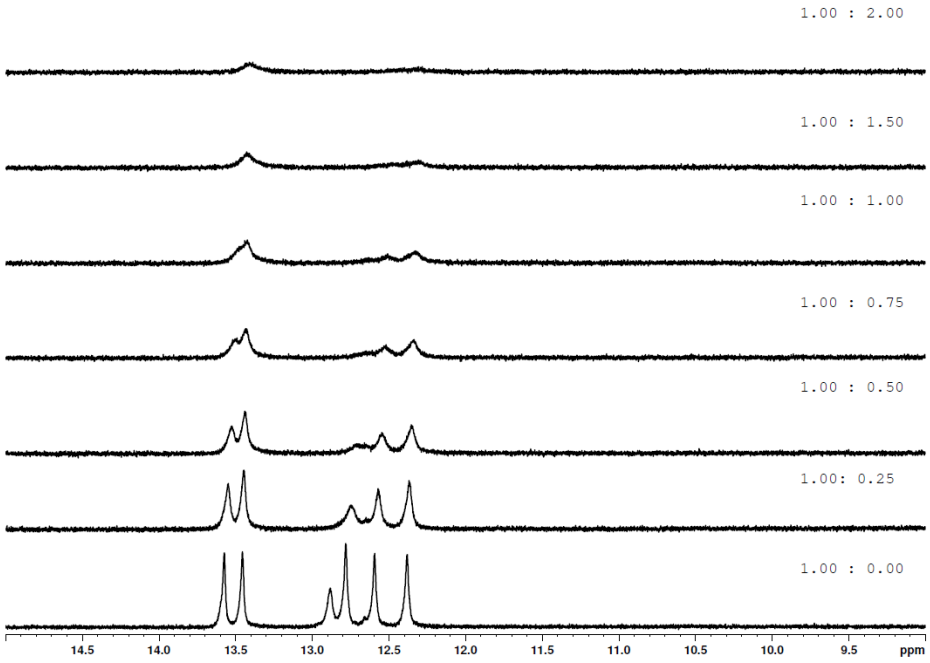

Figure 71. 1D ^{1}H-NMR spectra showing the imino proton resonances of DDD with methylene blue. All NMR data showed was collected in 10 mM $Na_xH_yPO_4$, 140 mM NaCl, pH 7.4 and 10% D_2O at 5°C. Data was collected by Yunus Kaiyum. The molar ratio of aptamer: ligand is noted to the right of each spectrum.

This result is almost similar to the NMR result of amodiaquine binding DDD. A study was done by Slavkovic *et al.* to understand the exceptionally high affinity interaction between the cocaine-binding aptamer and amodiaquine.[43] This was achieved by analyzing interactions of DNA structures with amodiaquine, which includes DDD. The conclusion made from this study was that amodiaquine binds tightly to all duplex DNA structures examined and appears to exhibit non-specific DNA-binding properties.[43] When looking at Figure 72, the spectrum shows the DNA duplex of DDD and upon titration of 0.33 equivalents of amodiaquine, there is a significant reduction in the intensity of the peaks shown to a point where the peaks are almost no longer present. However, there also seems to be a peak forming around 9.8 ppm and the intensity of the

peak slowly starts to increase until 2.0 equivalents of amodiaquine is titrated (Figure 72). When comparing this result with DDD binding methylene blue, the peaks shown on the spectrum also reduce in intensity until they are almost no longer present but, this observation is seen when 2.00 equivalents of methylene blue is titrated (Figure 71). In addition, no new peaks are starting to form as seen with the peak starting to slowly increase in intensity around 9.8 ppm for DDD binding amodiaquine. This can show how methylene blue binds weaker than amodiaquine to DDD as higher equivalents of methylene blue are needed to observe an equivalent reduction in the intensity of peaks on the spectra.

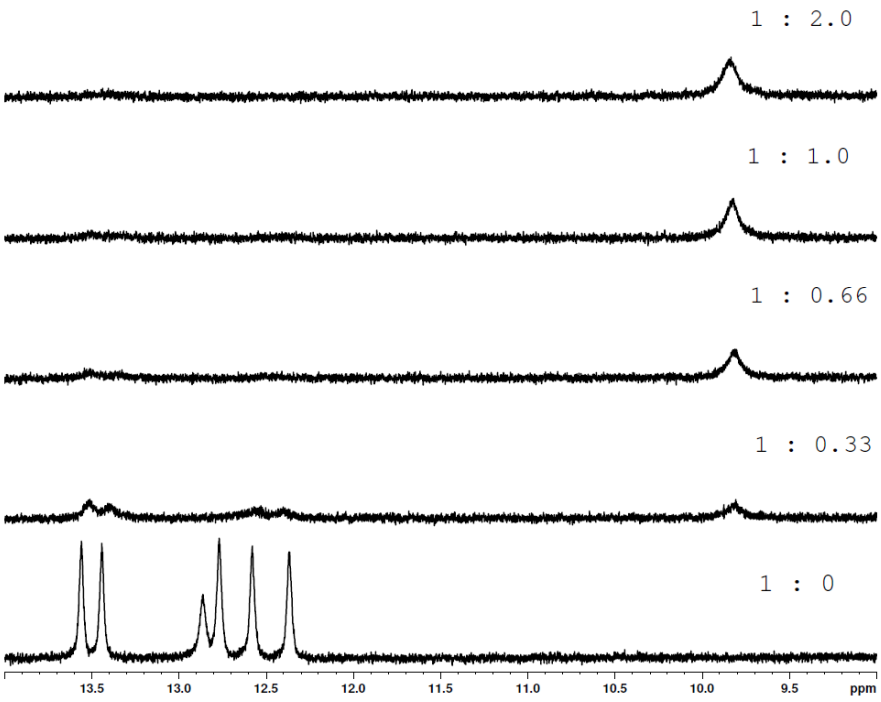

Figure 72. 1D ^{1}H-NMR spectra showing the imino proton resonances of DDD with amodiaquine. All NMR data showed was collected in 10 mM $Na_xH_yPO_4$, 140 mM NaCl, pH 6.8 and 10% D_2O at 5°C. Data was collected by Yunus Kaiyum. The molar ratio of aptamer: ligand is noted to the right of each spectrum.

Lastly, NMR was conducted to track the binding between the RKEC1 aptamer and methylene blue since the actual structure is known for an aptamer instead of a predicted secondary structure. The spectrum shows that the aptamer has a preformed structure in the free state and upon titration of methylene blue, there is a reduction in the intensity of the peaks (Figure 73). At 10.0 ppm, a shift in the peaks is observed where they become resolved from one another. Magnesium was added at 1.00 equivalents of methylene blue to see if there was a

change in NMR spectra and no significant changes were observed. Further reduction in the intensity of peaks is observed once higher equivalents of methylene blue are titrated. The results indicate that methylene blue binds to the RKEC1 aptamer and may disrupt base-pairing of the aptamer.

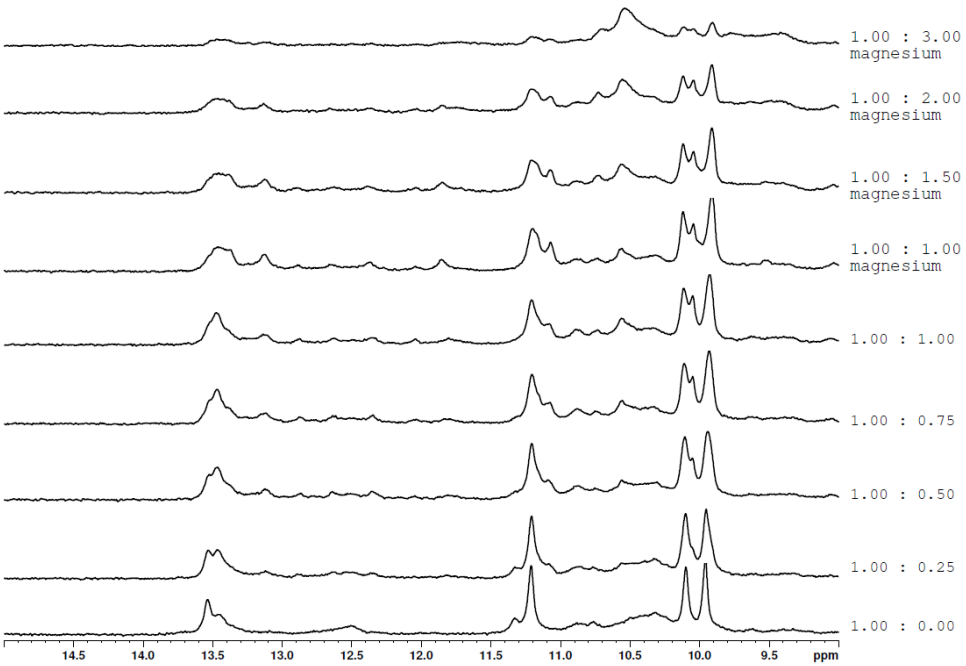

Figure 73. 1D ^{1}H-NMR spectra showing the imino proton resonances of the RKEC1 aptamer with methylene blue. All NMR data showed was collected in 10 mM $Na_xH_yPO_4$, 140 mM NaCl, pH 7.4 and 10% D_2O at 5°C. 2 mM $MgCl_2$ was added into the buffer conditions at 1.00 equivalents of methylene blue. Data was collected by Yunus Kaiyum. The molar ratio of aptamer: ligand is noted to the right of each spectrum.

When comparing this result to the data of the DA-5bp aptamer, the parent aptamer of the dopamine-binding aptamer, binding dopamine, it is not evident that the RKEC1 aptamer has structure formation upon addition of methylene blue, but the aptamer becomes more dynamic and loses rigidity in its structure. The NMR spectra of DA-5bp shows that the aptamer has a preformed structure in the free state. Upon addition of dopamine in 0.25 equivalent increments, there is a significant amount of structure change observed (Figure 74). New peaks start to appear both upfield and downfield of the previously detected peaks in the free state. The peak observed at around 13.5 ppm increases in intensity and peaks also start to shift to become resolved from one another observed between 12.0 and 13.0 ppm. Therefore, it shows that DA-5bp has a ligand-induced structure-switching binding mechanism towards dopamine as it is observed with the

structural changes in the NMR spectra. In contrast, RKEC1 has its structure disrupted upon binding methylene blue as observed with the reduction in the intensity of pre-existing peaks.

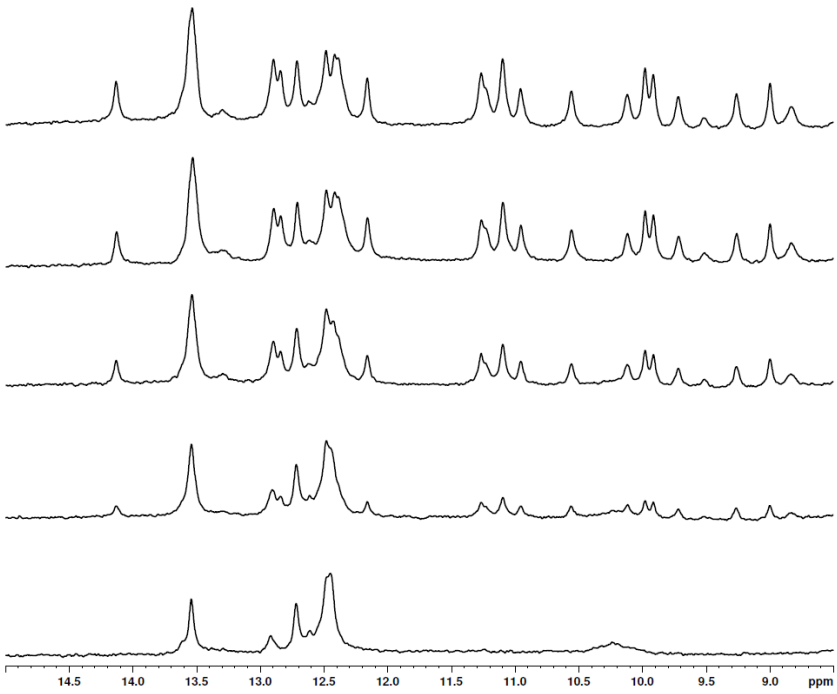

Figure 74. 1D ^{1}H-NMR spectra showing the imino proton resonances of the DA-5bp aptamer with dopamine. All NMR data showed was collected in 20 mM $Na_xH_yPO_4$, pH 7.4 and 10% D_2O at 5°C. Dopamine was added in 0.25 equivalent increments with the first spectrum being DA-5bp in the free state. Data was collected by Yunus Kaiyum.

Conclusions

It was shown through a direct plot analysis that methylene blue binds very weakly to duplex DNA sequences such as DDD and SJH but binds tightly to aptamer structures containing a bulge or stem-loop structure. The titration plots also showed how a sigmoidal fit was inappropriate to fit the data for the DDD and SJH titration as a modelled behaviour could not be observed and the midpoint could not be identified to calculate the K_d. The plots showed nearly a horizontal line which indicates that there is almost no effect of the titration of the DNA sequences on the fluorescence intensity of methylene blue. Also, some K_d values obtained from the titration plots for the aptamers were close to or in line with the values obtained from the direct plot, however, it was still determined that the direct plot would be a more accurate method to analyze the data. This is because a sigmoidal fit was determined to be inappropriate to fit some data sets of the titration plots for the aptamers. As a result, midpoints could not be identified, and

K_d values could not be calculated. The plots also showed a sigmoidal fit with low sigmoidicity which determined that binding occurred between the aptamer and methylene blue but did not quantify how tight or weak the binding was. Furthermore, NMR showed that binding occurs with the MB1 and RKEC1 aptamer and the DDD duplex DNA sequence. There was slight structure formation observed with the MB1 aptamer when titrated with methylene blue. There was a reduction in the intensity of the peaks when methylene blue was titrated into DDD and RKEC1 which indicates that methylene blue interacts with them and may be disrupting base-pairing. Overall, it can be shown that methylene blue intercalates DDD as expected with NMR, but binding affinity can be accurately determined with a direct plot analysis of fluorescence. This is because results obtained with fluorescence are achieved by working at aptamer/DNA concentrations lower than the K_d value while NMR requires higher concentrations that exceed the K_d value to obtain reliable data. In conclusion, by looking at the results, methylene blue may be binding tightly to aptamer structures such as bulges and stem-loops but show a weak binding interaction with duplex DNA.

Chapter 4. Future Work

In the structure-switching aptamers project, we observed that the affinity of the MN19 aptamer for its ligand quinine decreases as we increase the NaCl concentration from 140 mM to 1000 mM. However, the contribution of electrostatics was less for MN19 binding quinine than MN4 binding quinine at 140 mM NaCl. It was also seen how the binding affinity increases again as the NaCl concentration is increased to 2000 mM. Even though this trend was like the one seen for the DaMut3 aptamer binding dopamine, more data points are needed to confirm this increase in affinity as only one data point was obtained. Also, this project will include working on other structure-switching aptamers that do not have two-site binding. As mentioned with the MN19 aptamer, when NaCl concentration is decreased below 140 mM, two-site binding is observed and prevents the analysis of the binding affinity of the structure-switching aptamer at lower NaCl concentrations. Furthermore, a structure-switching aptamer that depends on NaCl concentration should not be chosen as this would also not allow the analysis of the binding affinity at lower NaCl concentrations. This is due to the aptamer requiring higher NaCl concentrations to function appropriately. Some structure-switching aptamers that are candidates for this study are Caff209, a variant of the caffeine-binding aptamer, TRP94, a tryptophan-binding aptamer, and HMX38, a methotrexate-binding aptamer.[32-34]

In the methylene blue project, it was seen that methylene blue binds tightly to aptamer structures such as bulges and stem-loops but binds very weakly to duplex DNA as seen with DDD and SJH. For future work, each aptamer's corresponding ligand can be added to the methylene blue-aptamer complex to see if it competes with methylene blue for the same binding site. If methylene blue is displaced, an increase in its fluorescence intensity is expected.

References

1. Minchin, S.; Lodge, J. Understanding biochemistry: structure and function of nucleic acids. *Essays in Biochemistry*. **2019**, *63* (4), 433-456. DOI:10.1042/EBC20180038
2. Guan, B.; Zhang, X. Aptamers as Versatile Ligands for Biomedical and Pharmaceutical Applications. *International Journal of Nanomedicine*. **2020**, *15*, 1059–1071. DOI:10.2147/IJN.S237544
3. Ni, X.; Castanares, M.; Mukherjee, A.; Lupold, S.E. Nucleic acid aptamers: clinical applications and promising new horizons. *Current Medicinal Chemistry*. **2011**, *18* (27), 4206-4214. DOI:10.2174/092986711797189600
4. Kim, D.H.; Seo, J.M.; Shin, K.J.; Yang, S.G. Design and clinical developments of aptamer-drug conjugates for targeted cancer therapy. *Biomaterials Research*. **2021**, *25* (1), 42. DOI:10.1186/s40824-021-00244-4
5. Chheda, U.; Pradeepan, S.; Esposito, E.; Strezsak, S.; Fernandez-Delgado, O.; Kranz, J. Factors Affecting Stability of RNA - Temperature, Length, Concentration, pH, and Buffering Species. *Journal of Pharmaceutical Sciences*. **2024**, *113* (2), 377-385. DOI: 10.1016/j.xphs.2023.11.023
6. Odeh, F.; Nsairat, H.; Alshaer, W.; Ismail, M.A.; Esawi, E.; Qaqish, B.; Bawab, A.A.; Ismail, S.I. Aptamers Chemistry: Chemical Modifications and Conjugation Strategies. *Molecules*. **2019**, *25* (1), 3. DOI:10.3390/molecules25010003
7. Wu, Y.X.; Kwon, Y.J. Aptamers: The "evolution" of SELEX. *Methods*. **2016**, *106*, 21-28. DOI: 10.1016/j.ymeth.2016.04.020

8. Tuerk, C.; Gold, L. Systematic evolution of ligands by exponential enrichment: RNA ligands to bacteriophage T4 DNA polymerase. *Science*. **1990**, *249* (4968), 505-510. DOI:10.1126/science.2200121
9. Ellington, A.D.; Szostak, J.W. In vitro selection of RNA molecules that bind specific ligands. *Nature*. **1990**, *346* (6287), 818-822. DOI:10.1038/346818a0
10. Lam, S.Y.; Lau, H.L.; Kwok, C.K. Capture-SELEX: Selection Strategy, Aptamer Identification, and Biosensing Application. *Biosensors*. **2022**, *12* (12), 1142. DOI:10.3390/bios12121142
11. Hasegawa, H.; Savory, N.; Abe, K.; Ikebukuro, K. Methods for Improving Aptamer Binding Affinity. *Molecules*. **2016**, *21* (4), 421. DOI:10.3390/molecules21040421
12. Shraim, A.S.; Abdel Majeed, B.A.; Al-Binni, M.A.; Hunaiti, A. Therapeutic Potential of Aptamer-Protein Interactions. *ACS Pharmacology and Translational Science*. **2022**, *5* (12), 1211-1227. DOI:10.1021/acsptsci.2c00156
13. Stojanović, M.N.; de Prada, P.; Landry, D.W. Aptamer-based folding fluorescent sensor for cocaine. *Journal of the American Chemical Society*. **2001**, *123* (21), 4928-4931. DOI:10.1021/ja0038171
14. Neves, M.A.D.; Slavkovic, S.; Churcher, Z.R.; Johnson, P.E. Salt-mediated two-site ligand binding by the cocaine-binding aptamer. *Nucleic Acids Research*. **2017**, *45* (3), 1041-1048. DOI:10.1093/nar/gkw1294
15. Reinstein, O.; Yoo, M.; Han, C.; Palmo, T.; Beckham, S. A.; Wilce, M. C.; Johnson, P. E. Quinine binding by the cocaine-binding aptamer. Thermodynamic and hydrodynamic analysis of high-affinity binding of an off-target ligand. *Biochemistry*. **2013,** *52* (48), 8652–8662. DOI:10.1021/bi4010039

16. Churcher, Z.R.; Garaev, D.; Hunter, H.N.; Johnson, P.E. Reduction in Dynamics of Base pair Opening upon Ligand Binding by the Cocaine-Binding Aptamer. *Biophysical Journal*. **2020**, *119* (6), 1147-1156. DOI: 10.1016/j.bpj.2020.08.012

17. Zhang, Y.; Lai, B.S.; Juhas, M. Recent Advances in Aptamer Discovery and Applications. *Molecules*. **2019**, *24* (5), 941. DOI:10.3390/molecules24050941

18. Wu, X.; Zhao, Z.; Bai, H.; Fu, Ting.; Yang, Chao.; Hu, Xiaoxiao.; Liu, Qiaoling.; Champanhac, Carole.; Teng, I.T.; Ye, Mao.; Tan, Weihong. DNA Aptamer Selected against Pancreatic Ductal Adenocarcinoma for in vivo Imaging and Clinical Tissue Recognition. *Theranostics*. **2015**, *5* (9), 985-994. DOI:10.7150/thno.11938

19. Iwagawa, T.; Ohuchi, S.P.; Watanabe, S.; Nakamura, Y. Selection of RNA aptamers against mouse embryonic stem cells. *Biochimie*. **2012**, *94* (1), 250-257. DOI: 10.1016/j.biochi.2011.10.017

20. Dauphin-Ducharme, P.; Churcher, Z.R.; Shoara, A.A.; Rabarimehr, E.; Slavkovic, S.; Fontaine, N.; Boisvert, O.; Johnson, P.E. Redox Reporter - Ligand Competition to Support Signaling in the Cocaine-Binding Electrochemical Aptamer-Based Biosensor. *Chemistry*. **2023**, *29*(35), e202300618. DOI:10.1002/chem.202300618

21. Thiviyanathan, V.; Gorenstein, D.G. Aptamers and the next generation of diagnostic reagents. *Proteomics-Clinical Applications*. **2012**, *6* (11-12), 563-573. DOI:10.1002/prca.201200042

22. Jing, M.; Bowser, M. T. Methods for measuring aptamer-protein equilibria: a review. *Analytica Chimica Acta*. **2011,** *686* (1-2), 9–18. DOI: 10.1016/j.aca.2010.10.032

23. Slavkovic, S.; Johnson, P.E. Isothermal titration calorimetry studies of aptamer-small molecule interactions: practicalities and pitfalls – Aptamers. *Aptamers.* **2018**, *2*, 45-51

24. Zacharioudaki, D.E.; Fitilis, I.; Kotti, M. Review of Fluorescence Spectroscopy in Environmental Quality Applications. *Molecules*. **2022**, *27* (15), 4801. DOI:10.3390/molecules27154801

25. Shoara, A.A.; Johnson, P.E. Fluorometry studies of aptamers that bind intrinsically fluorescent ligands: techniques, obstacles and optimizations. *Aptamers*. **2022**, *2*, 19-27

26. Churcher, Z.R.; Johnson, P.E. NMR for non-experts; a practical guide for applying NMR methods in studies of aptamer-ligand interactions. *Aptamers.* **2020**, *4*, 3-9

27. Pendergrast, P. S.; Marsh, H. N.; Grate, D.; Healy, J. M.; Stanton, M. Nucleic acid aptamers for target validation and therapeutic applications. *Journal of Biomolecular Techniques*. **2005,** *16* (3), 224–234.

28. Hianik, T.; Ostatná, V.; Sonlajtnerova, M.; Grman, I. Influence of ionic strength, pH and aptamer configuration for binding affinity to thrombin. *Bioelectrochemistry.* **2007,** *70* (1), 127–133. DOI: 10.1016/j.bioelechem.2006.03.012

29. Schmidt, C.; Kammel, A.; Tanner, J. A.; Kinghorn, A. B.; Khan, M. M.; Lehmann, W.; Menger, M.; Schedler, U.; Schierack, P.; Rödiger, S. A multiparametric fluorescence assay for screening aptamer-protein interactions based on microbeads. *Scientific Reports*. **2022,** *12* (1), 2961. DOI:10.1038/s41598-022-06817-0

30. Selvam, S.; Sarkar, I. Bile salt induced solubilization of methylene blue: Study on methylene blue fluorescence properties and molecular mechanics calculation. *Journal of Pharmaceutical Analysis*. **2017**, *7* (1), 71-75. DOI: 10.1016/j.jpha.2016.07.006

31. Shoara, A.A.; Slavkovic, S.; Donaldson, L.; Johnson, P.E. Analysis of the Interaction between the Cocaine-Binding Aptamer and its Ligands using Fluorescence Spectroscopy. *Canadian Journal of Chemistry.* **2017**, *95* (12)

32. Huang, P.J.; Liu, J. Selection of Aptamers for Sensing Caffeine and Discrimination of Its Three Single Demethylated Analogues. *Analytical Chemistry*. **2022**, *94* (7), 3142-3149. DOI: 10.1021/acs.analchem.1c04349

33. Wu, Y.; Ranallo, S.; Del Grosso, E.; Chamoro-Garcia, A.; Ennis, H.L.; Milosavić, N.; Yang, K.; Kippin, T.; Ricci, F.; Stojanović, M.N.; Plaxo, K.W. Using Spectroscopy to Guide the Adaptation of Aptamers into Electrochemical Aptamer-Based Sensors. *Bioconjugate Chemistry*. **2023**, *34* (1), 124-132. DOI: 10.1021/acs.bioconjchem.2c00275

34. He, J.; Wang, J.; Zhang, M.; Shi, G. Selection of a Structure-Switching Aptamer for the Specific Methotrexate Detection. *ACS Sensors*. **2021**, *6* (6), 2436-2441. DOI:10.1021/acssensors.1c00749

35. Huang, P.J.; Liu, J. A DNA Aptamer for Theophylline with Ultrahigh Selectivity Reminiscent of the Classic RNA Aptamer. *ACS Chem Biology*. **2022**, *17* (8), 2121-2129. DOI:10.1021/acschembio.2c00179

36. Nakatsuka, N.; Yang, K.A.; Abendroth, J.M.; Cheung, K.M.; Xu, X.; Yang, H.; Zhao, C.; Zhu, B.; Rim, Y.S.; Yang, Y.; Weiss, P.S.; Stojanović, M.N.; Andrews, A.M. Aptamer-field-effect transistors overcome Debye length limitations for small-molecule sensing. *Science*. **2018**, *362* (6412), 319-324. DOI:10.1126/science. aao6750

37. Cruz-Aguado, J.A.; Penner, G. Determination of ochratoxin a with a DNA aptamer. *Journal of Agricultural and Food Chemistry*. **2008**, *56* (22), 10456-10461. DOI:10.1021/jf801957h

38. Yang, K.; Alkhamis, O.; Canoura, J.; Bryant, A.; Gong, E.M.; Barbu, M.; Taylor, S.; Nikic, D.; Banerjee, S.; Xiao, Y.; Stojanović, M.N.; Landry, D.W. Exploring the Landscape of Aptamers: From Cross-Reactive to Selective to Specific, High-Affinity Receptors for Cocaine. *JACS Au*. **2024**, *4* (2), 760-770. DOI:10.1021/jacsau.3c00781

39. Yang, K.; Mitchell, N.M.; Banerjee, S.; Cheung, Z.; Taylor, S.; Kostic, A.M.; Wong, I.; Sajjath, S.; Zhang, Y.; Stevens, J.; Mohan, S.; Landry, D.W.; Worgall, T.S.; Andrews, A.M.; Stojanović, M.N. A functional group-guided approach to aptamers for small molecules. *Science*. **2023**, *380* (6648), 942-948. DOI:10.1126/science. abn9859

40. Drew, H.R.; Wing, R.M.; Takano, T.; Broka, C.; Tanaka, S.; Itakura, K.; Dickerson, R.E. Structure of a B-DNA dodecamer: conformation and dynamics. *Proceedings of the National Academy of Sciences of the United States of America*. **1981**, *78* (4), 2179-2183. DOI:10.1073/pnas.78.4.2179

41. Hossain, M.; Giri, P.; Kumar, G.S. DNA intercalation by quinacrine and methylene blue: a comparative binding and thermodynamic characterization study. *DNA and Cell Biology*. **2008**, *27* (2), 81-90. DOI:10.1089/dna.2007.0652

42. Venugopal, S.; Sharma, V.; Mehra, A.; Singh, I.; Singh, G. DNA intercalators as anticancer agents. *Chemical Biology and Drug Design*. **2022**, *100*(4), 580-598. DOI:10.1111/cbdd.14116

43. Slavkovic, S.; Shoara, A.A.; Kaiyum, Y.A.; Churcher, Z.R.; Liu, T.; Simine, L.; Johnson, P.E. Amodiaquine Nonspecifically Binds Double Stranded and Three-Way Junction DNA Structures. *Chembiochem*. **2024**, *25* (14), e202400116. DOI:10.1002/cbic.202400116